Lamb Wave Propagation in Laminated Composite Plates

by

Bruce S. Tang

Dissertation submitted to the Faculty of the

Virginia Polytechnic Institute and State University

in partial fulfillment of the requirements for the degree of

Doctor of Philosophy

in

Engineering Mechanics

APPROVED:

E. G. Henneke, II, Chairman

R. O. Claus

J. C. Duke, Jr.

D. H. Morris

C. W. Smith

December, 1988

Blacksburg, Virginia

Lamb Wave Propagation in Laminated Composite Plates

by

Bruce S. Tang

E. G. Henneke, II, Chairman

Engineering Mechanics

(ABSTRACT)

Low frequency Lamb waves in composite laminates were investigated theoretically and experimentally. To have a general solution for Lamb wave propagation in multi-layered composite laminates is not practical due to a large number of boundary conditions needed to be satisfied at the interlaminar interfaces. Various approximate theories have been proposed to model low frequency Lamb wave propagation in composite laminates. In the present study, an approximate solution was derived from an elementary shear deformation plate theory and was shown to work well in the low frequency, long wavelength region.

A simple method, similar in configuration to the acousto-ultrasonic technique, was used to measure Lamb wave phase velocities. Low frequency Lamb waves, usually in the range of 10 kHz to 1 MHz, were generated. Dispersion curves of the lowest symmetric Lamb mode and the lowest antisymmetric Lamb mode were obtained. The experimental data were compared with the results obtained from the approximate solution for the lowest Lamb modes in the low frequency, long wavelength region for a unidirectional laminate, a symmetric cross-ply laminate, a symmetric quasi-isotropic laminate and an aluminum plate. There is good correlation between the data and the results obtained from the approximate solution, which suggests that the lowest Lamb

modes are modeled adequately by the present theory in these cases. This experimental procedure of measuring phase velocities can be used to characterize laminated composite plates with and without damage since each material and stacking sequence gives distinct lowest symmetric and antisymmetric curves.

Stiffness reduction of composite laminates caused by damage can be related to the change in Lamb wave propagation speed. Damage in the form of transverse cracks in the 90° plies of a $[90/90/90/0]_s$ graphite/epoxy laminate reduced the phase velocities of the Lamb modes. The lowest antisymmetric mode is sensitive to stiffness reduction in composite plates. Consequently, axial stiffness reduction in $[0/45/0/45/0/45]_s$ and $[0]_{12}$ woven graphite/polyimide composite laminates was monitored by the lowest antisymmetric Lamb mode.

DEDICATION

This work is dedicated to my wife, Kit-Ming and my parents.

ACKNOWLEDGEMENTS

The author would like to express his thanks and appreciation to the following people:

- Dr. Edmund G. Henneke, II for his guidance, friendship, encouragement and support in both academic and personal aspects.
- Dr. J. C. Duke, Jr. for his advice and helpful discussions.
- Dr. R. O. Claus, Dr. D. H. Morris and Prof. C. W. Smith for serving as committee members and for helping to edit this document.
- The faculty, staff and students of the Materials Response Group for their assistance and support.
- A special thanks to Kit-Ming, the author's wife, and Mr. and Mrs. Yick Tang, the author's parents, for their constant and endless love, encouragement, patience and support for the last four turbulent years.

Table of Contents

I. INTRODUCTION 1

II. LITERATURE REVIEW 5

2.1 Theoretical Background 5

2.2 Experimental Techniques 8

2.3 Summary 9

III. ANTISYMMETRIC LAMB MODES 11

3.1 Shear Deformation Theory 12

3.2 Exact Solutions for Transversely Isotropic Plates 20

3.3 Experimental Procedure 26

3.4 Results and Discussion 30

IV. SYMMETRIC LAMB MODES 44

4.1 Shear Deformation Theory 44

4.2 Exact Solutions for Transversely Isotropic Plates 45

V. DISPERSION CURVES OF LAMB WAVES 47
5.1 Exact Solutions 47
5.2 Approximate Theory 50

VI. APPLICATION TO MONITOR AXIAL STIFFNESS REDUCTION 64
6.1 Stiffness Reduction 64
6.2 Modified Method 72
6.3 Woven Materials 75

VII. CONCLUSIONS 80

REFERENCES 83

APPENDIX A 87

APPENDIX B 91

VITA 95

List of Illustrations

Figure 1. Acoustic waveguide. 4

Figure 2. Lamb modes. 6

Figure 3. Coordinate system of a plate. 13

Figure 4. Schematic diagram of the experimental setup for Lamb wave phase velocity measurements. 27

Figure 5. Typical input and output signals. 28

Figure 6. Change in arrival time for a phase point. 29

Figure 7. Theoretical dispersion curves for antisymmetric Lamb waves propagating along the fiber direction of a $[0]_8$ graphite/epoxy laminate. (1 in/sec = 0.0254 m/sec) 32

Figure 8. Theoretical dispersion curves for antisymmetric Lamb waves propagating perpendicular to the fiber direction of a $[0]_8$ graphite/epoxy laminate. (1 in/sec = 0.0254 m/sec) 33

Figure 9. Dispersion curves for antisymmetric Lamb waves propagating along the fiber direction of a $[0]_8$ graphite/epoxy laminate. (1 in/sec = 0.0254 m/sec) 34

Figure 10. Dispersion curves for antisymmetric Lamb waves propagating perpendicular to the fiber direction of a $[0]_8$ graphite/epoxy laminate. (1 in/sec = 0.0254 m/sec) 35

Figure 11. Dispersion curves for antisymmetric Lamb waves propagating along the x axis of a $[0/90]_{2s}$ graphite/epoxy laminate. (1 in/sec = 0.0254 m/sec) 37

Figure 12. Dispersion curves for antisymmetric Lamb waves propagating along the y axis of a $[0/90]_{2s}$ graphite/epoxy laminate. (1 in/sec = 0.0254 m/sec) 38

Figure 13. Dispersion curves for antisymmetric Lamb waves propagating along the x axis of a $[0/45/90/-45]_s$ graphite/epoxy laminate. (1 in/sec = 0.0254 m/sec) 39

Figure 14. Dispersion curves for antisymmetric Lamb waves propagating along the y axis of a $[0/45/90/-45]_s$ graphite/epoxy laminate. (1 in/sec = 0.0254 m/sec) 40

Figure 15. Dispersion curves for antisymmetric Lamb wave propagation in a 6061-T4 aluminum plate. (1 in/sec = 0.0254 m/sec) 41

Figure 16. Lamb wave dispersion curves for wave propagation along the fiber direction of a unidirectional laminate. 48

Figure 17. Lamb wave dispersion curves for wave propagation perpendicular to the fiber direction of a unidirectional laminate. 49

Figure 18. Regions of the lowest Lamb modes for symmetric laminates. Upper region corresponds to symmetric modes and lower region corresponds to antisymmetric modes. 51

Figure 19. Region of the second lowest symmetric modes for symmetric laminates. 52

Figure 20. Region of the second lowest antisymmetric modes for symmetric laminates. 53

Figure 21. Theoretical results and data for Lamb wave propagation along the fiber direction of a unidirectional laminate. 54

Figure 22. Theoretical results and data for Lamb wave propagation perpendicular to the fiber direction of a unidirectional laminate. 55

Figure 23. Theoretical results and data for low frequency Lamb wave propagation in the x direction of a $[0/90]_{2s}$ laminate. 57

Figure 24. Theoretical results and data for low frequency Lamb wave propagation in the y direction of a $[0/90]_{2s}$ laminate. 58

Figure 25. Theoretical results and data for low frequency Lamb wave propagation in the x direction of a $[0/45/90/-45]_s$ laminate. 59

Figure 26. Theoretical results and data for low frequency Lamb wave propagation in the y direction of a $[0/45/90/-45]_s$ laminate. 60

Figure 27. Theoretical results and data for low frequency Lamb wave propagation in a 6061-T4 aluminum plate. 61

Figure 28. Upper and lower limits of approximate solutions. 63

Figure 29. Data and theoretical results from the shear deformation theory (SDT) for a $[0/90]_{2s}$ graphite/epoxy laminate. 65

Figure 30. Schematic representation of transverse cracks in a $[0/90]_{2s}$ laminate. . . . 67

Figure 31. Theoretical dispersion curves for Lamb wave propagation in the 0° direction of a $[0/90]_{2s}$ laminate. 68

Figure 32. Theoretical dispersion curves for Lamb wave propagation in the 0° direction of a $[90/90/90/0]_s$ laminate. 69

Figure 33. Experimental data for Lamb wave propagation in the 0° direction of a $[90/90/90/0]_s$ graphite/epoxy laminate. 70

Figure 34. Experimental data for the lowest antisymmetric Lamb mode in the 0° direction of a $[90/90/90/0]_s$ graphite/epoxy laminate. 71

Figure 35. Schematic diagram of the experimental setup for the modified method. . 74

Figure 36. Experimental data for the lowest antisymmetric Lamb mode in the 0° direction of two $[0/45/0/45/0/45]_s$ woven graphite/polyimide specimens. . . 76

Figure 37. X-ray radiograph of a $[0/45/0/45/0/45]_s$ woven graphite/polyimide specimen after axial stiffness reduction of 4.9%. 77

Figure 38. X-ray radiograph of a $[0/45/0/45/0/45]_s$ woven graphite/polyimide specimen after axial stiffness reduction of 7.7%. 78

Figure 39. Experimental data for the lowest antisymmetric Lamb mode in the 0° direction of a $[0]_{12}$ woven graphite/polyimide specimen. 79

I. INTRODUCTION

Owing to the advantage of very large strength-to-weight and stiffness-to-weight ratios, composite materials are attractive for a wide range of applications. Increasingly, more and more high performance engineering structures are being built with critical structural components made from composite materials. Many of these components are in the form of plates. Usually, in the high performance engineering structures, these laminated composite plates are in a complex state of stress. Appropriate nondestructive evaluation techniques and procedures are needed to evaluate and predict the mechanical properties of these composite plates in the as-received condition and during service loading to monitor damage development and to assure the reliability of the engineering structures.

Damage development in laminated composite plates is a complex sequence of matrix cracking, delamination, fiber breakage, fiber/matrix debonding, and so on. A number of testing methods has been developed to interrogate and to monitor damage development in composite laminates. Different tests have been found to be sensitive to different types of damage. Generally, a more complete understanding of the damage development and damage state is obtained if several tests are used. From this information, it is expected that one will be able to model the damage state and estimate the residual stiffness, residual strength and life of the composite laminates.

Ultrasonic testing is one way to monitor damage development [1-4]. Cracks and delaminations can be detected by reflection of ultrasonic signals. Moreover, the measurement of ultrasonic wave speed is directly related to material stiffness and hence is a quantitative parameter which yields information about the mechanical state of the material [5-10]. It may also be related indirectly to information concerning strength and life, although knowledge at the present stage is too immature to state this definitely. The measurements of ultrasonic wave speed and attenuation in the thickness direction of a plate are relatively straightforward, especially when the material to be studied is thick enough to allow pulse delays of sufficiently long time to be monitored by standard ultrasonic testing instrumentation. Much work has been performed using through-the-thickness ultrasonic attenuation and velocity measurements to monitor damage and evaluate material properties in laminated composite plates. However, little information about the in-plane properties can be obtained from such tests. Evaluation of in-plane properties of laminated composite plates will provide information which is more useful to designers and users than measurement of through-the-thickness properties since laminated composite plates are designed to carry load in the plane of the plate in most cases. Thus, there is a need for ultrasonic testing methods, such as measurement of in-plane wave speeds, to evaluate material properties and to monitor damage in the in-plane directions of laminated composite plates in the as-received condition and during service loading.

In applied electromagnetism, waveguides have been widely used for a number of decades. The same waveguide concept can be applied to elastic wave propagation in a plate of finite thickness. In this case, the plate is considered as an acoustic waveguide (Figure 1). Generally speaking, acoustic waveguide problems are significantly more difficult to solve than are electromagnetic waveguide problems, and the basic characteristics of the solutions themselves are often more complicated. Every acoustic waveguide structure is capable of supporting an infinite number of different guided wave solutions, called waveguide modes, each with a different propagation speed and a different particle displacement field. In a traction-free plate, several different types of waveguide modes can coexist. The simplest mode is the shear horizontal (SH) mode, in which particle motions are parallel to the plate surface and the wave is a pure shear wave. In the Lamb wave modes, which have particle motions in a plane normal to the plate surfaces, both shear and longitudinal wave components are needed to satisfy the boundary conditions at the surfaces of the plate. For composite laminates, unlike wave propagation in layered media as discussed by Brekhovskikh [11] and Ewing, Jardetzky and Press [12], Lamb waves use the whole laminate as the wave medium. Lamb waves may be the most adequate nondestructive means to interrogate and to evaluate material properties of laminated composite plates in the plane of the plate, which usually coincides with the direction of applied loads. However, in order to utilize Lamb waves to their full potential, it is necessary that we have a complete understanding of the characteristics of Lamb waves.

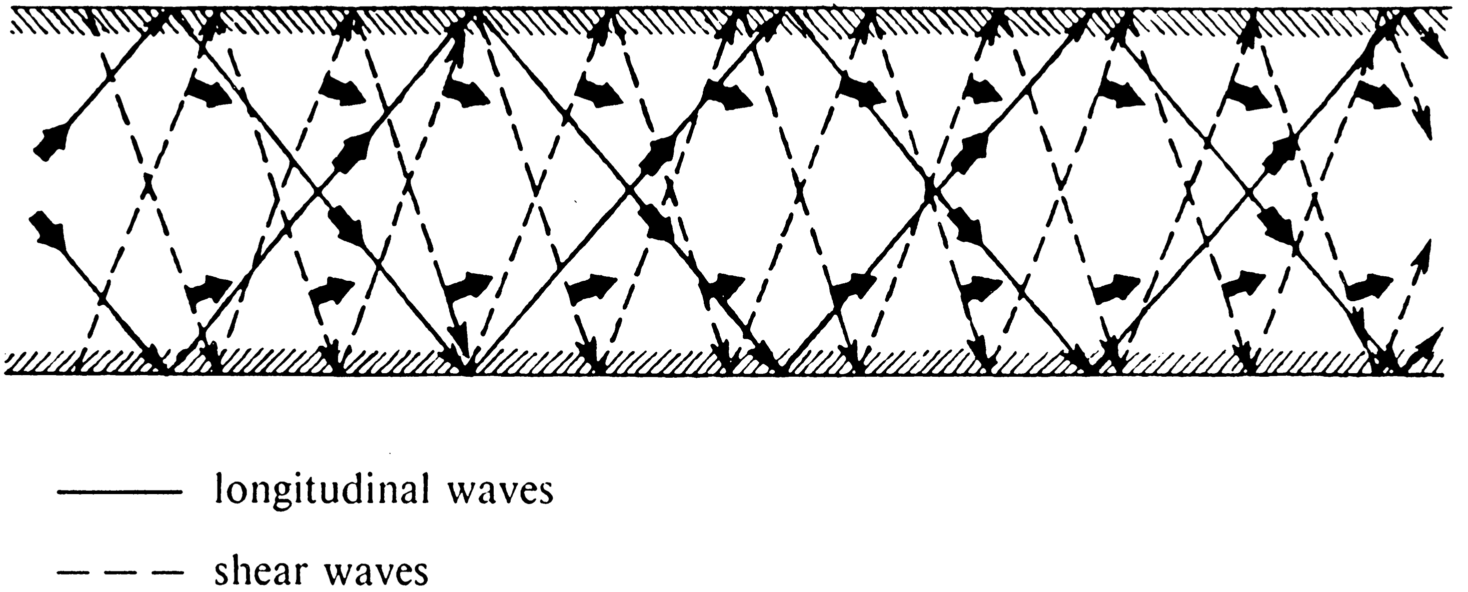

Figure 1. Acoustic waveguide.

II. LITERATURE REVIEW

2.1 Theoretical Background

Lamb wave propagation in isotropic and anisotropic plates has been the subject of numerous investigations for many years. The theories of Lamb wave propagation in isotropic and orthotropic plates are well established [13-15]. More recently, Lamb wave propagation in laminated composite plates has drawn much attention. There are two distinct types of harmonic motion in Lamb waves, symmetric (or dilatational) modes and antisymmetric (or flexural) modes (Figure 2). In a homogeneous isotropic solid bounded by two parallel surfaces, waves will propagate as symmetric Lamb modes, antisymmetric Lamb modes or SH modes having their wave vectors in the plane of the solid. These wave types will be set up in such a manner as to maintain the traction-free boundary conditions at the surfaces. For a given frequency, a number of modes can exist that will satisfy the traction-free boundary conditions. Standing waves will be established in the transverse direction and traveling waves will be propagated in the plane of the plate. The analysis for SH modes is straightforward

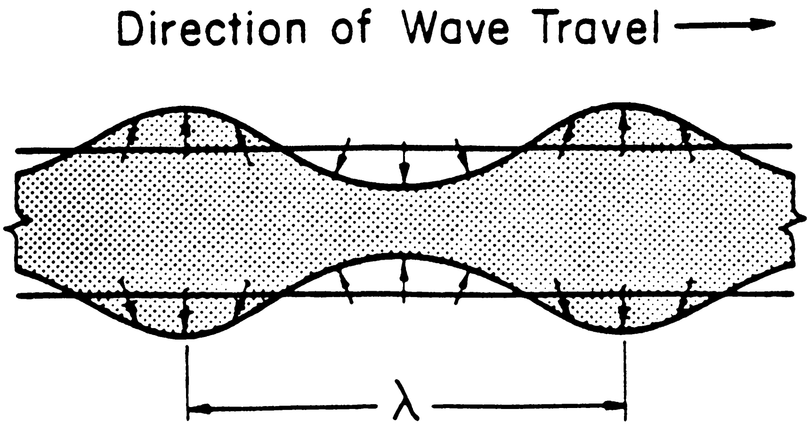

Symmetric Mode

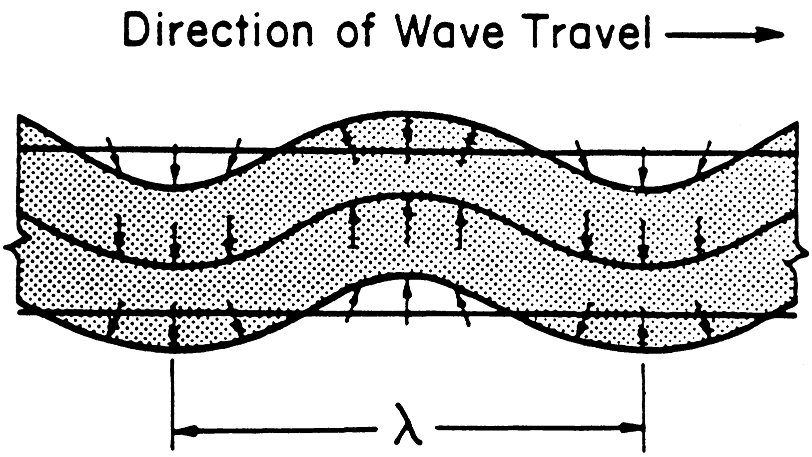

Antisymmetric Mode

Figure 2. Lamb modes.

while the analysis for symmetric and antisymmetric Lamb modes is much more complicated.

The Lamb modes were first discussed by Lamb [13] in 1917. Lamb formulated the problem by using potentials and arrived at the well-known Rayleigh-Lamb relation for wave propagation in isotropic plates. Solie and Auld [14] investigated waves in anisotropic plates theoretically and compared the results to the uncoupled shear vertical and longitudinal modes, which in turn were related to the slowness curves for bulk waves. This approach provides a means of approximating Lamb wave dispersion curves from the behavior of the slowness curves. Habeger, Mann, and Baum [15] conducted a theoretical and experimental study of ultrasonic Lamb waves in machine-made papers. The papers were modeled as homogeneous orthotropic plates. The dispersion equation for Lamb wave propagation in the principal directions was developed analytically and verified experimentally.

For Lamb wave propagation, unidirectional composite plates can be considered as homogeneous, orthotropic plates as long as the wavelength of the Lamb wave of interest is much larger than the ply thickness. Thus, the solution for orthotropic plates can be applied to unidirectional laminates. To obtain a general solution for Lamb wave propagation in multilayered composite laminates is not practical, due to a large number of boundary conditions needed to be satisfied at the interlaminar interfaces. Owing to the difficulty of this problem, various approximate theories have been proposed to model low frequency Lamb wave propagation in composite laminates. Moon [16] used a variational method to obtain an approximate solution for Lamb wave propagation in laminated composite plates. Sun and Tan [17] derived an approximate solution based on Mindlin's plate theory for isotropic materials. Stiffler and Henneke [18] obtained a low frequency Lamb wave solution using elementary plate theory.

2.2 *Experimental Techniques*

There are many methods to generate and detect Lamb waves in composite materials. The most popular method is the leaky Lamb wave method. In this particular method, two transducers and a composite plate are immersed in a water tank. By varying the sending and receiving angles of the transducers, relative maxima corresponding to Lamb modes are detected when the Lamb wave energy leaks from the surfaces of the plate. By knowing the angles and the excitation frequencies, dispersion curves can be obtained experimentally. Worlton [19] was the first one to confirm the theory of Lamb waves and determined the dispersion curves for aluminum and zirconium experimentally by using this method. Chimenti and Nayfeh [20] verified their approximate solution for unidirectional composite plates in the fiber direction by the detection of null zones which indicated the presence of leaky Lamb waves. Bar-Cohen and Chimenti [21] studied the application of leaky Lamb waves for non-destructive testing of composite laminates. They observed a correlation between the character of the excited Lamb modes and the presence of certain defects such as porosity and delaminations. Martin and Chimenti [22] refined this method by signal processing. While the results of the leaky Lamb wave method look promising, the technique may not be particularly well suited for field inspection of composite laminates since the method requires the composite plates to be immersed in water. Using plexiglass variable angle beam wedges instead of water as the elastic wave medium may solve the problem. A simple method similar to the acousto-ultrasonic technique [23,24] has been studied by Stiffler and Henneke [18,25,26] to generate and detect Lamb waves in composite laminates. The experimental data obtained by this simple method generally belong to the lowest symmetric and antisymmetric Lamb modes. In this method, two piezoelectric transducers acoustically coupled to the plate by water soluble couplant are directly in contact with the composite plate to create and receive Lamb waves. The Lamb wave speed can be determined by measuring the change in arrival time of a phase point on the receiving signal while moving the receiver a certain distance. Chapman [27] used the same idea in the detection of debonding in fiberglass reinforced plastic lap joints. In a similar approach, Rose, Rokhlin and Adler [28] measured Lamb wave speeds with energy flux deviation in composite laminates. Liu [29] generated Lamb modes and SH modes in a unidirectional graphite/aluminum composite plate by a shear wave transducer, and used an electromagnetic acoustic transducer (EMAT), which was not sensitive to the SH modes, to detect the signals. Wormley and Thompson [30], who used two EMATs as receivers, determined the wave speed by cross-correlation between the two receiving signals and thus evaluated the texture of rolled metal plates.

2.3 Summary

Lamb waves may be the most adequate nondestructive means to interrogate and to evaluate in-plane properties of laminated composite plates. The theories of Lamb wave propagation in isotropic and orthotropic plates are well established. However, to have a general solution for Lamb wave propagation in multilayered composite laminates is not practical, and hence approximate theory is needed to model Lamb wave propagation in this situation. The method studied by Stiffler and Henneke may be an easier technique to implement in field inspection of laminated composite plates than the leaky Lamb wave method, since the leaky Lamb wave method requires composite plates to be immersed in water.

III. ANTISYMMETRIC LAMB MODES

There are two distinct types of harmonic motion in Lamb waves. They are called symmetric (or dilatational) modes and antisymmetric (or flexural) modes. Stiffler and Henneke [18,25,26] employed the classical plate theory in their analysis of antisymmetric Lamb modes. The classical plate theory is based on the Kirchhoff hypothesis, which assumes that normals to the midplane before deformation remain straight and normal to the midplane after deformation, and hence neglects transverse shear deformation effects. For homogeneous isotropic thin plates, the effects of the transverse shear deformation are negligible. However, these effects are significant in the case of laminated composite plates due to the relatively low transverse shear modulus. Thus, the effects of transverse shear deformation should be included in the formulation. The present study deals with an analysis of antisymmetric Lamb waves using a shear deformation theory which incorporates the effects of transverse shear deformation and rotary inertia. Exact solutions for the antisymmetric Lamb wave propagation in transversely isotropic plates are also presented.

3.1 Shear Deformation Theory

The classical plate theory is a special case of the shear deformation theory. In the classical plate theory, the shear moduli are taken to be very large so that the transverse shear deformation can be neglected. A variety of shear deformation theories have been proposed to date. The analysis presented here is based on the work of Yang, Norris and Stavsky [31] who extended Mindlin's theory for homogeneous plates [32] to laminates consisting of an arbitrary number of anisotropic layers.

Considering a laminated composite plate of thickness h, the origin of the global coordinate system is located at the midplane, with the z axis being normal to the midplane, and the x and y axes in the midplane of the plate (Figure 3). The approach of Yang, Norris and Stavsky, which takes into account the effects of transverse shear deformation and rotary inertia, assumes the following displacement field:

$$u = u_0(x,y,t) + z\psi_x(x,y,t)$$

$$v = v_0(x,y,t) + z\psi_y(x,y,t) \tag{1}$$

$$w = w(x,y,t)$$

where u, v, w are the displacement components in the x, y and z directions, u_0 and v_0 are the midplane displacement components, and ψ_x and ψ_y are the rotation components along the x and y axes, respectively. From the strain-displacement relations, we have

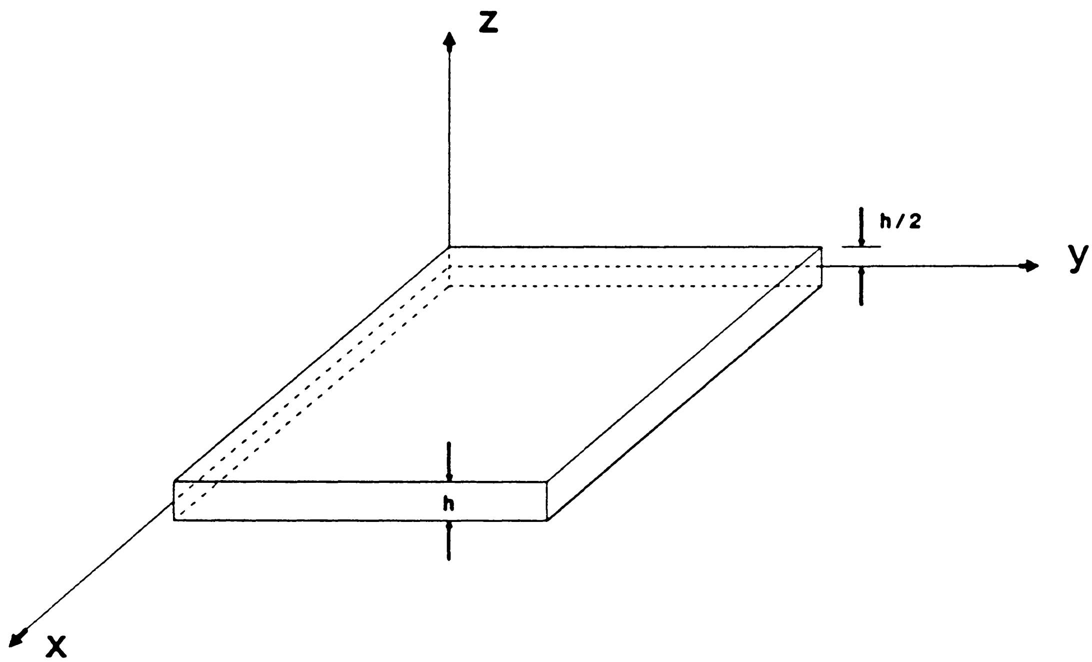

Figure 3. Coordinate system of a plate.

$$\varepsilon_x = \frac{\partial u_0}{\partial x} + z\frac{\partial \psi_x}{\partial x}$$

$$\varepsilon_y = \frac{\partial v_0}{\partial y} + z\frac{\partial \psi_y}{\partial y}$$

$$\varepsilon_z = 0$$

$$\gamma_{xy} = \frac{\partial u_0}{\partial y} + \frac{\partial v_0}{\partial x} + z\left(\frac{\partial \psi_x}{\partial y} + \frac{\partial \psi_y}{\partial x}\right) \tag{2}$$

$$\gamma_{xz} = \psi_x + \frac{\partial w}{\partial x}$$

$$\gamma_{yz} = \psi_y + \frac{\partial w}{\partial y}$$

The stress-strain relations for any layer are given by

$$\begin{bmatrix} \sigma_x \\ \sigma_y \\ \tau_{yz} \\ \tau_{xz} \\ \tau_{xy} \end{bmatrix} = \begin{bmatrix} \overline{Q}_{11} & \overline{Q}_{12} & 0 & 0 & \overline{Q}_{16} \\ \overline{Q}_{12} & \overline{Q}_{22} & 0 & 0 & \overline{Q}_{26} \\ 0 & 0 & \overline{Q}_{44} & \overline{Q}_{45} & 0 \\ 0 & 0 & \overline{Q}_{45} & \overline{Q}_{55} & 0 \\ \overline{Q}_{16} & \overline{Q}_{26} & 0 & 0 & \overline{Q}_{66} \end{bmatrix} \begin{bmatrix} \varepsilon_x \\ \varepsilon_y \\ \gamma_{yz} \\ \gamma_{xz} \\ \gamma_{xy} \end{bmatrix} \tag{3}$$

where $\overline{Q}_{ij}$ for $i,j = 1,2,6$ are plane-stress reduced stiffnesses, and $\overline{Q}_{ij}$ for $i,j = 4,5$ are transverse shear stiffnesses. Defining the force and moment resultants per unit length as

$$(N_x, N_y, N_{xy}) = \int_{-h/2}^{h/2} (\sigma_x, \sigma_y, \tau_{xy})dz$$

$$(Q_x , Q_y) = \int_{-h/2}^{h/2} (\tau_{xz}, \tau_{yz}) dz \tag{4}$$

$$(M_x, M_y, M_{xy}) = \int_{-h/2}^{h/2} (\sigma_x, \sigma_y, \tau_{xy}) z dz$$

where h is the thickness of the plate, we have

$$\begin{bmatrix} N_x \\ N_y \\ Q_y \\ Q_x \\ N_{xy} \\ M_x \\ M_y \\ M_{xy} \end{bmatrix} = \begin{bmatrix} A_{11} & A_{12} & 0 & 0 & A_{16} & B_{11} & B_{12} & B_{16} \\ A_{12} & A_{22} & 0 & 0 & A_{26} & B_{12} & B_{22} & B_{26} \\ 0 & 0 & A_{44} & A_{45} & 0 & 0 & 0 & 0 \\ 0 & 0 & A_{45} & A_{55} & 0 & 0 & 0 & 0 \\ A_{16} & A_{26} & 0 & 0 & A_{66} & B_{16} & B_{26} & B_{66} \\ B_{11} & B_{12} & 0 & 0 & B_{16} & D_{11} & D_{12} & D_{16} \\ B_{12} & B_{22} & 0 & 0 & B_{26} & D_{12} & D_{22} & D_{26} \\ B_{16} & B_{26} & 0 & 0 & B_{66} & D_{16} & D_{26} & D_{66} \end{bmatrix} \begin{bmatrix} \frac{\partial u_0}{\partial x} \\ \frac{\partial v_0}{\partial y} \\ \frac{\partial w}{\partial y} + \psi_y \\ \frac{\partial w}{\partial x} + \psi_x \\ \frac{\partial u_0}{\partial y} + \frac{\partial v_0}{\partial x} \\ \frac{\partial \psi_x}{\partial x} \\ \frac{\partial \psi_y}{\partial y} \\ \frac{\partial \psi_x}{\partial y} + \frac{\partial \psi_y}{\partial x} \end{bmatrix} \tag{5}$$

where the laminate stiffnesses are given by $(A_{ij}, B_{ij}, D_{ij}) = \int_{-h/2}^{h/2} (\overline{Q}_{ij})_k (1, z, z^2) dz$, $i,j = 1,2,6$ and $A_{ij} = k_i k_j \int_{-h/2}^{h/2} (\overline{Q}_{ij})_k dz$, $i,j = 4,5$ (see Appendix A). The shear correction factors k_i k_j are included to account for the fact that the transverse shear strain distributions are not uniform across the thickness of the plate. Neglecting body forces, the equations of motion are

$$\frac{\partial N_x}{\partial x} + \frac{\partial N_{xy}}{\partial y} = \bar{\rho}\frac{\partial^2 u_0}{\partial t^2} + R\frac{\partial^2 \psi_x}{\partial t^2}$$

$$\frac{\partial N_{xy}}{\partial x} + \frac{\partial N_y}{\partial y} = \bar{\rho}\frac{\partial^2 v_0}{\partial t^2} + R\frac{\partial^2 \psi_y}{\partial t^2}$$

$$\frac{\partial Q_x}{\partial x} + \frac{\partial Q_y}{\partial y} = \bar{\rho}\frac{\partial^2 w}{\partial t^2} \tag{6}$$

$$\frac{\partial M_x}{\partial x} + \frac{\partial M_{xy}}{\partial y} - Q_x = R\frac{\partial^2 u_0}{\partial t^2} + I\frac{\partial^2 \psi_x}{\partial t^2}$$

$$\frac{\partial M_{xy}}{\partial x} + \frac{\partial M_y}{\partial y} - Q_y = R\frac{\partial^2 v_0}{\partial t^2} + I\frac{\partial^2 \psi_y}{\partial t^2}$$

where $(\bar{\rho}, R, I) = \int_{-h/2}^{h/2} \rho(1, z, z^2)dz$ and ρ is the mass density. Substituting equation (5) into (6), we obtain the equations of motion in terms of the displacements and the rotations as

$$\begin{aligned}
&A_{11}\frac{\partial^2 u_0}{\partial x^2} + 2A_{16}\frac{\partial^2 u_0}{\partial x \partial y} + A_{66}\frac{\partial^2 u_0}{\partial y^2} + A_{16}\frac{\partial^2 v_0}{\partial x^2} + (A_{12} + A_{66})\frac{\partial^2 v_0}{\partial x \partial y} + A_{26}\frac{\partial^2 v_0}{\partial y^2} \\
&+ B_{11}\frac{\partial^2 \psi_x}{\partial x^2} + 2B_{16}\frac{\partial^2 \psi_x}{\partial x \partial y} + B_{66}\frac{\partial^2 \psi_x}{\partial y^2} + B_{16}\frac{\partial^2 \psi_y}{\partial x^2} + (B_{12} + B_{66})\frac{\partial^2 \psi_y}{\partial x \partial y} + B_{26}\frac{\partial^2 \psi_y}{\partial y^2} \\
&\qquad = \bar{\rho}\frac{\partial^2 u_0}{\partial t^2} + R\frac{\partial^2 \psi_x}{\partial t^2}
\end{aligned}$$

$$A_{16}\frac{\partial^2 u_0}{\partial x^2}+(A_{12}+A_{66})\frac{\partial^2 u_0}{\partial x\partial y}+A_{26}\frac{\partial^2 u_0}{\partial y^2}+A_{66}\frac{\partial^2 v_0}{\partial x^2}+2A_{26}\frac{\partial^2 v_0}{\partial x\partial y}+A_{22}\frac{\partial^2 v_0}{\partial y^2}$$
$$+B_{16}\frac{\partial^2 \psi_x}{\partial x^2}+(B_{12}+B_{66})\frac{\partial^2 \psi_x}{\partial x\partial y}+B_{26}\frac{\partial^2 \psi_x}{\partial y^2}+B_{66}\frac{\partial^2 \psi_y}{\partial x^2}+2B_{26}\frac{\partial^2 \psi_y}{\partial x\partial y}+B_{22}\frac{\partial^2 \psi_y}{\partial y^2}$$
$$=\bar{\rho}\frac{\partial^2 v_0}{\partial t^2}+R\frac{\partial^2 \psi_y}{\partial t^2}$$

$$A_{55}(\frac{\partial \psi_x}{\partial x}+\frac{\partial^2 w}{\partial x^2})+A_{45}(\frac{\partial \psi_x}{\partial y}+\frac{\partial \psi_y}{\partial x}+2\frac{\partial^2 w}{\partial x\partial y})+A_{44}(\frac{\partial \psi_y}{\partial y}+\frac{\partial^2 w}{\partial y^2})$$
$$=\bar{\rho}\frac{\partial^2 w}{\partial t^2} \tag{7}$$

$$B_{11}\frac{\partial^2 u_0}{\partial x^2}+2B_{16}\frac{\partial^2 u_0}{\partial x\partial y}+B_{66}\frac{\partial^2 u_0}{\partial y^2}+B_{16}\frac{\partial^2 v_0}{\partial x^2}+(B_{12}+B_{66})\frac{\partial^2 v_0}{\partial x\partial y}+B_{26}\frac{\partial^2 v_0}{\partial y^2}$$
$$+D_{11}\frac{\partial^2 \psi_x}{\partial x^2}+2D_{16}\frac{\partial^2 \psi_x}{\partial x\partial y}+D_{66}\frac{\partial^2 \psi_x}{\partial y^2}+D_{16}\frac{\partial^2 \psi_y}{\partial x^2}+(D_{12}+D_{66})\frac{\partial^2 \psi_y}{\partial x\partial y}+D_{26}\frac{\partial^2 \psi_y}{\partial y^2}$$
$$-A_{55}(\psi_x+\frac{\partial w}{\partial x})-A_{45}(\psi_y+\frac{\partial w}{\partial y})=R\frac{\partial^2 u_0}{\partial t^2}+I\frac{\partial^2 \psi_x}{\partial t^2}$$

$$B_{16}\frac{\partial^2 u_0}{\partial x^2}+(B_{12}+B_{66})\frac{\partial^2 u_0}{\partial x\partial y}+B_{26}\frac{\partial^2 u_0}{\partial y^2}+B_{66}\frac{\partial^2 v_0}{\partial x^2}+2B_{26}\frac{\partial^2 v_0}{\partial x\partial y}+B_{22}\frac{\partial^2 v_0}{\partial y^2}$$
$$+D_{16}\frac{\partial^2 \psi_x}{\partial x^2}+(D_{12}+D_{66})\frac{\partial^2 \psi_x}{\partial x\partial y}+D_{26}\frac{\partial^2 \psi_x}{\partial y^2}+D_{66}\frac{\partial^2 \psi_y}{\partial x^2}+2D_{26}\frac{\partial^2 \psi_y}{\partial x\partial y}+D_{22}\frac{\partial^2 \psi_y}{\partial y^2}$$
$$-A_{45}(\psi_x+\frac{\partial w}{\partial x})-A_{44}(\psi_y+\frac{\partial w}{\partial y})=R\frac{\partial^2 v_0}{\partial t^2}+I\frac{\partial^2 \psi_y}{\partial t^2}$$

For symmetric laminates, the coupling stiffnesses B_{ij}'s and the coupling normal-rotary inertia coefficient R are identically zero. The equations of motion decouple into two sets of equations governing the in-plane and the transverse motions respectively:

$$A_{11}\frac{\partial^2 u_0}{\partial x^2} + 2A_{16}\frac{\partial^2 u_0}{\partial x\partial y} + A_{66}\frac{\partial^2 u_0}{\partial y^2} + A_{16}\frac{\partial^2 v_0}{\partial x^2} + (A_{12}+A_{66})\frac{\partial^2 v_0}{\partial x\partial y} + A_{26}\frac{\partial^2 v_0}{\partial y^2} = \bar{\rho}\frac{\partial^2 u_0}{\partial t^2}$$

$$A_{16}\frac{\partial^2 u_0}{\partial x^2} + (A_{12}+A_{66})\frac{\partial^2 u_0}{\partial x\partial y} + A_{26}\frac{\partial^2 u_0}{\partial y^2} + A_{66}\frac{\partial^2 v_0}{\partial x^2} + 2A_{26}\frac{\partial^2 v_0}{\partial x\partial y} + A_{22}\frac{\partial^2 v_0}{\partial y^2} = \bar{\rho}\frac{\partial^2 v_0}{\partial t^2} \tag{8}$$

and

$$A_{55}(\frac{\partial \psi_x}{\partial x} + \frac{\partial^2 w}{\partial x^2}) + A_{45}(\frac{\partial \psi_x}{\partial y} + \frac{\partial \psi_y}{\partial x} + 2\frac{\partial^2 w}{\partial x\partial y}) + A_{44}(\frac{\partial \psi_y}{\partial y} + \frac{\partial^2 w}{\partial y^2}) = \bar{\rho}\frac{\partial^2 w}{\partial t^2}$$

$$D_{11}\frac{\partial^2 \psi_x}{\partial x^2} + 2D_{16}\frac{\partial^2 \psi_x}{\partial x\partial y} + D_{66}\frac{\partial^2 \psi_x}{\partial y^2} + D_{16}\frac{\partial^2 \psi_y}{\partial x^2} + (D_{12}+D_{66})\frac{\partial^2 \psi_y}{\partial x\partial y} + D_{26}\frac{\partial^2 \psi_y}{\partial y^2} - A_{55}(\psi_x + \frac{\partial w}{\partial x}) - A_{45}(\psi_y + \frac{\partial w}{\partial y}) = I\frac{\partial^2 \psi_x}{\partial t^2} \tag{9}$$

$$D_{16}\frac{\partial^2 \psi_x}{\partial x^2} + (D_{12}+D_{66})\frac{\partial^2 \psi_x}{\partial x\partial y} + D_{26}\frac{\partial^2 \psi_x}{\partial y^2} + D_{66}\frac{\partial^2 \psi_y}{\partial x^2} + 2D_{26}\frac{\partial^2 \psi_y}{\partial x\partial y} + D_{22}\frac{\partial^2 \psi_y}{\partial y^2} - A_{45}(\psi_x + \frac{\partial w}{\partial x}) - A_{44}(\psi_y + \frac{\partial w}{\partial y}) = I\frac{\partial^2 \psi_y}{\partial t^2}$$

For wave propagation, we consider plane waves of the type

$$w = W\ \exp\{i[k(l_1x + l_2y) - \omega t]\}$$

$$\psi_x = \Psi_x\ \exp\{i[k(l_1x + l_2y) - \omega t]\} \tag{10}$$

$$\psi_y = \Psi_y \ \exp\{i[k(l_1 x + l_2 y) - \omega t]\}$$

where k is the wave number, l_1 and l_2 are the direction cosines of the wave vector in the x and y directions, respectively, ω is the circular frequency, and W, Ψ_x and Ψ_y are the amplitudes of the plane harmonic waves. Substituting equation (10) into equation (9), the determinant of this resulting set of equations gives the characteristic equation for antisymmetric Lamb modes. For symmetric quasi-isotropic laminates, in addition to $B_{ij} = 0$ and $R = 0$, we have $A_{16} = A_{26} = A_{45} = 0$ and $D_{16} = D_{26}$. The characteristic equation for antisymmetric Lamb modes is

$$\begin{vmatrix} \begin{matrix} D_{11}k^2 l_1^2 + 2D_{16}k^2 l_1 l_2 \\ + D_{66}k^2 l_2^2 + A_{55} - I\omega^2 \end{matrix} & D_{16}k^2 + (D_{12} + D_{66})k^2 l_1 l_2 & iA_{55}kl_1 \\ D_{16}k^2 + (D_{12} + D_{66})k^2 l_1 l_2 & \begin{matrix} D_{66}k^2 l_1^2 + 2D_{16}k^2 l_1 l_2 \\ + D_{22}k^2 l_2^2 + A_{44} - I\omega^2 \end{matrix} & iA_{44}kl_2 \\ iA_{55}kl_1 & iA_{44}kl_2 & \begin{matrix} - A_{55}k^2 l_1^2 - A_{44}k^2 l_2^2 \\ + \bar{\rho}\omega^2 \end{matrix} \end{vmatrix} = 0 \quad (11)$$

If $l_1 = 1$ and $l_2 = 0$ (i.e., waves propagating in the x direction), equation (11) gives

$$\begin{aligned} &(D_{11}k^2 + A_{55} - I\omega^2)(D_{66}k^2 + A_{44} - I\omega^2)(A_{55}k^2 - \bar{\rho}\omega^2) \\ &\quad - (D_{16}k^2)^2(A_{55}k^2 - \bar{\rho}\omega^2) - (A_{55}k)^2(D_{66}k^2 + A_{44} - I\omega^2) = 0 \end{aligned} \quad (12)$$

If $l_1 = 0$ and $l_2 = 1$, the characteristic equation is

$$(D_{22}k^2 + A_{44} - I\omega^2)(D_{66}k^2 + A_{55} - I\omega^2)(A_{44}k^2 - \bar{\rho}\omega^2) \\ - (D_{16}k^2)^2(A_{44}k^2 - \bar{\rho}\omega^2) - (A_{44}k)^2(D_{66}k^2 + A_{55} - I\omega^2) = 0 \tag{13}$$

For symmetric cross-ply laminates, if $l_1 = 1$ and $l_2 = 0$, we obtain

$$(D_{11}k^2 + A_{55} - I\omega^2)(A_{55}k^2 - \bar{\rho}\omega^2) - A_{55}^2k^2 = 0 \tag{14}$$

and if $l_1 = 0$ and $l_2 = 1$, we have

$$(D_{22}k^2 + A_{44} - I\omega^2)(A_{44}k^2 - \bar{\rho}\omega^2) - A_{44}^2k^2 = 0 \tag{15}$$

In each situation, the characteristic equation has more than one root. However, only one of these roots approaches zero circular frequency as the wave number approaches zero, and this is the root corresponding to the lowest antisymmetric mode. It is apparent that the phase velocity ω/k of the antisymmetric Lamb modes is dispersive since it is a function of the wave number. Equations (12-15) are the dispersion relations for antisymmetric Lamb waves traveling in symmetric quasi-isotropic and symmetric cross-ply laminates. A similar approach has been investigated by Sun and Tan [17]. However, shear correction factors are not included in their model. The relation for wave propagation at an angle with respect to the x direction can be obtained in a similar fashion.

3.2 Exact Solutions for Transversely Isotropic Plates

Lamb [13] analyzed the problem of wave propagation in isotropic plates using potentials and arrived at the well-known Rayleigh-Lamb relation. Habeger, Mann, and

Baum [15] studied Lamb wave propagation in machine-made paper. In their study, the paper was assumed as a homogeneous orthotropic plate. A relatively straightfoward approach for transversely isotropic plates suggested by Green [33] is presented here.

Considering an infinite plate of transversely isotropic material with the boundary surfaces at $z = \pm h/2$ and the axis of symmetry in the x direction, the stress-strain relations for the transversely isotropic material are given by

$$\begin{bmatrix} \sigma_x \\ \sigma_y \\ \sigma_z \\ \tau_{yz} \\ \tau_{xz} \\ \tau_{xy} \end{bmatrix} = \begin{bmatrix} C_{11} & C_{12} & C_{12} & 0 & 0 & 0 \\ C_{12} & C_{22} & C_{23} & 0 & 0 & 0 \\ C_{12} & C_{23} & C_{22} & 0 & 0 & 0 \\ 0 & 0 & 0 & (C_{22} - C_{23})/2 & 0 & 0 \\ 0 & 0 & 0 & 0 & C_{55} & 0 \\ 0 & 0 & 0 & 0 & 0 & C_{55} \end{bmatrix} \begin{bmatrix} \varepsilon_x \\ \varepsilon_y \\ \varepsilon_z \\ \gamma_{yz} \\ \gamma_{xz} \\ \gamma_{xy} \end{bmatrix} \tag{16}$$

Also, the strain-displacement relations are

$$\varepsilon_x = \frac{\partial u}{\partial x}$$

$$\varepsilon_y = \frac{\partial v}{\partial y}$$

$$\varepsilon_z = \frac{\partial w}{\partial z}$$

$$\gamma_{xy} = \frac{\partial u}{\partial y} + \frac{\partial v}{\partial x} \tag{17}$$

$$\gamma_{xz} = \frac{\partial u}{\partial z} + \frac{\partial w}{\partial x}$$

$$\gamma_{yz} = \frac{\partial v}{\partial z} + \frac{\partial w}{\partial y}$$

where u, v, w are the displacement components in the x, y and z directions, respectively. Our problem is to solve the equations of motion

$$\frac{\partial \sigma_x}{\partial x} + \frac{\partial \tau_{xy}}{\partial y} + \frac{\partial \tau_{xz}}{\partial z} = \rho \frac{\partial^2 u}{\partial t^2}$$

$$\frac{\partial \tau_{xy}}{\partial x} + \frac{\partial \sigma_y}{\partial y} + \frac{\partial \tau_{yz}}{\partial z} = \rho \frac{\partial^2 v}{\partial t^2} \qquad (18)$$

$$\frac{\partial \tau_{xz}}{\partial x} + \frac{\partial \tau_{yz}}{\partial y} + \frac{\partial \sigma_z}{\partial z} = \rho \frac{\partial^2 w}{\partial t^2}$$

subjected to the traction-free boundary conditions

$$\sigma_z = \tau_{xz} = \tau_{yz} = 0 \qquad \text{at} \qquad z = \pm h/2 \qquad (19)$$

Green [33] suggested that for waves propagating in the plane of the plate in a direction making an angle with the x axis the displacements have the form

$$u = U(z)\ \sin[k(l_1 x + l_2 y) - \omega t]$$

$$v = V(z)\ \sin[k(l_1 x + l_2 y) - \omega t] \qquad (20)$$

$$w = W(z)\ \cos[k(l_1 x + l_2 y) - \omega t]$$

For antisymmetric Lamb waves, the lateral displacement w must be an even function of z, while the in-plane displacements u and v must be odd in z. Substituting equation (20) into equations (17) and (16), we obtain

$$\sigma_x = [C_{11}kl_1U + C_{12}(kl_2V + \frac{\partial W}{\partial z})]\cos[k(l_1x + l_2y) - \omega t]$$

$$\sigma_y = [C_{12}kl_1U + C_{22}kl_2V + C_{23}\frac{\partial W}{\partial z}]\cos[k(l_1x + l_2y) - \omega t]$$

$$\sigma_z = [C_{12}kl_1U + C_{23}kl_2V + C_{22}\frac{\partial W}{\partial z}]\cos[k(l_1x + l_2y) - \omega t] \qquad (21)$$

$$\tau_{xy} = C_{55}k(l_2U + l_1V)\cos[k(l_1x + l_2y) - \omega t]$$

$$\tau_{xz} = C_{55}(\frac{\partial U}{\partial z} - kl_1W)\sin[k(l_1x + l_2y) - \omega t]$$

$$\tau_{yz} = [(C_{22} - C_{23})/2](\frac{\partial V}{\partial z} - kl_2W)\sin[k(l_1x + l_2y) - \omega t]$$

Introducing the stresses (21) into equation (18), the equations of motion become

$$\begin{aligned}
&- C_{55}\frac{\partial^2 U}{\partial z^2} + k^2(C_{11}l_1^2 + C_{55}l_2^2 - \rho v^2)U + (C_{12} + C_{55})k^2l_1l_2V \\
&\qquad + (C_{12} + C_{55})kl_1\frac{\partial W}{\partial z} = 0 \\[2ex]
&(C_{12} + C_{55})k^2l_1l_2U - [(C_{22} - C_{23})/2]\frac{\partial^2 V}{\partial z^2} + k^2(C_{55}l_1^2 + C_{22}l_2^2 - \rho v^2)V \\
&\qquad + \{[(C_{22} - C_{23})/2] + C_{23}\}kl_2\frac{\partial W}{\partial z} = 0 \qquad (22) \\[2ex]
&(C_{12} + C_{55})kl_1\frac{\partial U}{\partial z} + \{[(C_{22} - C_{23})/2] + C_{23}\}kl_2\frac{\partial V}{\partial z} + C_{22}\frac{\partial^2 W}{\partial z^2} \\
&\qquad - k^2(C_{55}l_1^2 + [(C_{22} - C_{23})/2]l_2^2 - \rho v^2)W = 0
\end{aligned}$$

where v, which is equivalent to ω/k, is the phase velocity. From the solution of the isotropic plate problem [13,34-37] and the requirements that $W(z)$ must be even, and

$U(z)$ and $V(z)$ must be odd for antisymmetric Lamb waves propagating in the plate, we let

$$U = A \sinh kpz$$

$$V = B \sinh kpz \tag{23}$$

$$W = C \cosh kpz$$

Substituting these expressions into the equations of motion (22) and setting the determinant of the resulting system of three homogeneous equations to zero for nontrivial solutions, the outcome takes the form

$$\begin{vmatrix} C_{11}l_1^2 + C_{55}l_2^2 - C_{55}p^2 - \rho v^2 & (C_{12} + C_{55})l_1 l_2 & (C_{12} + C_{55})pl_1 \\ (C_{12} + C_{55})l_1 l_2 & C_{55}l_1^2 + C_{22}l_2^2 - [(C_{22} - C_{23})/2]p^2 - \rho v^2 & \{[(C_{22} - C_{23})/2] + C_{23}\}pl_2 \\ (C_{12} + C_{55})pl_1 & \{[(C_{22} - C_{23})/2] + C_{23}\}pl_2 & - C_{55}l_1^2 - [(C_{22} - C_{23})/2]l_2^2 + C_{22}p^2 + \rho v^2 \end{vmatrix} = 0 \tag{24}$$

If $l_1 = 1$ and $l_2 = 0$ (i.e. waves propagating in the x direction), V is uncoupled from U and W in equation (22). Therefore, equation (24) gives

$$(C_{11} - C_{55}p^2 - \rho v^2)(C_{55} - C_{22}p^2 - \rho v^2) + (C_{12} + C_{55})^2 p^2 = 0 \tag{25}$$

for nontrivial solutions of U and W. Consequently, the general solution of equation (22) is

$$U = A_1 \sinh kp_1 z + A_2 \sinh kp_2 z$$

$$W = -\frac{(C_{11} - C_{55}p_1^2 - \rho v^2)}{(C_{12} + C_{55})} \frac{A_1}{p_1} \cosh kp_1 z - \frac{(C_{11} - C_{55}p_2^2 - \rho v^2)}{(C_{12} + C_{55})} \frac{A_2}{p_2} \cosh kp_2 z \tag{26}$$

where A_1 and A_2 are arbitrary constants, and p_1^2 and p_2^2 are the roots of equation (25). With the boundary conditions (19), we arrive at

$$\begin{aligned} &A_1[C_{12}(C_{12} + C_{55}) - C_{22}(C_{11} - C_{55}p_1^2 - \rho v^2)] \sinh kp_1(h/2) \\ &\qquad + A_2[C_{12}(C_{12} + C_{55}) - C_{22}(C_{11} - C_{55}p_2^2 - \rho v^2)] \sinh kp_2(h/2) = 0 \\ &A_1(C_{11} + C_{12}p_1^2 - \rho v^2)\frac{\cosh kp_1(h/2)}{p_1} + A_2(C_{11} + C_{12}p_2^2 - \rho v^2)\frac{\cosh kp_2(h/2)}{p_2} = 0 \end{aligned} \tag{27}$$

Finally, in order to have a solution to our problem, equation (27) yields the condition

$$\begin{aligned} &(C_{11} + C_{12}p_2^2 - \rho v^2)[C_{12}(C_{12} + C_{55}) - C_{22}(C_{11} - C_{55}p_1^2 - \rho v^2)]p_1 \tanh kp_1(h/2) \\ &- (C_{11} + C_{12}p_1^2 - \rho v^2)[C_{12}(C_{12} + C_{55}) - C_{22}(C_{11} - C_{55}p_2^2 - \rho v^2)]p_2 \tanh kp_2(h/2) = 0 \end{aligned} \tag{28}$$

Thus, the phase velocity v is a function of kh and equation (28) is the dispersion relation for antisymmetric Lamb waves traveling in the x direction. Similarly, the condition for antisymmetric Lamb waves traveling in the y direction of an infinite transversely isotropic plate having traction-free boundary surfaces is

$$[(C_{22} - C_{23}) - \rho v^2]^2 \tanh kp_1(h/2) = (C_{22} - C_{23})^2 p_1 p_2 \tanh kp_2(h/2) \tag{29}$$

with p_1^2 and p_2^2 satisfying the equation

$$(C_{22} - C_{22}p^2 - \rho v^2)\{[(C_{22} - C_{23})/2] - [(C_{22} - C_{23})/2]p^2 - \rho v^2\} = 0 \tag{30}$$

3.3 Experimental Procedure

A simple method [18,25,26], similar in configuration to the acousto-ultrasonic technique [23,24], was used to measure Lamb wave phase velocities. Low frequency Lamb waves, usually in the range of 10 kHz to 1 MHz, were generated. Figure 4 is a schematic diagram of the experimental setup. A piezoelectric transducer was excited by gated sinewaves. Lamb waves were generated at a transmitter and detected by a receiving transducer. The position of the receiver was advanced a known distance relative to the transmitter in the direction of the phase velocity, and the change in time for a particular phase point of the wave was noted on a digital oscilloscope. From this information, the phase velocity was calculated. Then, the wave number was obtained from the phase velocity for the frequency at which the measurement was made. Finally, the frequency f and the wave number k were each multiplied by the thickness of the plate h, and fh was plotted against kh with data obtained at different frequencies. For any fh, the phase velocity is related to the ratio fh/kh, while the group velocity is related to the slope of the tangent to the curve. Since the curve is normalized with respect to the thickness of the composite plate, the curve is independent of the ply thickness. Typical input and output signals are shown in Figure 5. Figure 6 indicates the change in time for a particular phase point as the receiver changes its position. In this figure, the effect of the difference between phase velocity and group velocity is apparent.

During the measurement, as the frequency of the excitation signal was increased, it was observed that there existed a frequency at which an abrupt change in the phase velocity took place. This occurred due to a change in modes from the lowest anti-

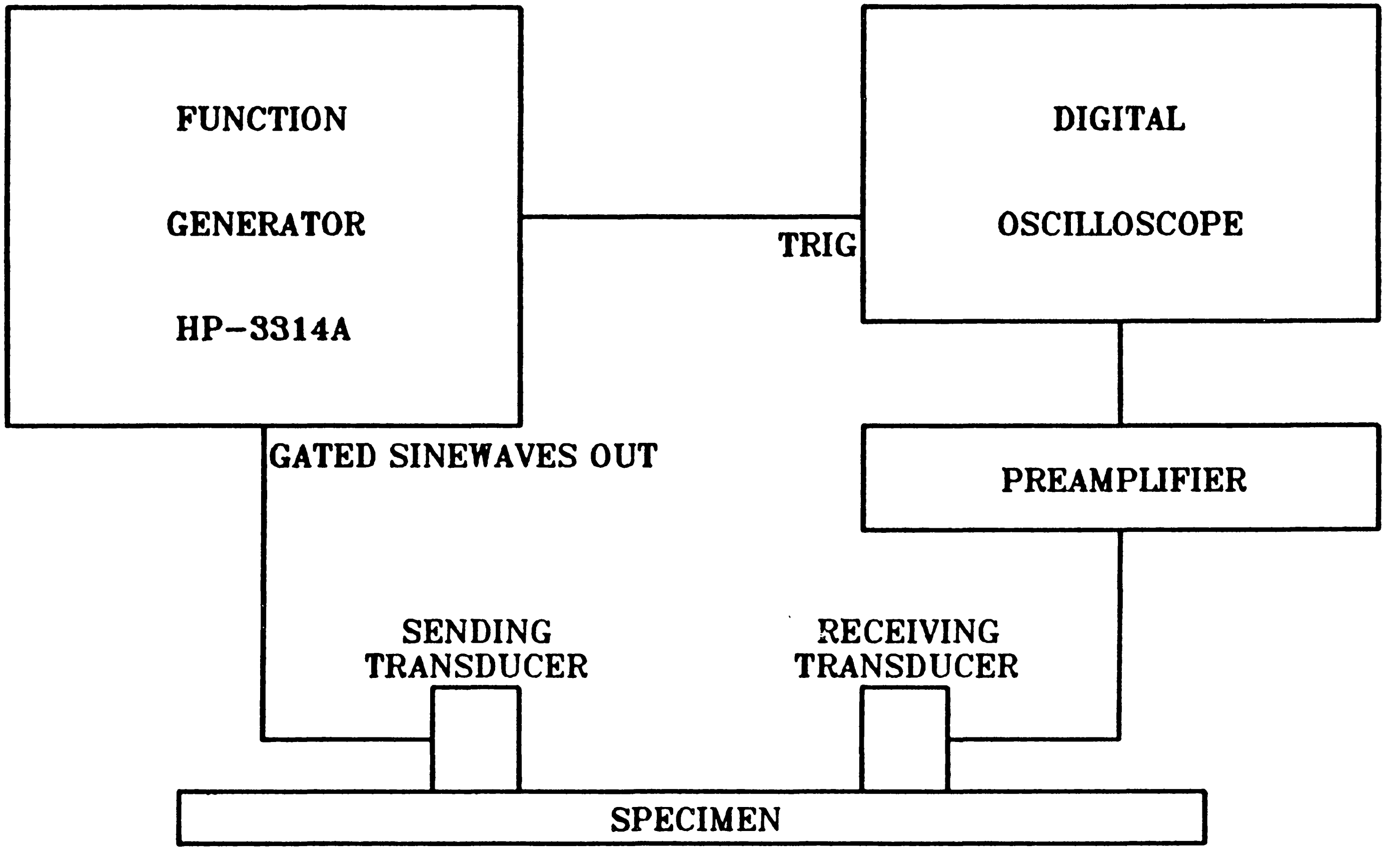

Figure 4. Schematic diagram of the experimental setup for Lamb wave phase velocity measurements.

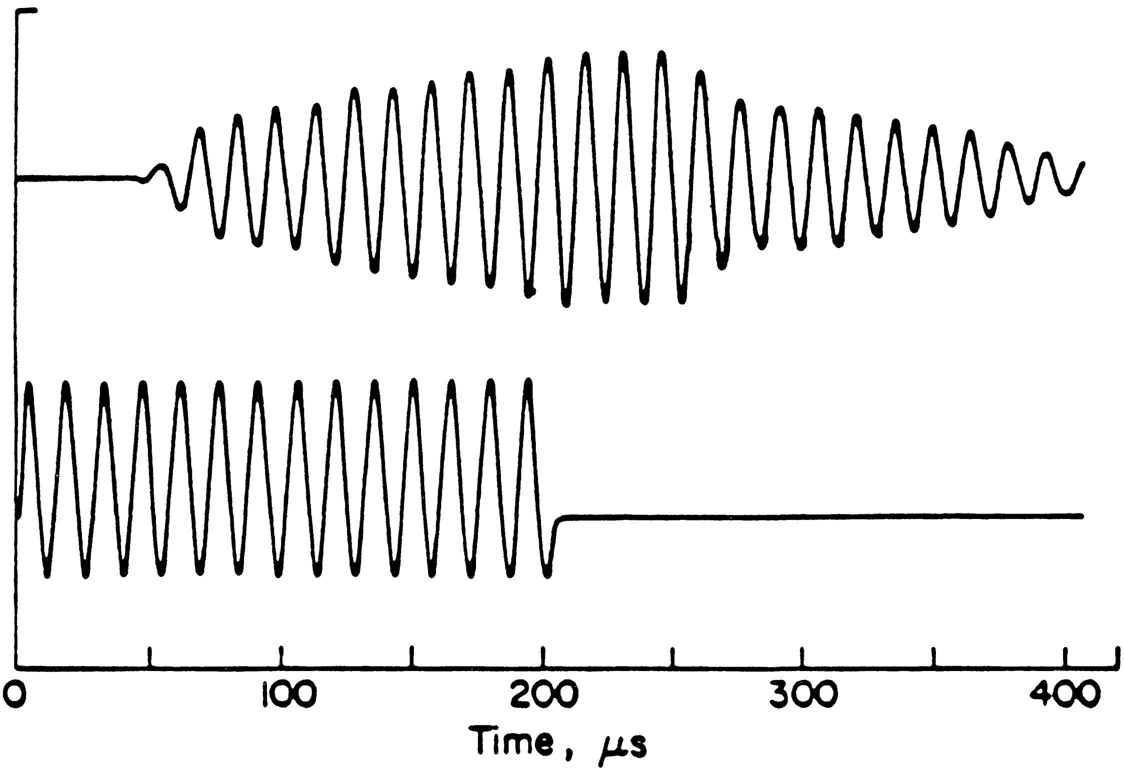

Figure 5. Typical input and output signals.

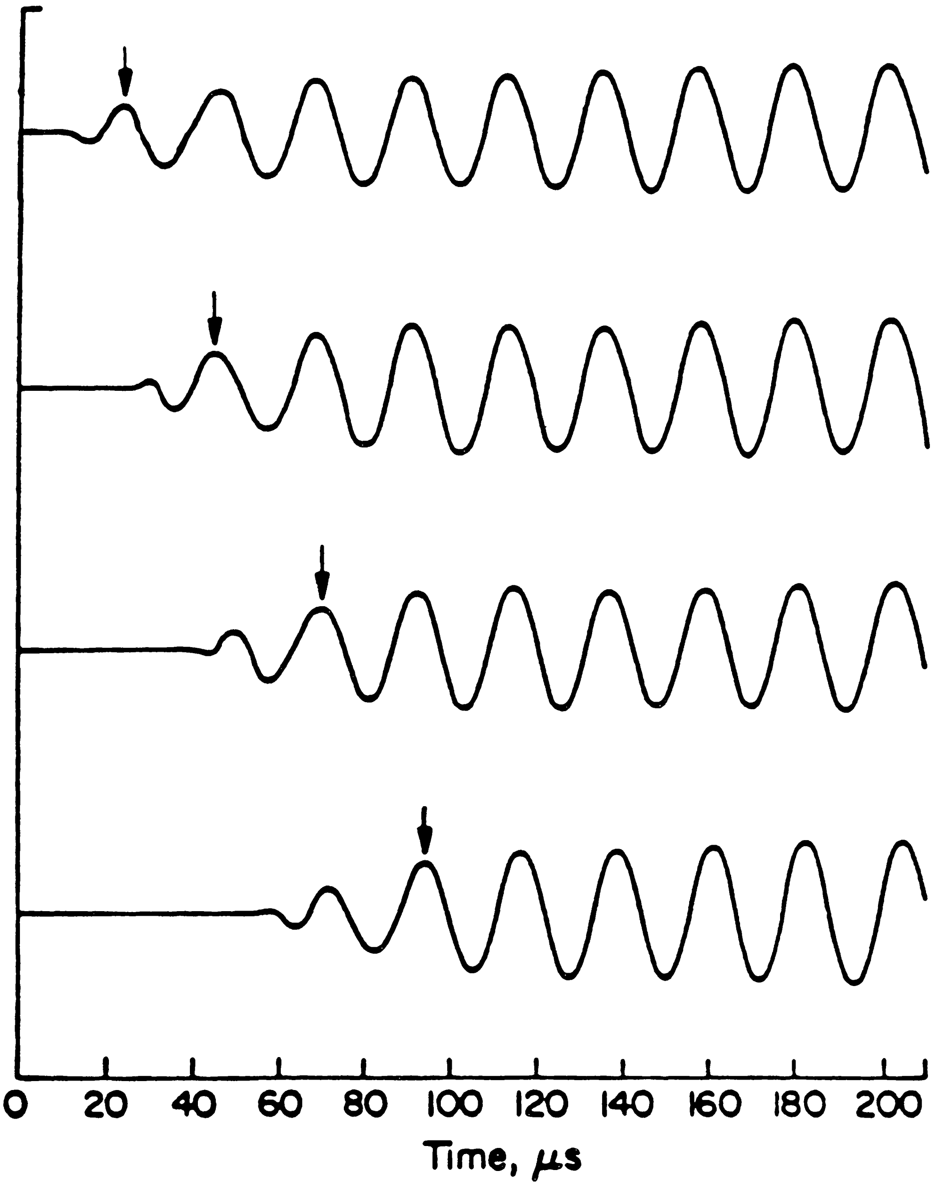

Figure 6. Change in arrival time for a phase point.

symmetric Lamb mode at low frequencies to the lowest symmetric Lamb mode at higher frequencies. This transitional frequency is related to the center frequency of the sending transducer and the thickness of the plate. The transitional frequency can be lowered by using a low center frequency sending transducer or a thick plate.

Owing to the anisotropy of composite laminates, there are energy flux deviations in Lamb waves as in the case of body waves propagating in composite materials [38,39]. Thus, one must take into account this phenomenon of energy flux deviation while measuring Lamb wave phase velocities in composite laminates [16,28].

3.4 Results and Discussion

The previous sections have provided the exact solutions for antisymmetric Lamb waves propagating in transversely isotropic plates and the approximate solutions obtained by shear deformation theory for antisymmetric Lamb waves traveling in composite laminates. An AS-4(Gr)/Pr 288 $[0]_8$ graphite/epoxy composite plate supplied by General Electric can be treated approximately as a transversely isotropic plate with the axis of symmetry in the fiber direction. The lamina properties of AS-4(Gr)/Pr 288 graphite/epoxy are $E_{11} = 18.30 \times 10^6$ lb/in^2 (1.26×10^2 GPa) , $E_{22} = 1.30 \times 10^6$ lb/in^2 (8.96 GPa) , $G_{12} = G_{13} = 0.66 \times 10^6$ lb/in^2 (4.55 GPa) , $G_{23} = 0.56 \times 10^6$ lb/in^2 (3.86 GPa) , $\nu_{12} = \nu_{13} = 0.32$ and $\rho = 1.487 \times 10^{-4}$ lbf-sec^2/in^4 (1,589 kg/m^3) . Since the data obtained using the experimental approach outlined above are mostly on the lowest antisymmetric and the lowest symmetric branches of the Lamb wave dispersion curves, the two lowest branches are used to characterize composite laminates. All the experimental data were taken with wavelengths which are much larger than the thickness of the plate; thus the interfaces between plies can be neglected.

In Figure 7, the lowest branch of the dispersion curves from the exact solution (ES) for antisymmetric Lamb waves traveling in the fiber direction of the $[0]_8$ graphite/epoxy laminate is plotted along with the numerical solutions obtained by the shear deformation theory with different values of shear correction factor k_5^2 for the $[0]_8$ laminate. The exact solution (ES) for waves propagating perpendicular to the fiber direction and the shear deformation theory solutions with different values of k_4^2 for the $[0]_8$ laminate are shown in Figure 8. Judging from these two figures, it is acceptable to assume that $k_4^2 = k_5^2 = 5/6$ for this unidirectional graphite/epoxy composite laminate in the low frequency, long wavelength range. Experimental data are compared with the results obtained by the classical plate theory (CPT) [18,25,26], the exact solution (ES) and the shear deformation theory (SDT) with $k_4^2 = k_5^2 = 5/6$ in Figures 9 and 10 for waves propagating parallel and perpendicular to the fiber direction, respectively.

In order to apply the shear deformation theory to multi-ply laminated composite plates, the selection of appropriate values for the shear correction factors is necessary. Chow [40] and Whitney [41], using a procedure which follows the approach of Reissner [42] for homogeneous isotropic plates, have determined k_4^2 and k_5^2 for cross-ply laminates under static cylindrical bending. In general, k_4^2 and k_5^2 have different values for symmetric laminates. The same procedure can be applied to symmetric quasi-isotropic laminates. It has been shown that the factors calculated from static cylindrical bending yield a good approximation to the exact solution for cross-ply laminates subjected to static or buckling loading [41,43]. Using this approach, the values of the

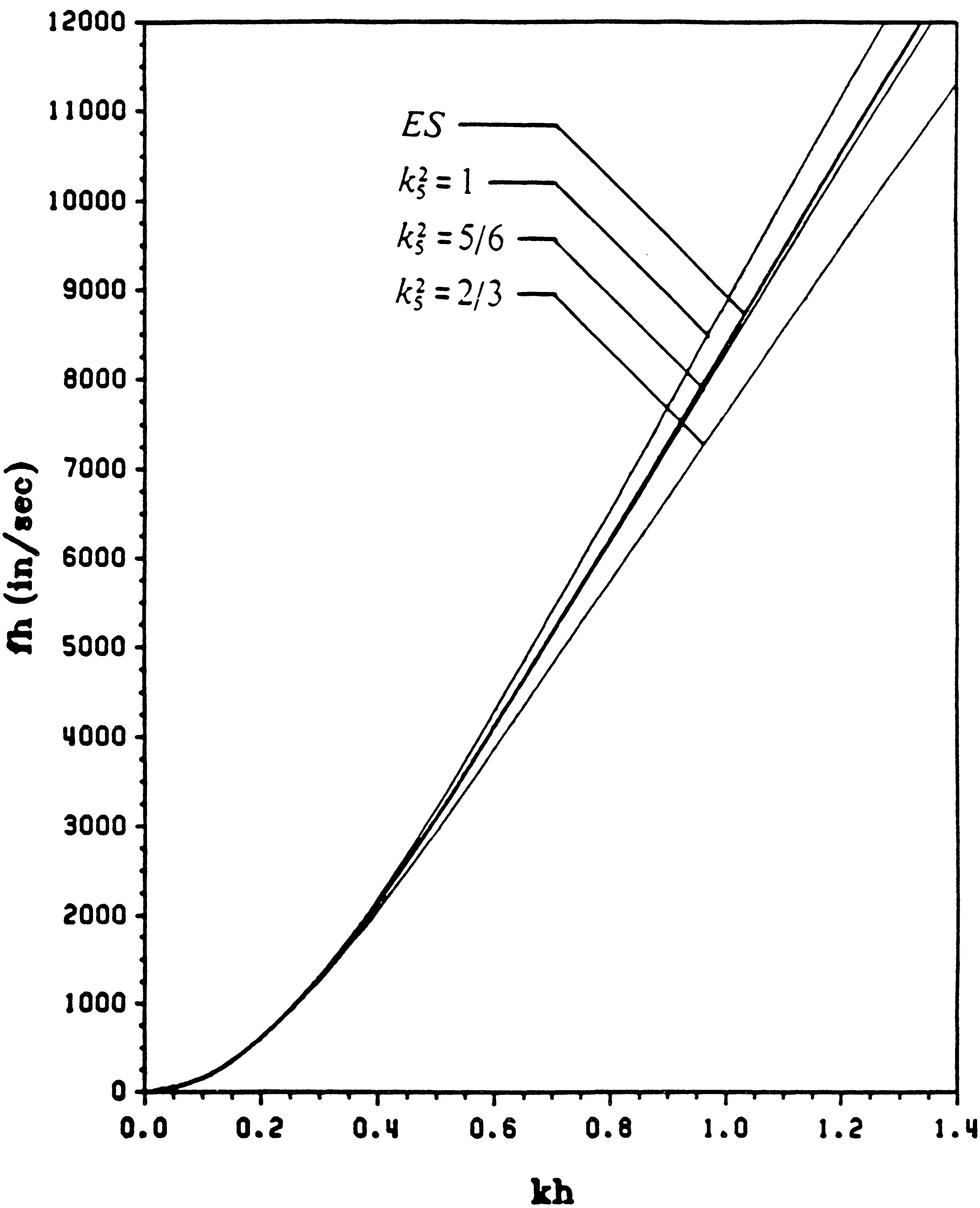

Figure 7. Theoretical dispersion curves for antisymmetric Lamb waves propagating along the fiber direction of a $[0]_8$ graphite/epoxy laminate. (1 in/sec = 0.0254 m/sec)

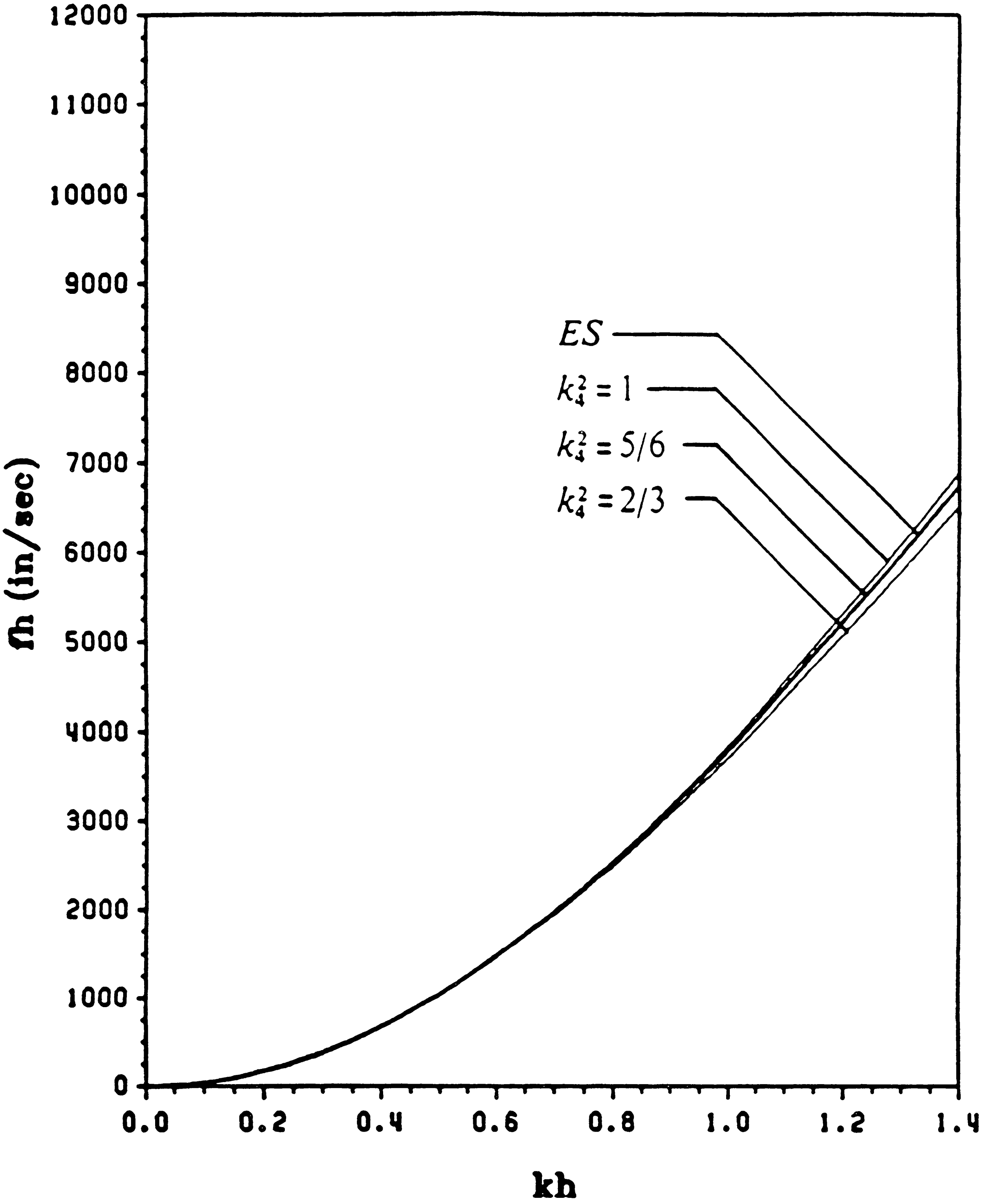

Figure 8. Theoretical dispersion curves for antisymmetric Lamb waves propagating perpendicular to the fiber direction of a $[0]_8$ graphite/epoxy laminate. (1 in/sec = 0.0254 m/sec)

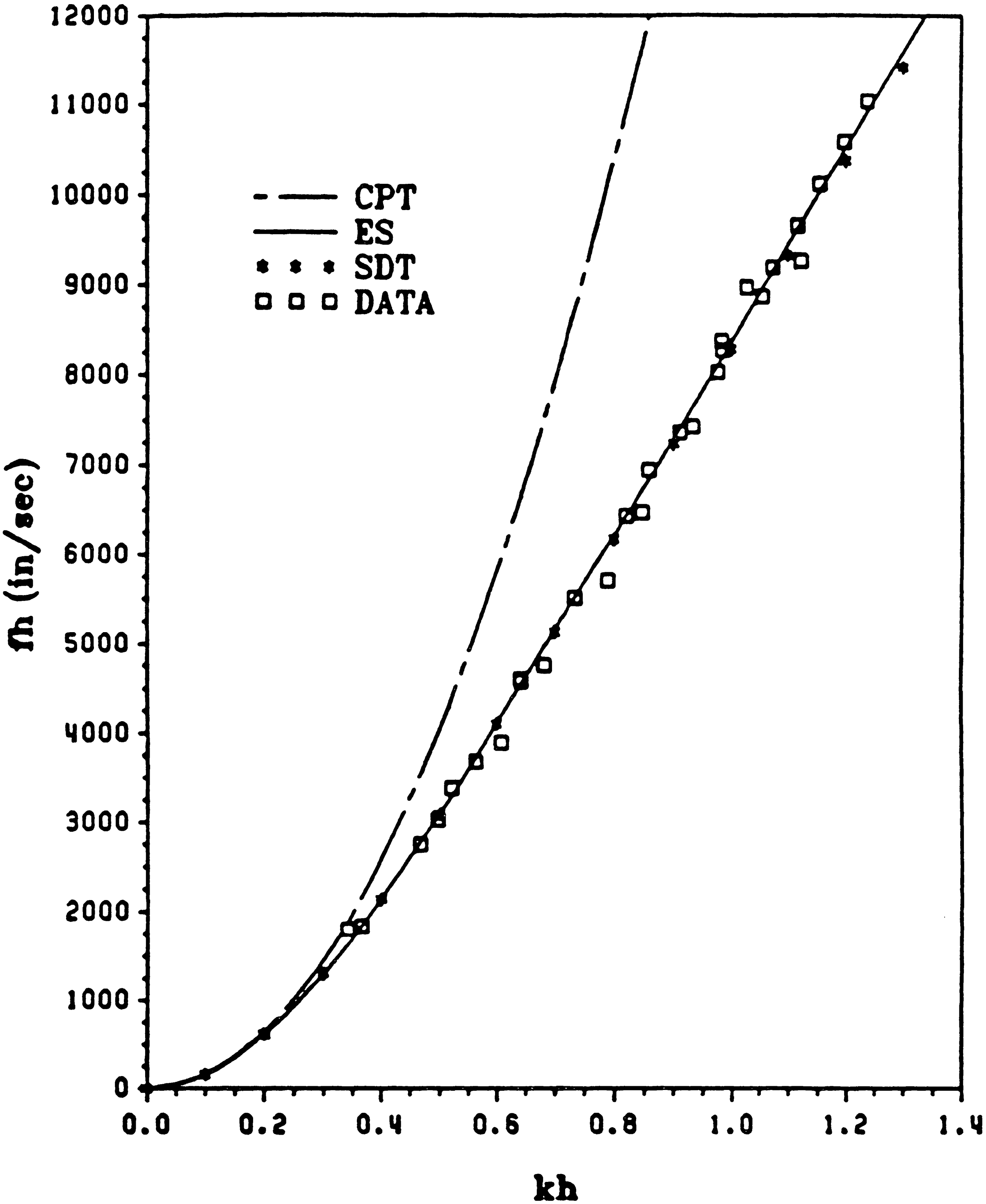

Figure 9. Dispersion curves for antisymmetric Lamb waves propagating along the fiber direction of a $[0]_8$ graphite/epoxy laminate. (1 in/sec = 0.0254 m/sec)

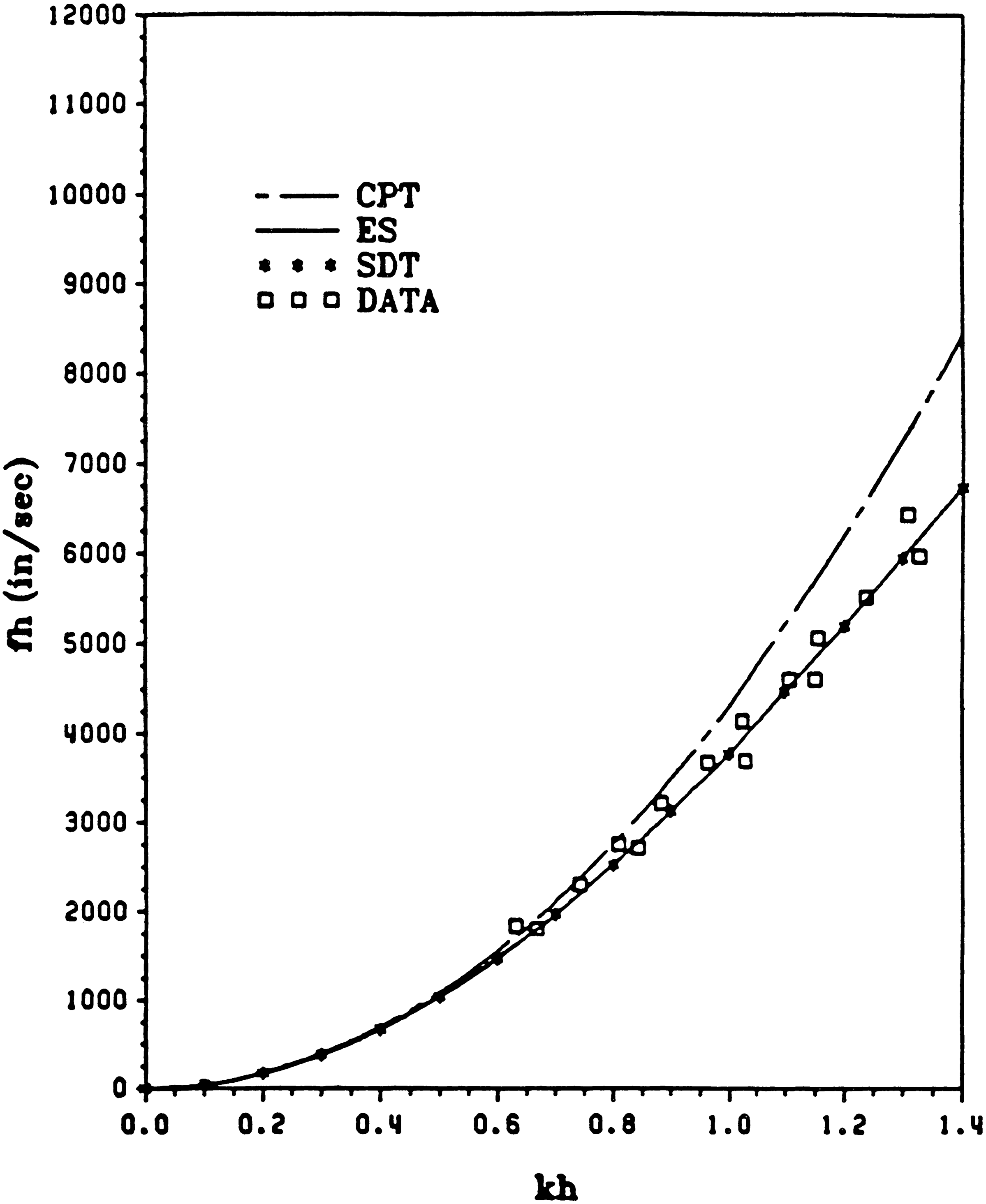

Figure 10. Dispersion curves for antisymmetric Lamb waves propagating perpendicular to the fiber direction of a $[0]_8$ graphite/epoxy laminate. (1 in/sec = 0.0254 m/sec)

shear correction factors are found to be 5/6 for homogeneous isotropic plates. This is the classic value determined by Reissner [42]. For unidirectional composite laminates, the same value of 5/6 is obtained for the shear correction factors. Thus, this is consistent with our results for antisymmetric Lamb waves propagating in the $[0]_8$ composite plate. For a $[0/90]_{2s}$ cross-ply graphite/epoxy laminate, we obtain $k_5^2 = 0.8607$ and $k_4^2 = 0.7133$, and for a $[0/45/90/-45]_s$ quasi-isotropic laminate, we have $k_5^2 = 0.8837$ and $k_4^2 = 0.6462$ (see Appendix B).

The results of the classical plate theory (CPT) [18,25,26] and the shear deformation theory (SDT) with the shear correction factors calculated from static cylindrical bending together with the experimental data are plotted in Figures 11 and 12 for the $[0/90]_{2s}$ cross-ply laminate. Figures 13 and 14 show the results for the symmetric quasi-isotropic laminate. For these laminates the experimental data for antisymmetric Lamb waves traveling in the x direction (i.e., the 0° direction) are slightly below our predicted curves obtained by the shear deformation theory, while the data for the y direction are slightly above our predicted dispersion curves. Figure 15 shows the results for a 6061-T4 aluminum plate. It is suspected that the shear correction factors for static cylindrical bending are not precisely applicable to the cross-ply and quasi-isotropic laminates and cause the predicted dispersion curves to deviate from the data since the transverse shear strain distributions in these cases are more complicated. Using a higher order shear deformation theory may improve the results. With regard to the validity of cylindrical bending in our experimental method, there is excellent correlation between the experimental data and the theoretical results in the aluminum plate and the unidirectional laminate, which suggests that the cylindrical bending assumption is appropriate for these cases. Other factors, such as the combined effects of residual thermal stresses and the bimodulus character of composite materials, may

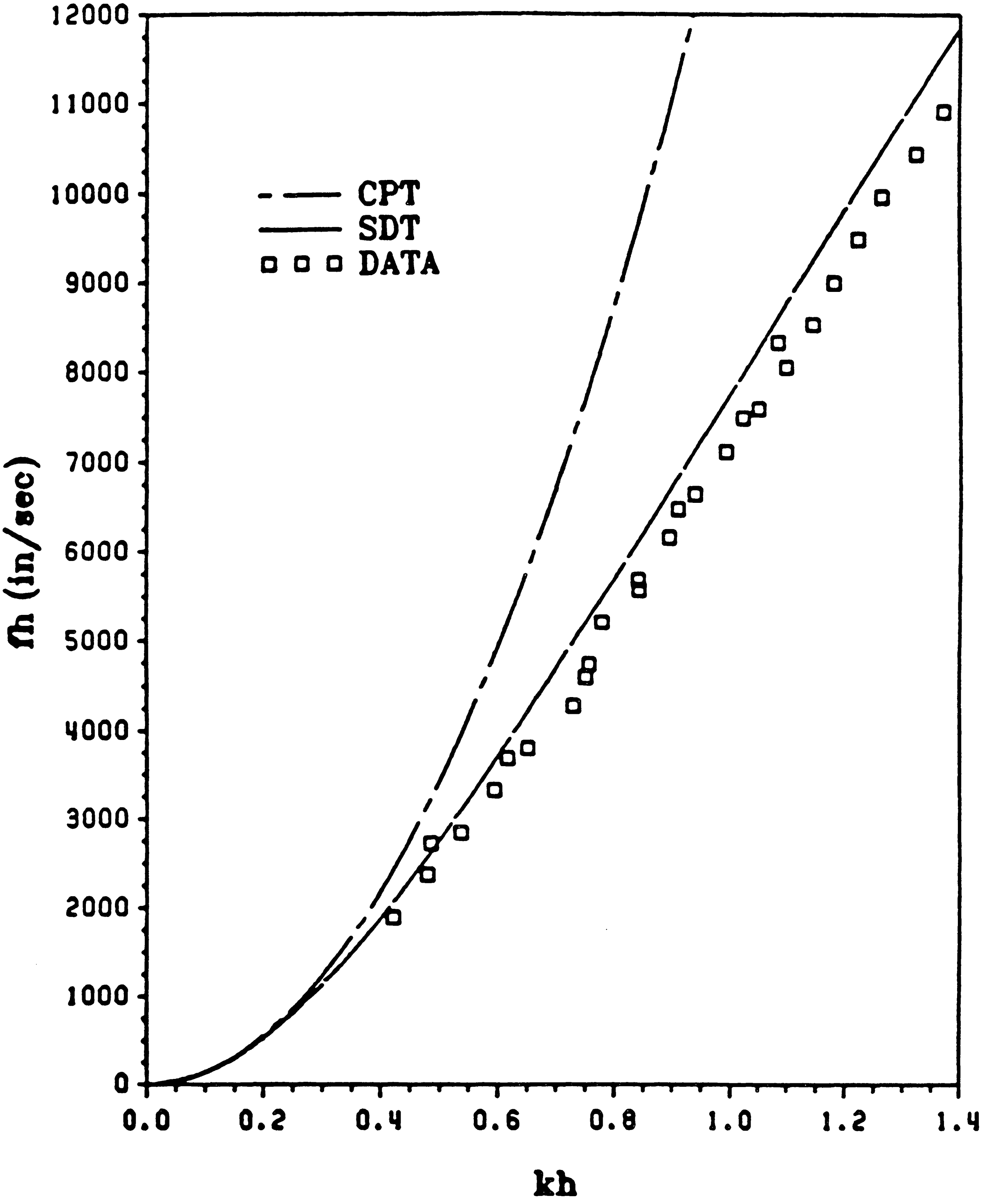

Figure 11. Dispersion curves for antisymmetric Lamb waves propagating along the x axis of a $[0/90]_{2s}$ graphite/epoxy laminate. (1 in/sec = 0.0254 m/sec)

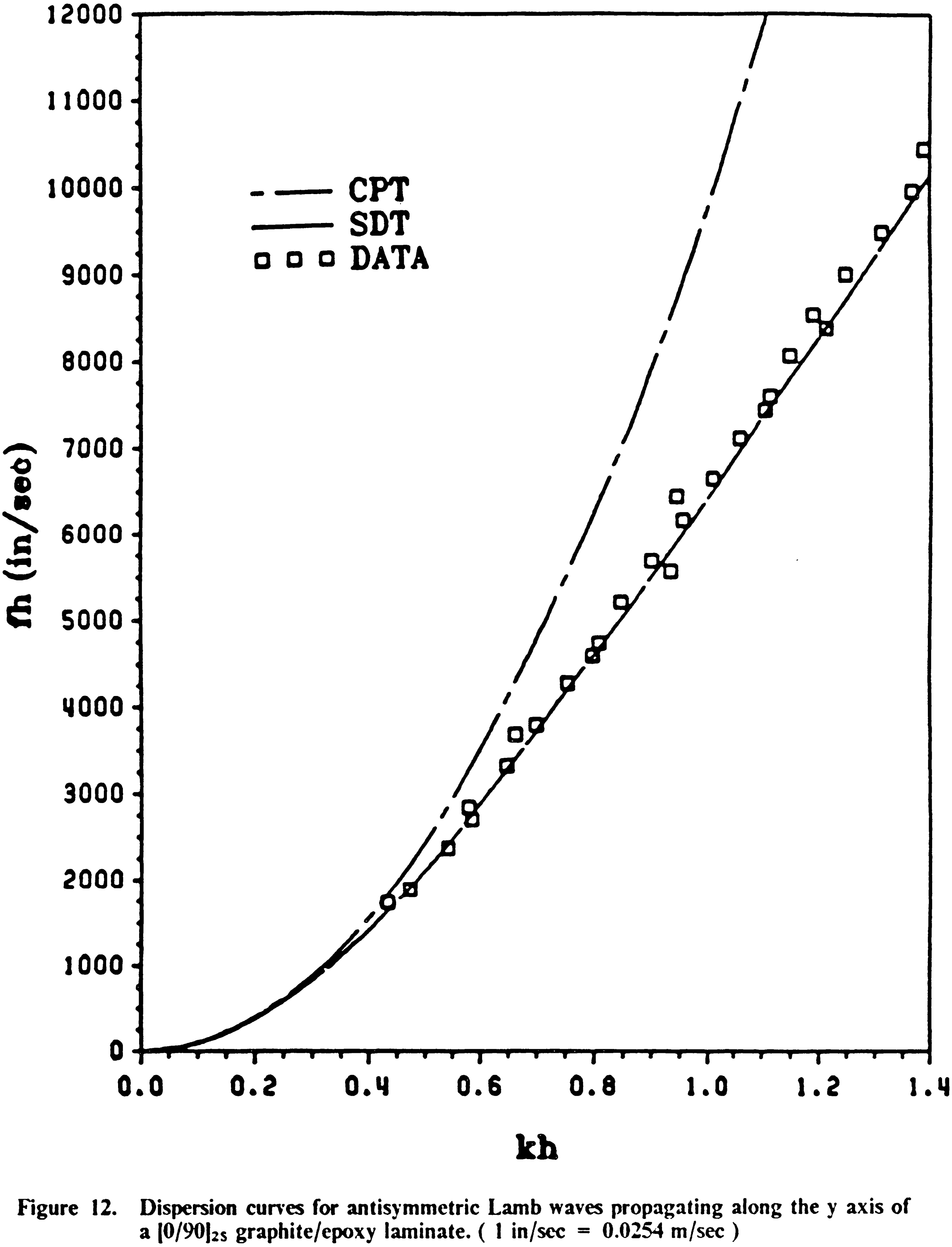

Figure 12. Dispersion curves for antisymmetric Lamb waves propagating along the y axis of a $[0/90]_{2S}$ graphite/epoxy laminate. (1 in/sec = 0.0254 m/sec)

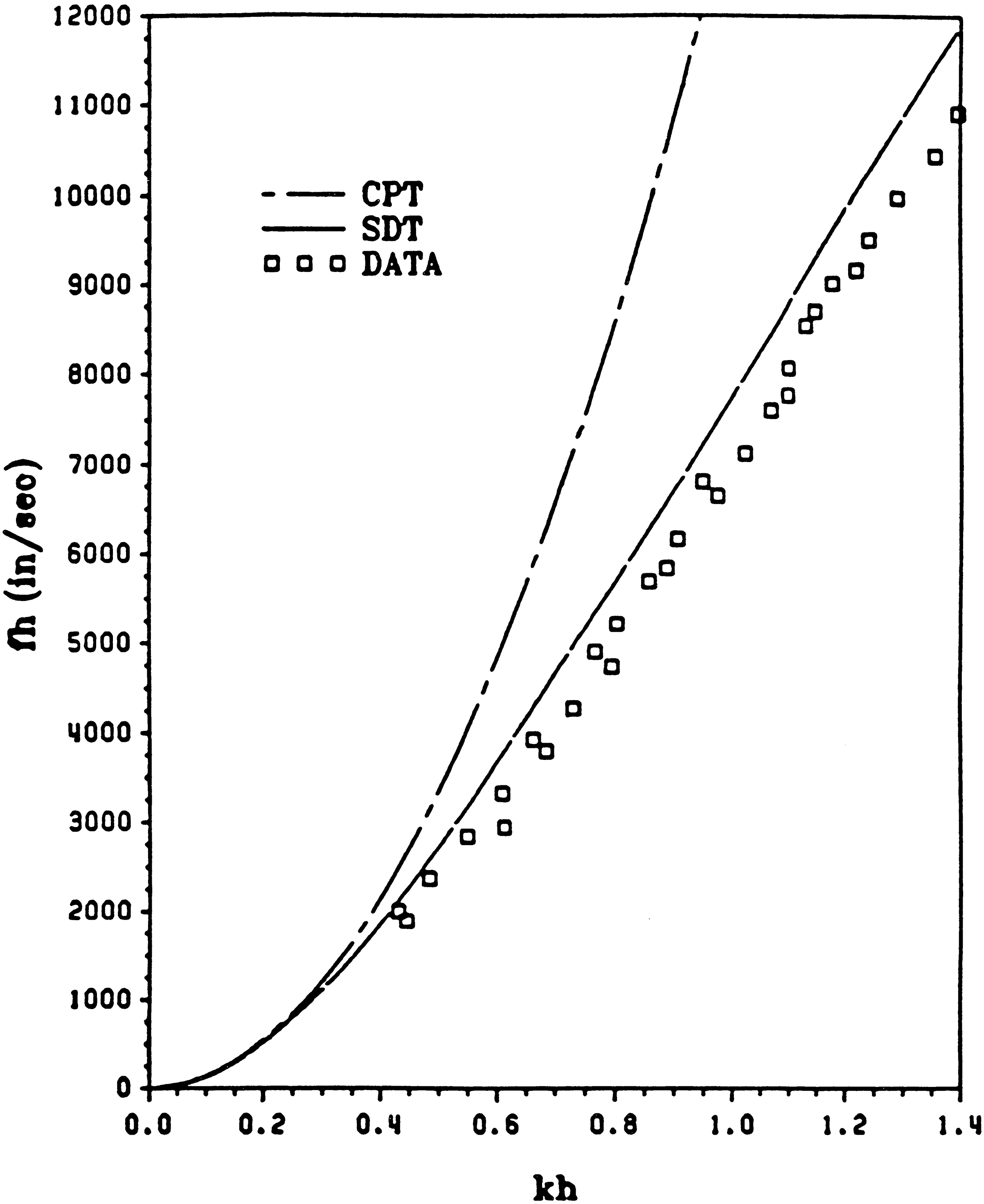

Figure 13. Dispersion curves for antisymmetric Lamb waves propagating along the x axis of a $[0/45/90/-45]_s$ graphite/epoxy laminate. (1 in/sec = 0.0254 m/sec)

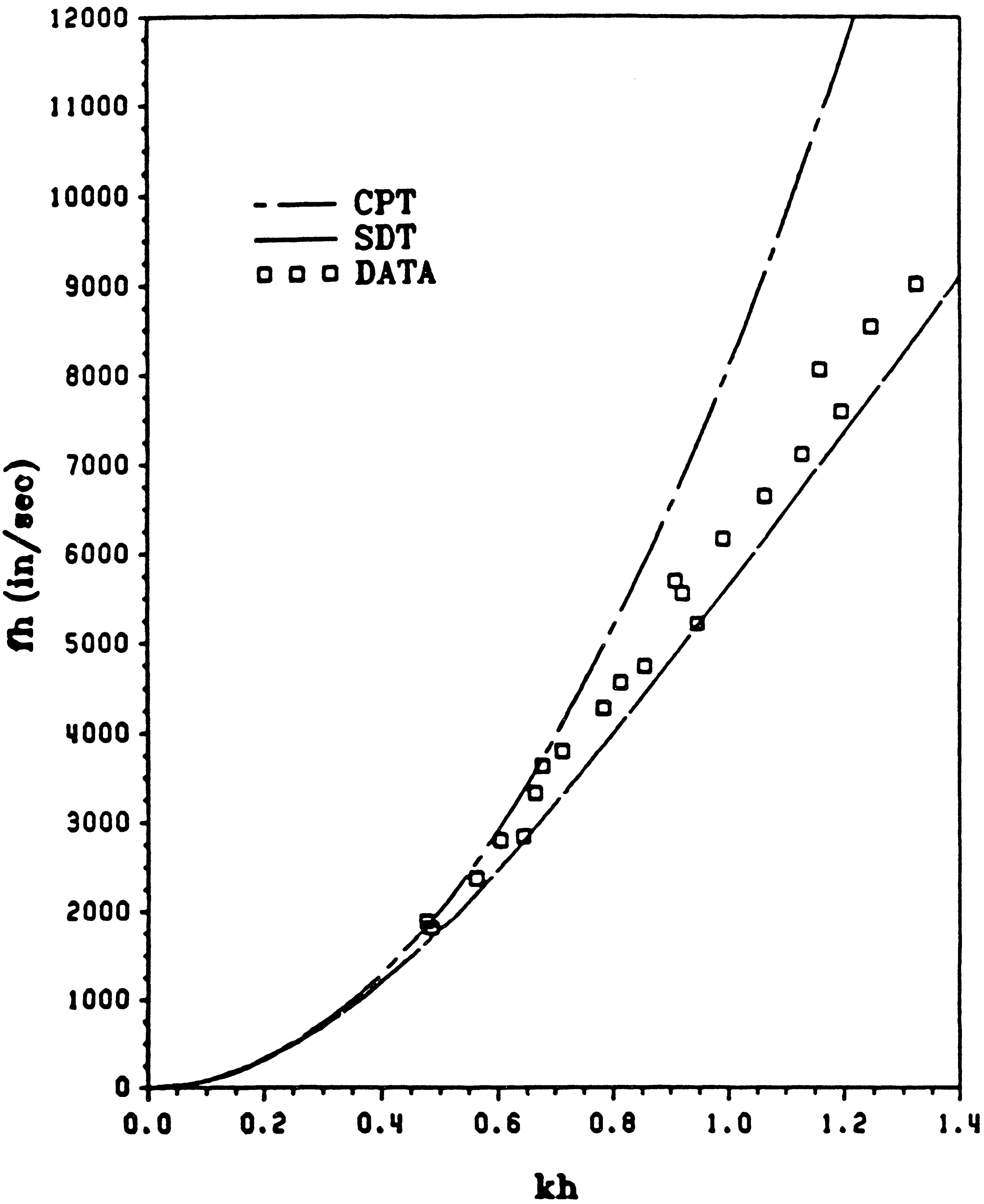

Figure 14. Dispersion curves for antisymmetric Lamb waves propagating along the y axis of a $[0/45/90/-45]_s$ graphite/epoxy laminate. (1 in/sec = 0.0254 m/sec)

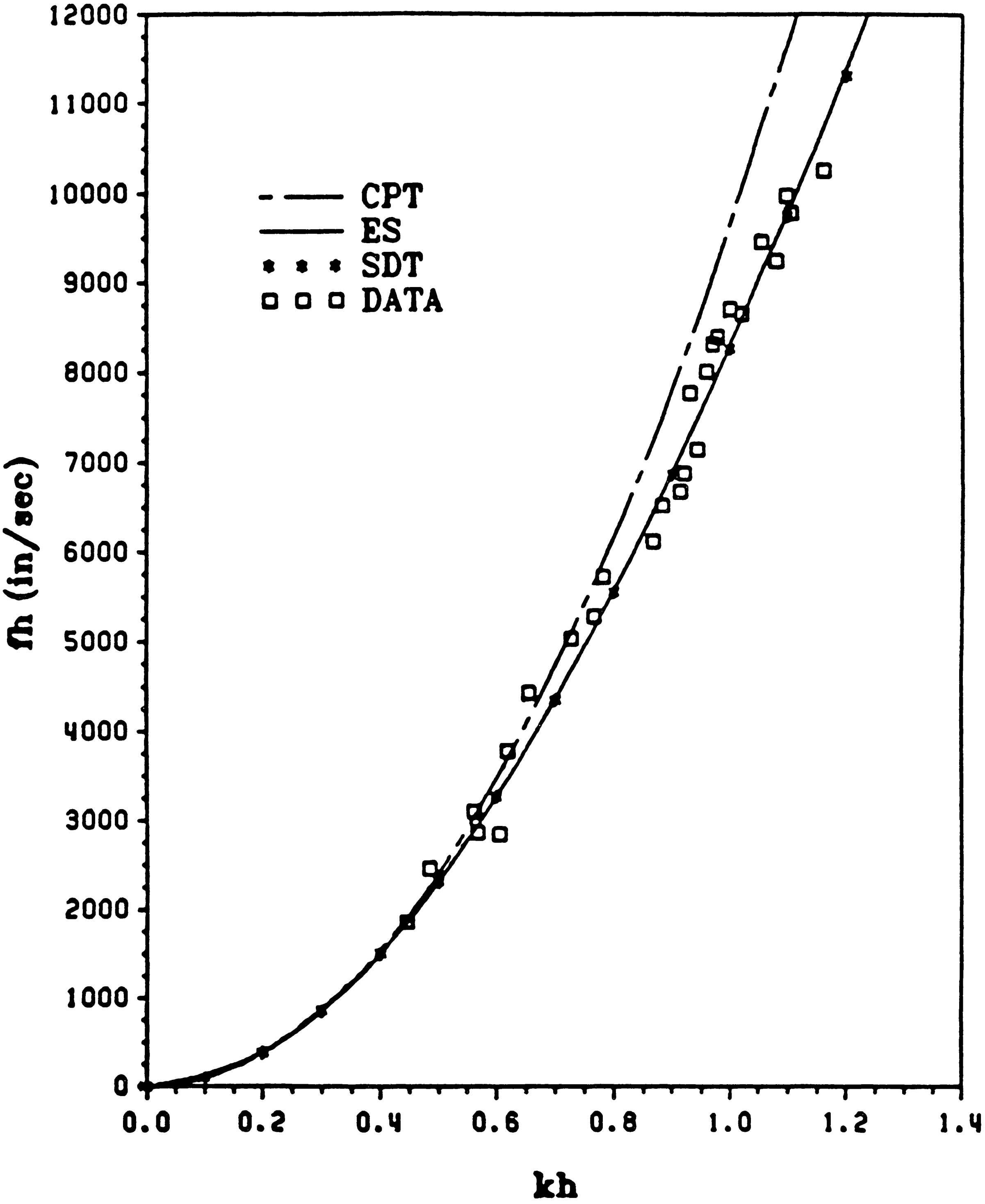

Figure 15. Dispersion curves for antisymmetric Lamb wave propagation in a 6061-T4 aluminum plate. (1 in/sec = 0.0254 m/sec)

also contribute to the deviation between the theory and the data. Further investigation is needed to identify the source of the deviation.

It is apparent that the effects of transverse shear deformation and rotary inertia are significant in laminated composite plates while the effects are relatively small in aluminum plates. For thin aluminum plates, in addition to the small thickness h , if the region of interest is in the low frequency, long wavelength range, the classical plate theory can be used instead of the shear deformation theory without much discrepancies. Surprisingly, in Figure 10, the inclusion of transverse shear deformation and rotary inertia in the plate theory has relatively little effect on the results of waves propagating perpendicular to the fiber direction in the $[0]_8$ graphite/epoxy composite plate. That is, there is little deviation from classical plate theory. This is a special situation for laminated composite plates because the ratio between the transverse shear modulus and the Young's modulus perpendicular to the fiber direction for this transversely isotropic plate and the similar ratio for the isotropic aluminum plate are of the same order of magnitude. Thus, the effects of transverse shear deformation and rotary inertia are relatively small as in the case of the aluminum plate in Figure 15.

Finally, the characteristic equation derived from the shear deformation theory has three distinct roots, however, only one approaches zero circular frequency as the wave number approaches zero. This is the root corresponding to the lowest antisymmetric branch of the dispersion curves for Lamb waves and is the one shown in the figures. In the case of waves propagating parallel or perpendicular to the fiber direction in the $[0]_8$ graphite/epoxy composite plate, this lowest root from the shear deformation theory with a static bending shear correction factor begins to deviate from the lowest branch of the exact solution as kh becomes large. A different value of shear correction factor is needed to correct the deviation. In addition, one of the two remaining roots correctly predicts the cut-off frequency of the second lowest antisymmetric branch. Similar results have been reported by Mindlin [32,34] for isotropic plates. The displacement field in the Yang, Norris and Stavsky approach is a one term approximation of the power series expansion of the displacement field in the elasticity approach for transversely isotropic plates. Using a higher order approximation may improve the results for transversely isotropic plates as well as the results for composite laminates.

IV. SYMMETRIC LAMB MODES

4.1 *Shear Deformation Theory*

The equations obtained from the shear deformation theory for the symmetric Lamb modes are not as complicated as the equations for the antisymmetric Lamb modes. Using the same procedure as in the antisymmetric Lamb modes and equation (8), the relations governing the lowest symmetric Lamb modes for symmetric cross-ply and quasi-isotropic laminates are:

$$A_{11}k^2 - \overline{\rho}\omega^2 = 0, \tag{31}$$

for wave propagation in the x direction, and,

$$A_{22}k^2 - \overline{\rho}\omega^2 = 0, \tag{32}$$

for wave propagation in the y direction, where k is the wave number, ω is the circular frequency, A_{ij} are the extensional stiffnesses, $\overline{\rho} = \int_{-h/2}^{h/2} \rho dz$ and ρ is the mass density.

It is easy to reconize that the equation is linear; this implies that the wave is nondispersive.

4.2 Exact Solutions for Transversely Isotropic Plates

The approach used to obtain the exact solutions for the antisymmetric Lamb modes in the transversely isotropic plates can be used to obtain the exact solutions for the symmetric Lamb modes. In this case, the lateral displacement w must be an odd function of z, while the in-plane displacements u and v must be even in z.

The equations for the symmetric Lamb modes are similar to the equations for the antisymmetric Lamb modes. The governing equation for the symmetric Lamb modes in the x direction is

$$\begin{aligned}&(C_{11} + C_{12}p_2^2 - \rho v^2)[C_{12}(C_{12} + C_{55}) - C_{22}(C_{11} - C_{55}p_1^2 - \rho v^2)]p_1 \tanh kp_2(h/2) \\ &- (C_{11} + C_{12}p_1^2 - \rho v^2)[C_{12}(C_{12} + C_{55}) - C_{22}(C_{11} - C_{55}p_2^2 - \rho v^2)]p_2 \tanh kp_1(h/2) = 0\end{aligned} \tag{33}$$

with p_1^2 and p_2^2 satisfying the equation

$$(C_{11} - C_{55}p^2 - \rho v^2)(C_{55} - C_{22}p^2 - \rho v^2) + (C_{12} + C_{55})^2 p^2 = 0 \tag{34}$$

which looks almost identical to the equation governing the antisymmetric Lamb modes

$$\begin{aligned}&(C_{11} + C_{12}p_2^2 - \rho v^2)[C_{12}(C_{12} + C_{55}) - C_{22}(C_{11} - C_{55}p_1^2 - \rho v^2)]p_1 \tanh kp_1(h/2) \\ &- (C_{11} + C_{12}p_1^2 - \rho v^2)[C_{12}(C_{12} + C_{55}) - C_{22}(C_{11} - C_{55}p_2^2 - \rho v^2)]p_2 \tanh kp_2(h/2) = 0\end{aligned} \tag{28}$$

with p_1^2 and p_2^2 satisfying the equation

$$(C_{11} - C_{55}p^2 - \rho v^2)(C_{55} - C_{22}p^2 - \rho v^2) + (C_{12} + C_{55})^2 p^2 = 0 \tag{25}$$

V. DISPERSION CURVES OF LAMB WAVES

Now, we have the approximate solutions from the shear deformation theory for both symmetric and antisymmetric Lamb modes in multilayered laminates and the exact solution for transversely isotropic plates. In order to test their validity, the theoretical solutions are compared with experimental data.

5.1 Exact Solutions

Lamb wave dispersion curves and experimental data for Lamb wave propagation parallel and perpendicular to the fiber direction of a unidirectional, AS-4(Gr)/Pr 288, graphite/epoxy composite plate are shown in Figures 16 and 17, respectively. The data obtained using the experimental procedure are mostly on the lowest antisymmetric and the lowest symmetric branches of the Lamb wave dispersion curves, although there is some cross over to higher order modes for the higher frequencies. For

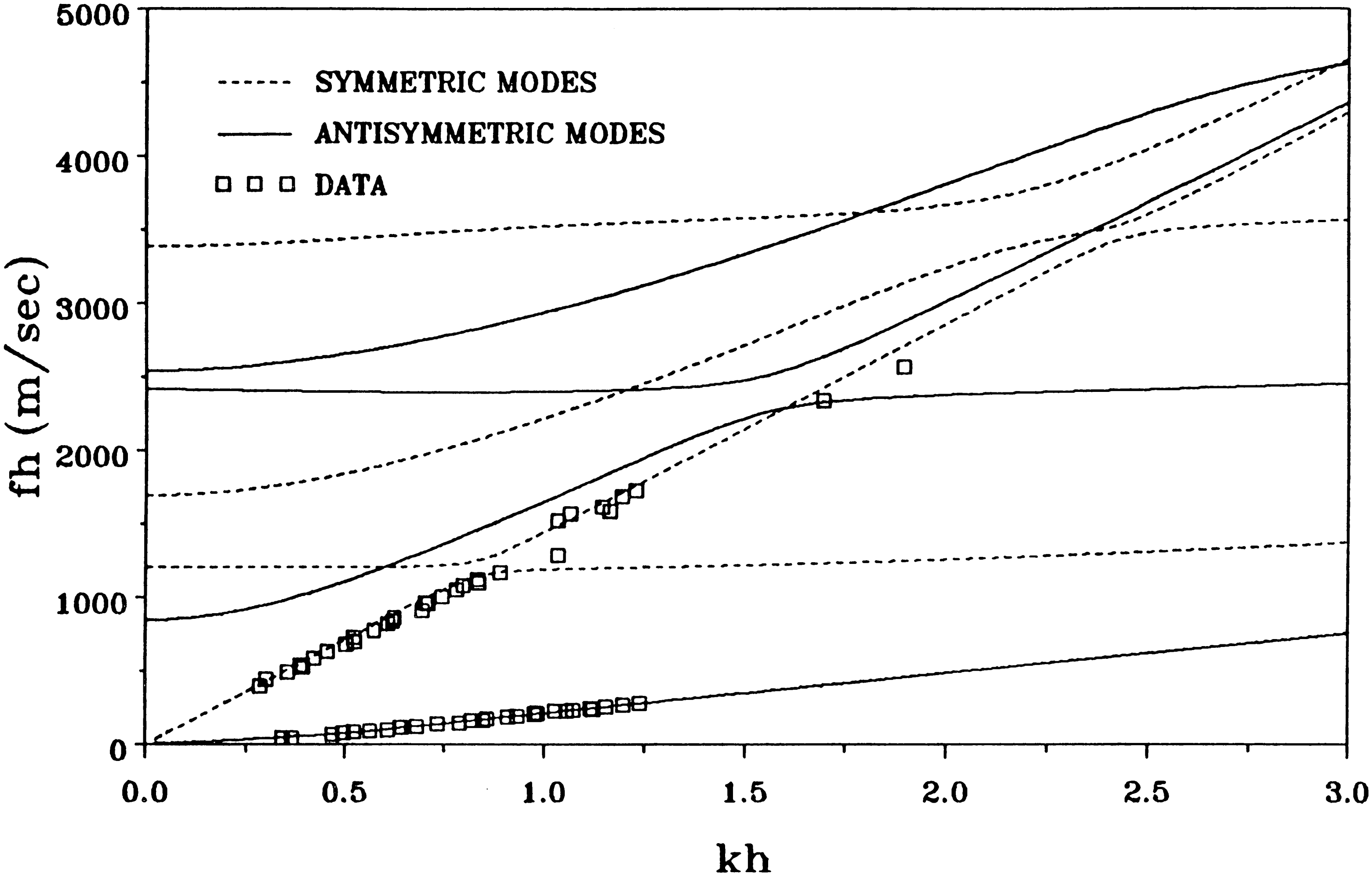

Figure 16. Lamb wave dispersion curves for wave propagation along the fiber direction of a unidirectional laminate.

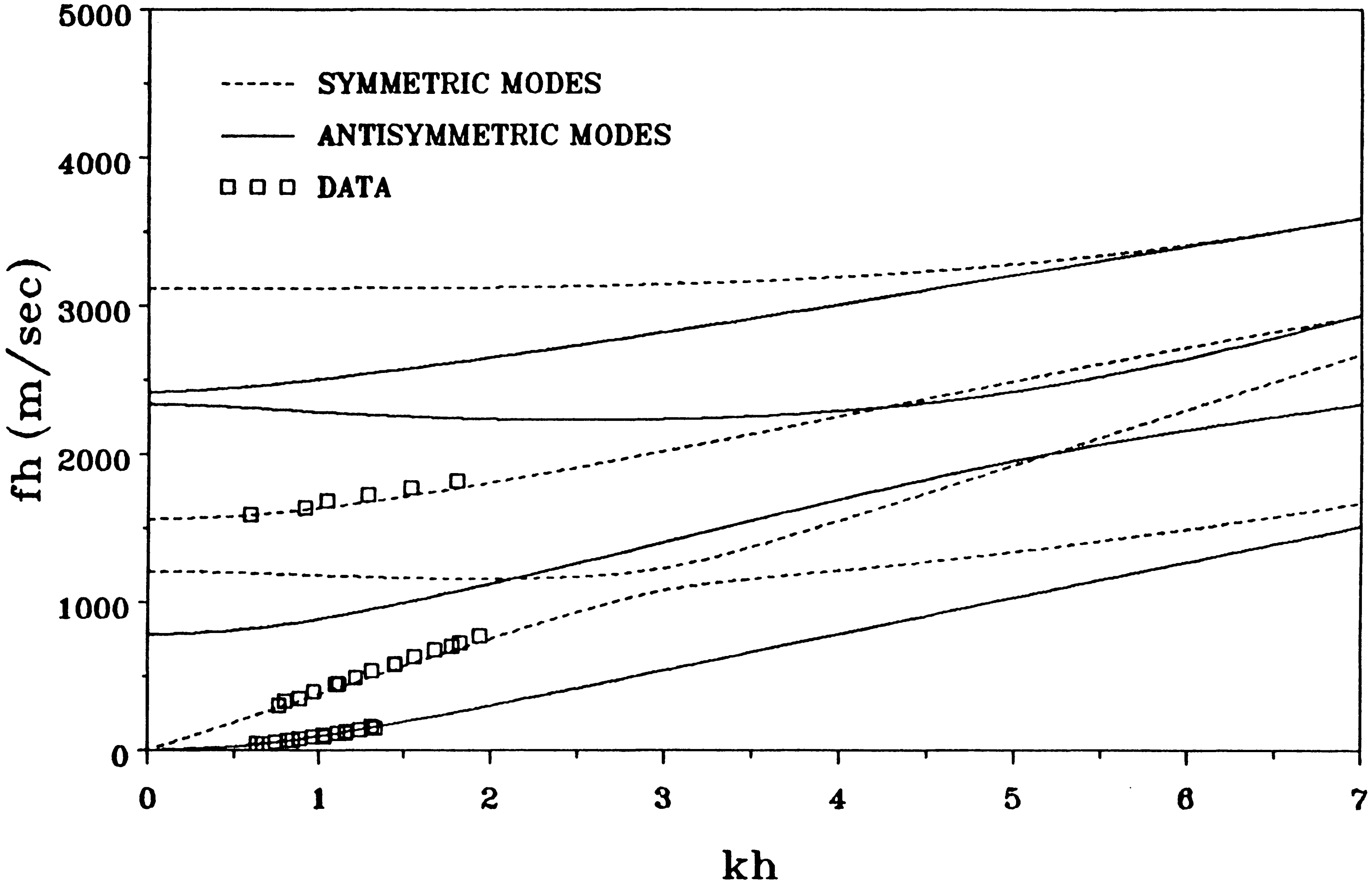

Figure 17. Lamb wave dispersion curves for wave propagation perpendicular to the fiber direction of a unidirectional laminate.

simplicity, we call the Lamb wave dispersion curves for Lamb wave propagation along the fiber direction of the unidirectional laminate the 0° dispersion curves, and the dispersion curves for wave propagation perpendicular to the fiber direction the 90° dispersion curves. The Lamb wave dispersion curves for multilayered composite laminates other than unidirectional laminates are unavailable since the elasticity formulation for Lamb wave propagation in multilayered composite laminates is not explicitly solvable. However, it is reasonable to assume that the dispersion curves for symmetric laminates of AS-4(Gr)/Pr 288, including the dispersion curves for wave propagation at an angle with the fiber direction of the unidirectional laminate, are bounded between the 0° dispersion curves and the 90° dispersion curves, with the 0° dispersion curves as the upper limit and the 90° dispersion curves as the lower limit. Figure 18 shows the regions where the lowest symmetric and antisymmetric modes of an AS-4(Gr)/Pr 288 graphite/epoxy symmetric laminate are most likely located. The regions for the second lowest symmetric and antisymmetric branches are shown in Figures 19 and 20, respectively.

5.2 Approximate Theory

Since the exact solution for multilayered laminates is not available, we turn our attention to our approximate theory, which holds for the low frequency, long wavelength region. Figures 21 and 22 show the results from the shear deformation theory (SDT), the lowest symmetric modes (S_0) and the lowest antisymmetric modes (A_0) for the exact solution from the theory of elasticity and the experimental data for the unidirectional laminate. It is apparent that the SDT dispersion relation is consistent

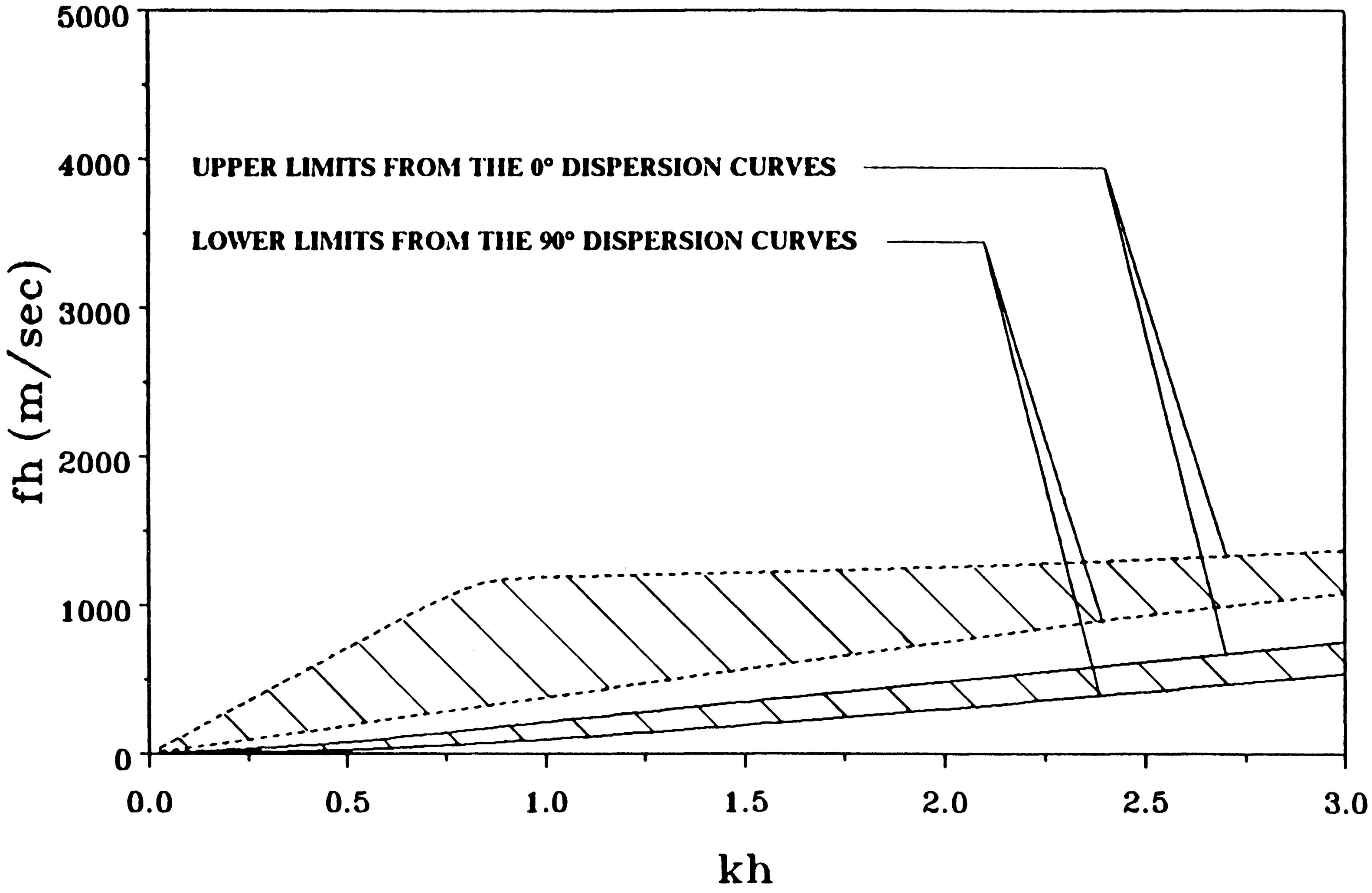

Figure 18. Regions of the lowest Lamb modes for symmetric laminates. Upper region corresponds to symmetric modes and lower region corresponds to antisymmetric modes.

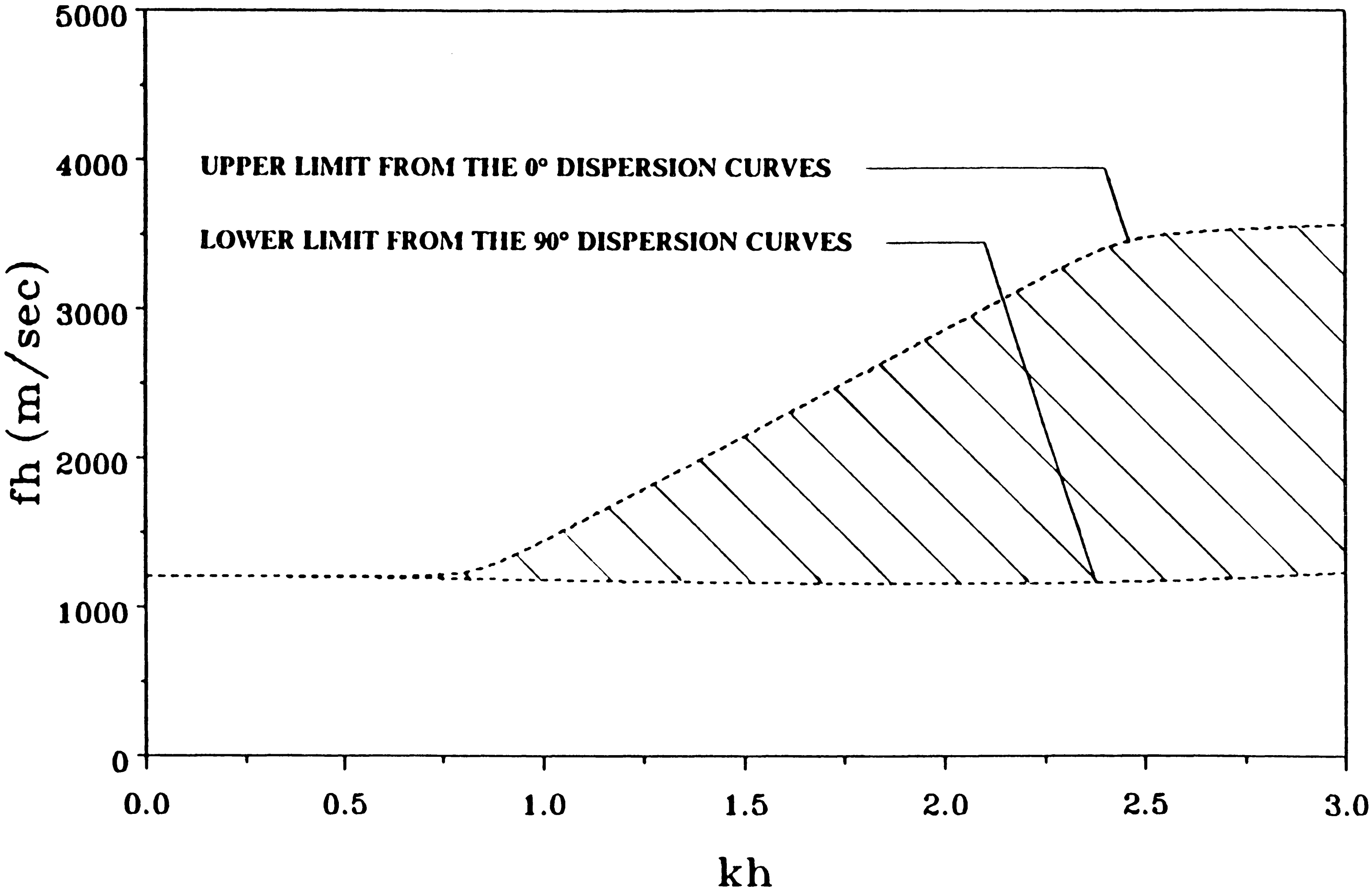

Figure 19. Region of the second lowest symmetric modes for symmetric laminates.

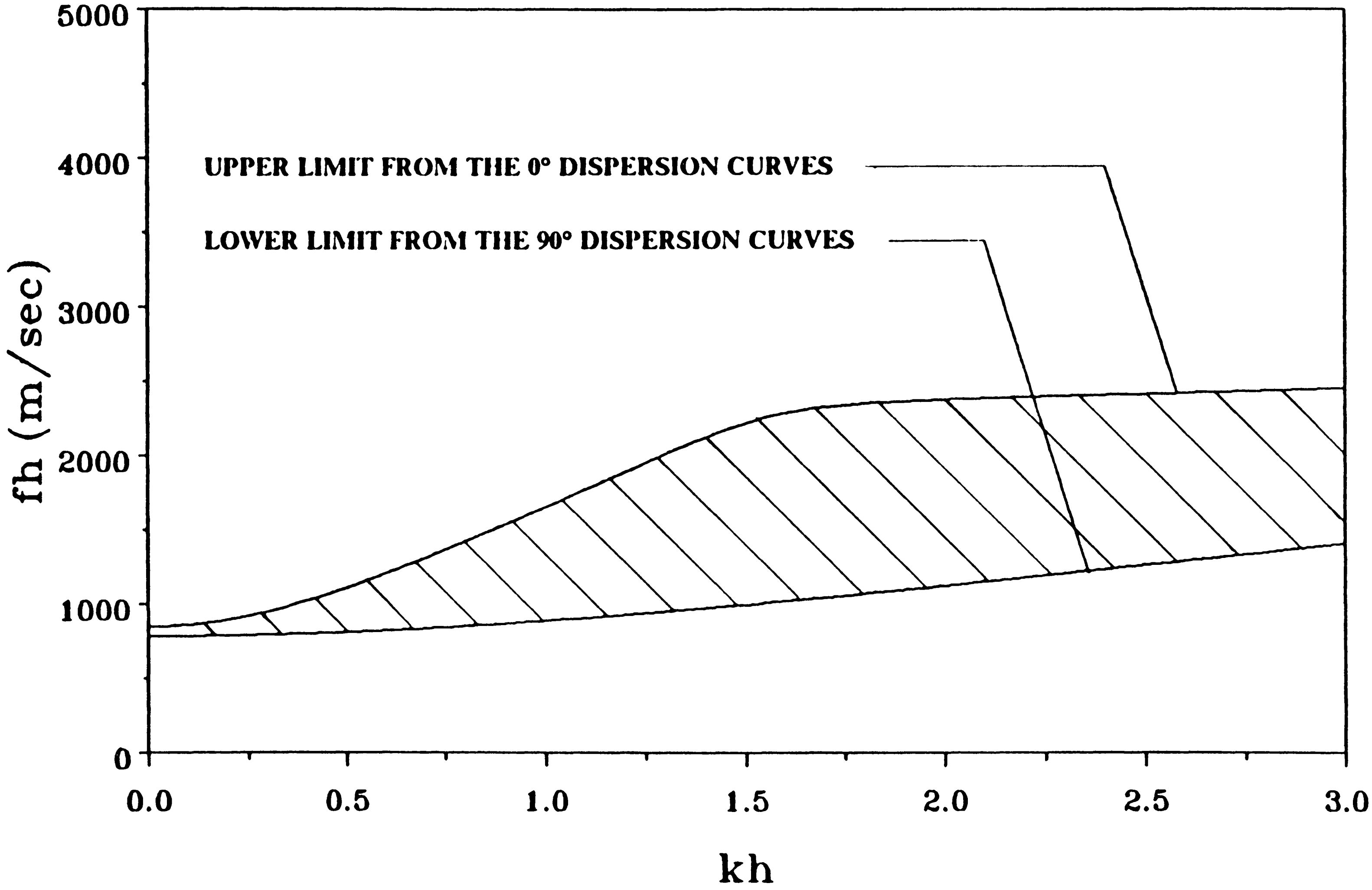

Figure 20. Region of the second lowest antisymmetric modes for symmetric laminates.

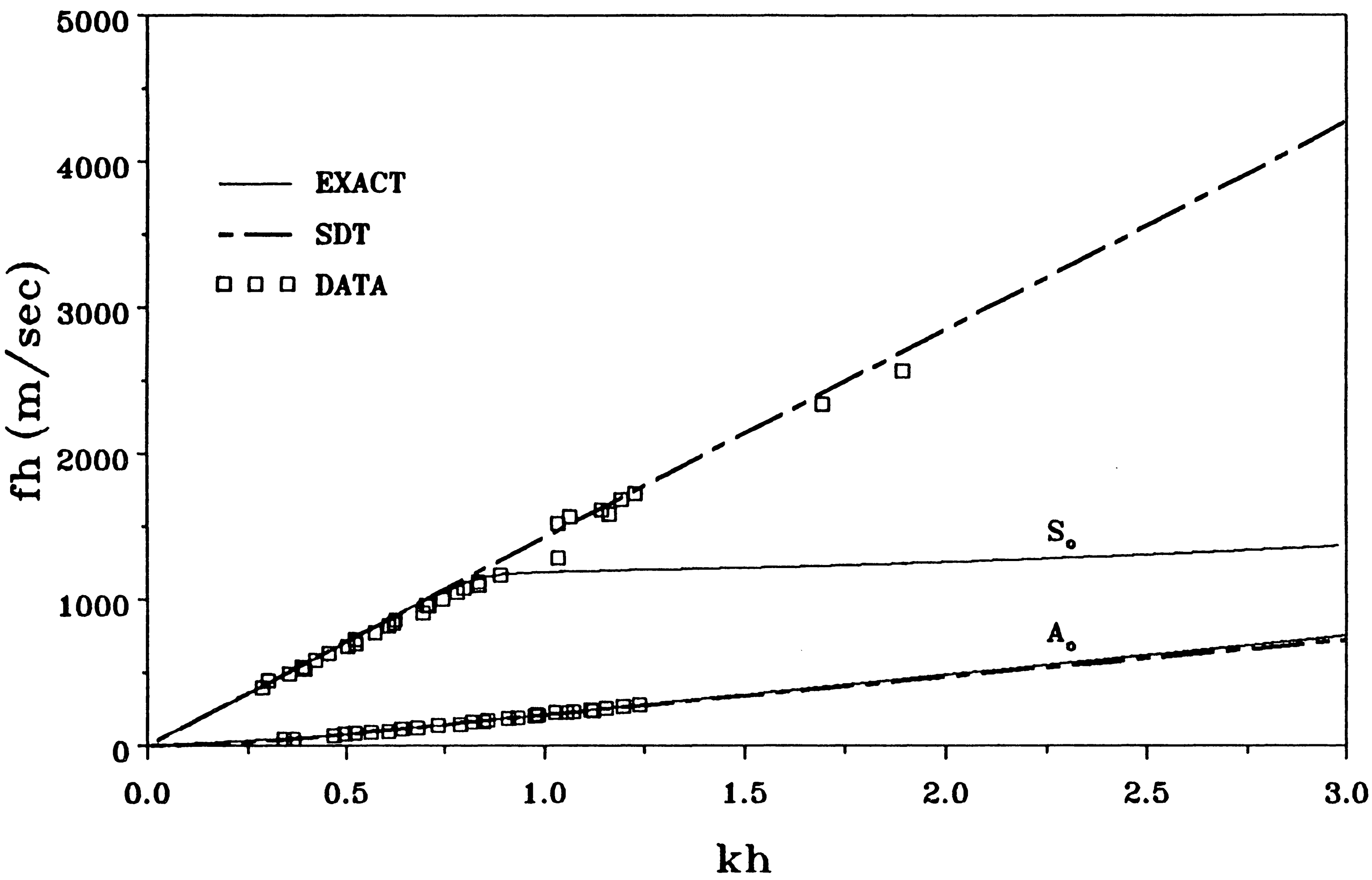

Figure 21. Theoretical results and data for Lamb wave propagation along the fiber direction of a unidirectional laminate.

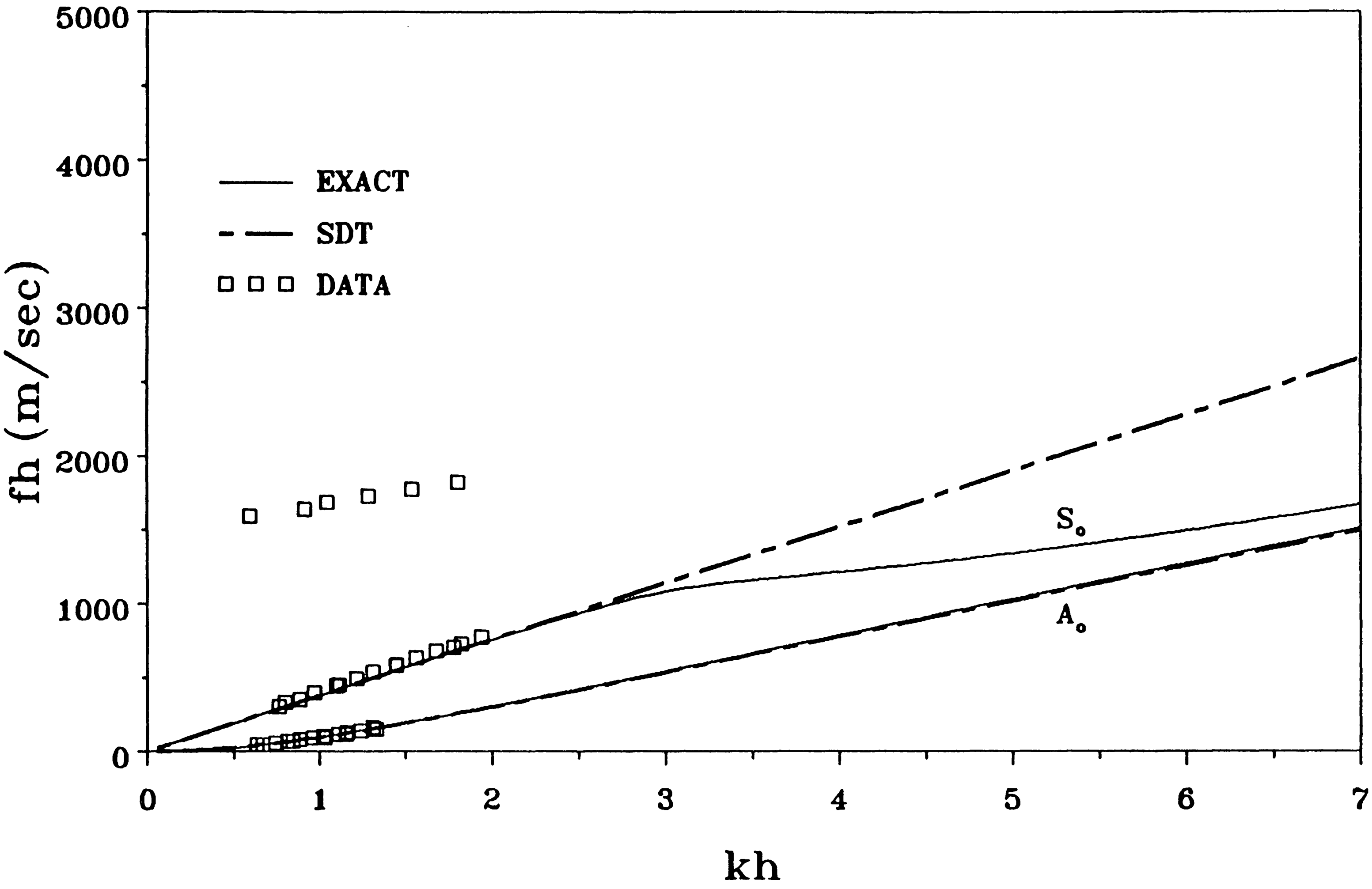

Figure 22. Theoretical results and data for Lamb wave propagation perpendicular to the fiber direction of a unidirectional laminate.

with the lowest antisymmetric branch, while the SDT nondispersion relation represents only the linear long wavelength portion of the lowest symmetric mode. In order to compare the nondispersion relation with the experimental data in the case where an elasticity solution is not available (i.e., for the multidirectional laminates), care must be taken to make sure that the data used for comparison belong to the linear long wavelength portion of the lowest symmetric mode instead of any higher order modes or other portions of the lowest symmetric mode. From Figure 22, the lowest symmetric mode of the 90° dispersion curves begins to deviate significantly from a straight line at 1,000 m/sec, while the corresponding value for the 0° dispersion curves is 1,200 m/sec (Figure 21). Hence, for the case of symmetric laminates, the corresponding values are probably in between 1,000 m/sec and 1,200 m/sec, in keeping with our assumption that the 0° and 90° dispersion curves represent the limits of the respective ranges. For symmetric composite laminates of AS-4(Gr)/Pr 288 graphite/epoxy, we assume that any data which are taken after the abrupt change in the phase velocity takes place, and below 1,000 m/sec, belong to the linear long wavelength region of the lowest symmetric mode. Thus, we can compare these data with the nondispersion relation which represents the linear long wavelength portion theoretically.

Figures 23-26 show the results from the shear deformation theory (SDT) and the experimental data for a symmetric cross-ply laminate and a symmetric quasi-isotropic laminate. Figure 27 shows the results for an aluminum plate. There is agreement between the experimental data and the results from the shear deformation theory, which suggests that the shear deformation theory works for the lowest symmetric and antisymmetric modes in the low frequency, long wavelength region. Data for the lowest symmetric mode at lower frequencies can be generated by a modified exper-

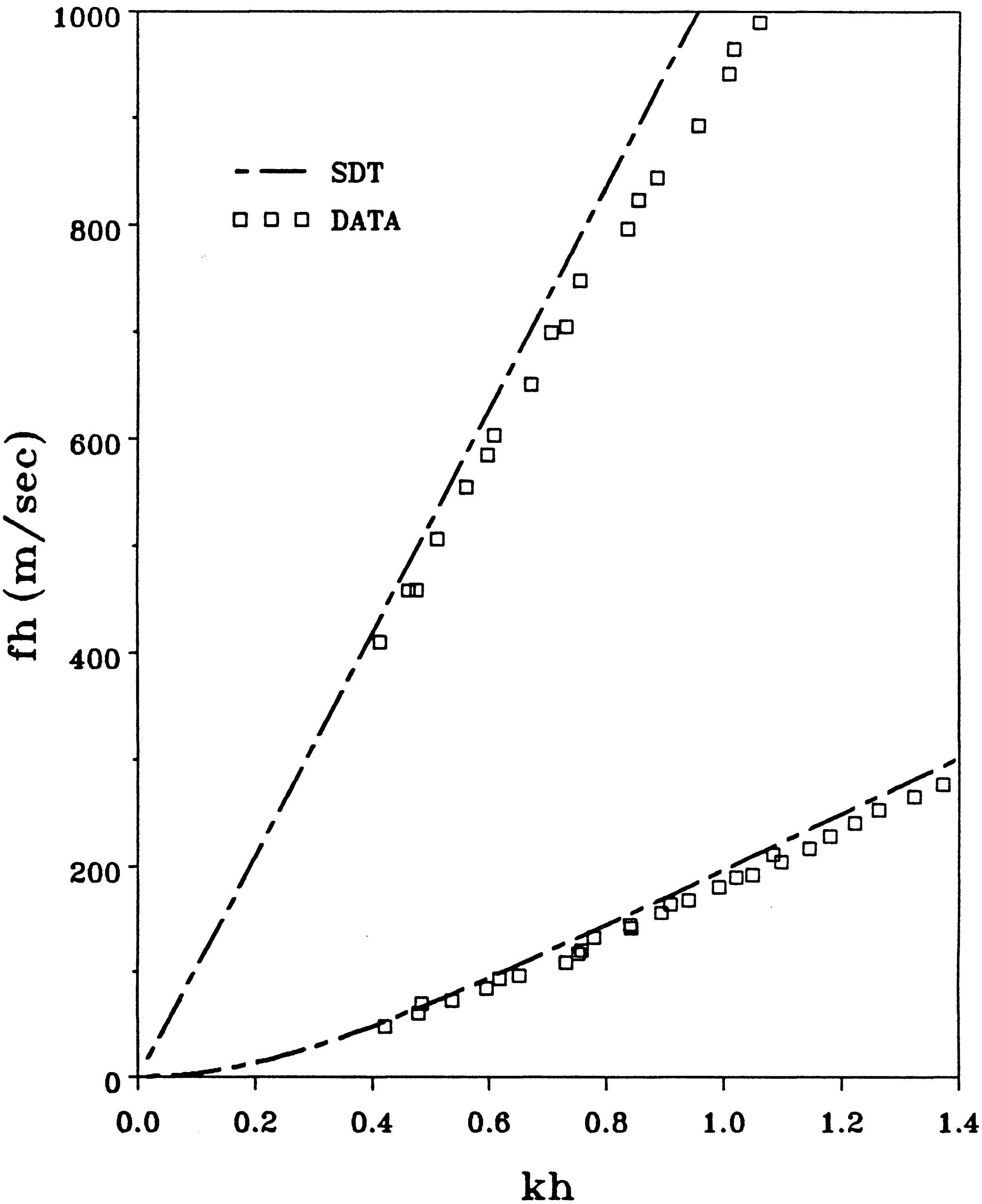

Figure 23. Theoretical results and data for low frequency Lamb wave propagation in the x direction of a $[0/90]_{2S}$ laminate.

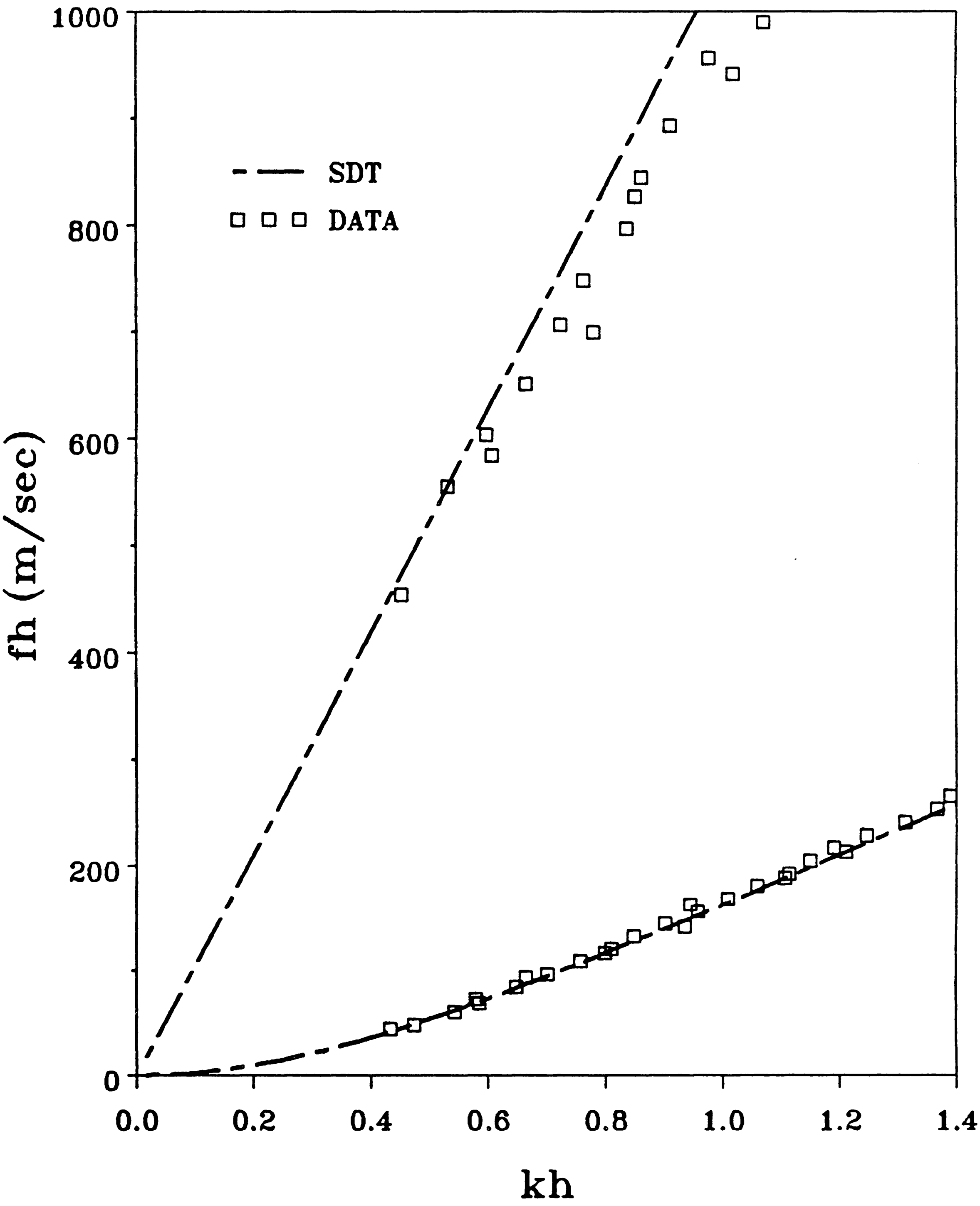

Figure 24. Theoretical results and data for low frequency Lamb wave propagation in the y direction of a $[0/90]_{2S}$ laminate.

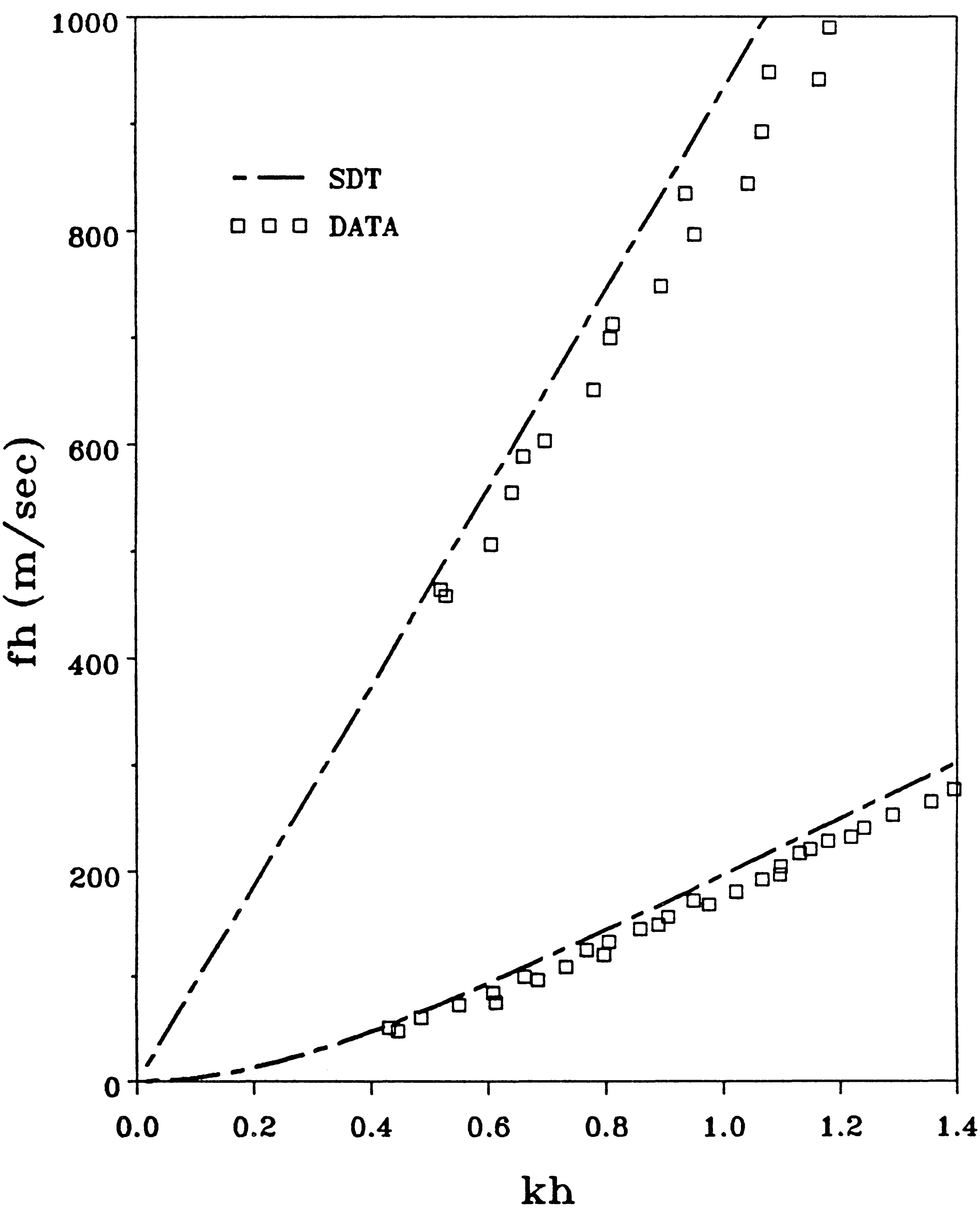

Figure 25. Theoretical results and data for low frequency Lamb wave propagation in the x direction of a $[0/45/90/-45]_s$ laminate.

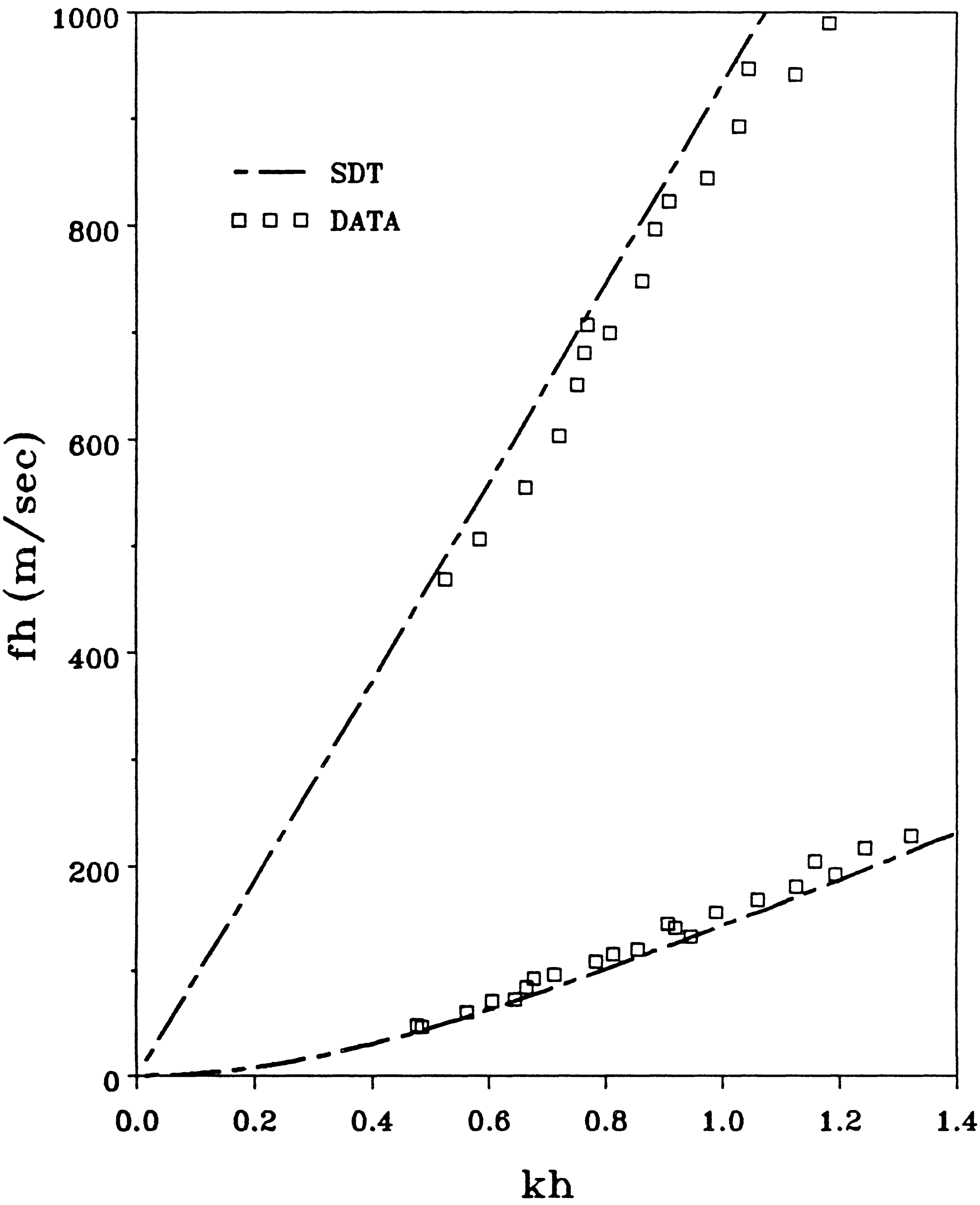

Figure 26. Theoretical results and data for low frequency Lamb wave propagation in the y direction of a $[0/45/90/-45]_s$ laminate.

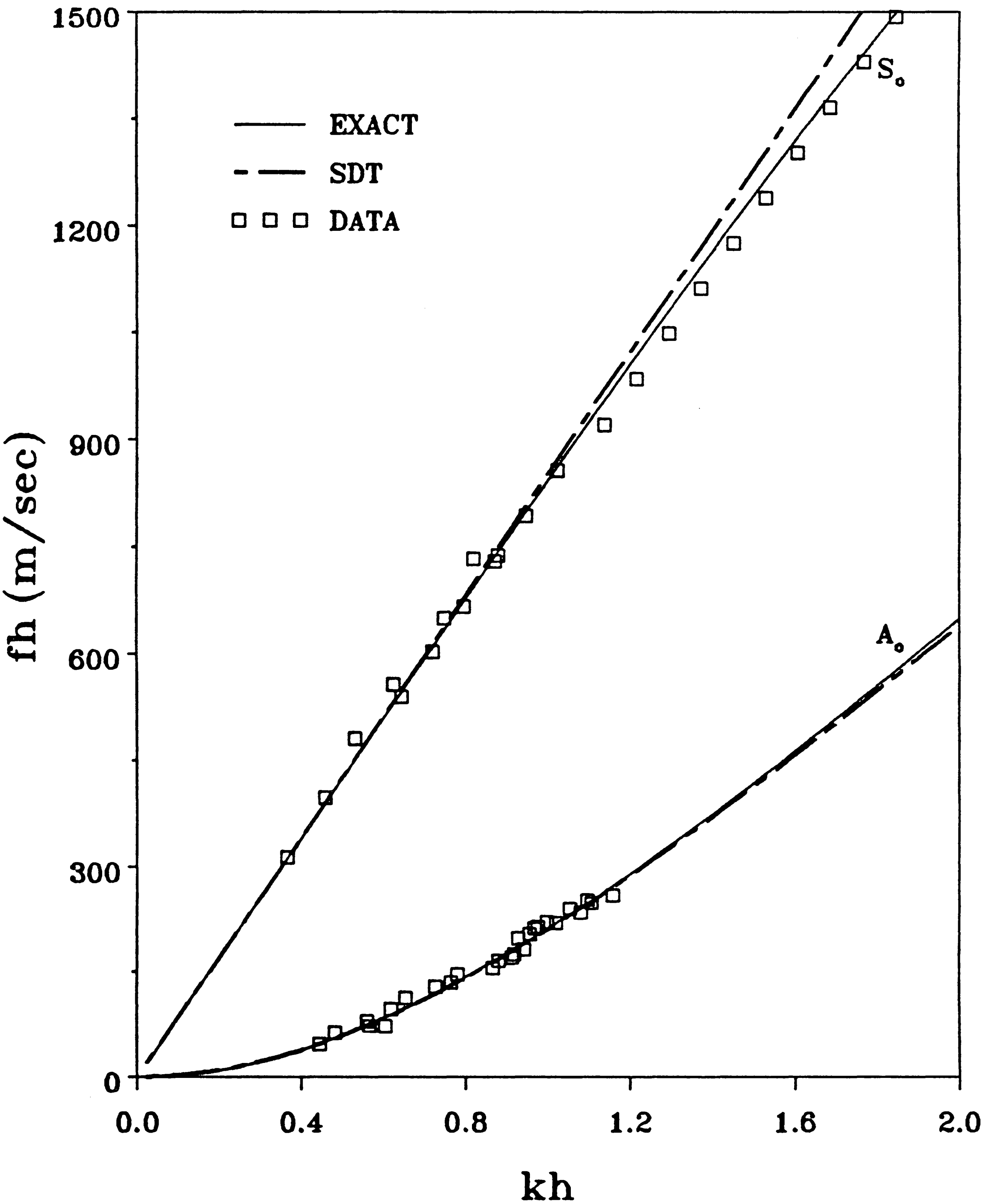

Figure 27. Theoretical results and data for low frequency Lamb wave propagation in a 6061-T4 aluminum plate.

imental approach. In this approach, the sending transducer in Figure 4 is placed at the edge of the plate. Figure 28 shows that the results from the shear deformation theory for the symmetric cross-ply and quasi-isotropic laminates are in between the upper limit and the lower limit, and this is what we expected.

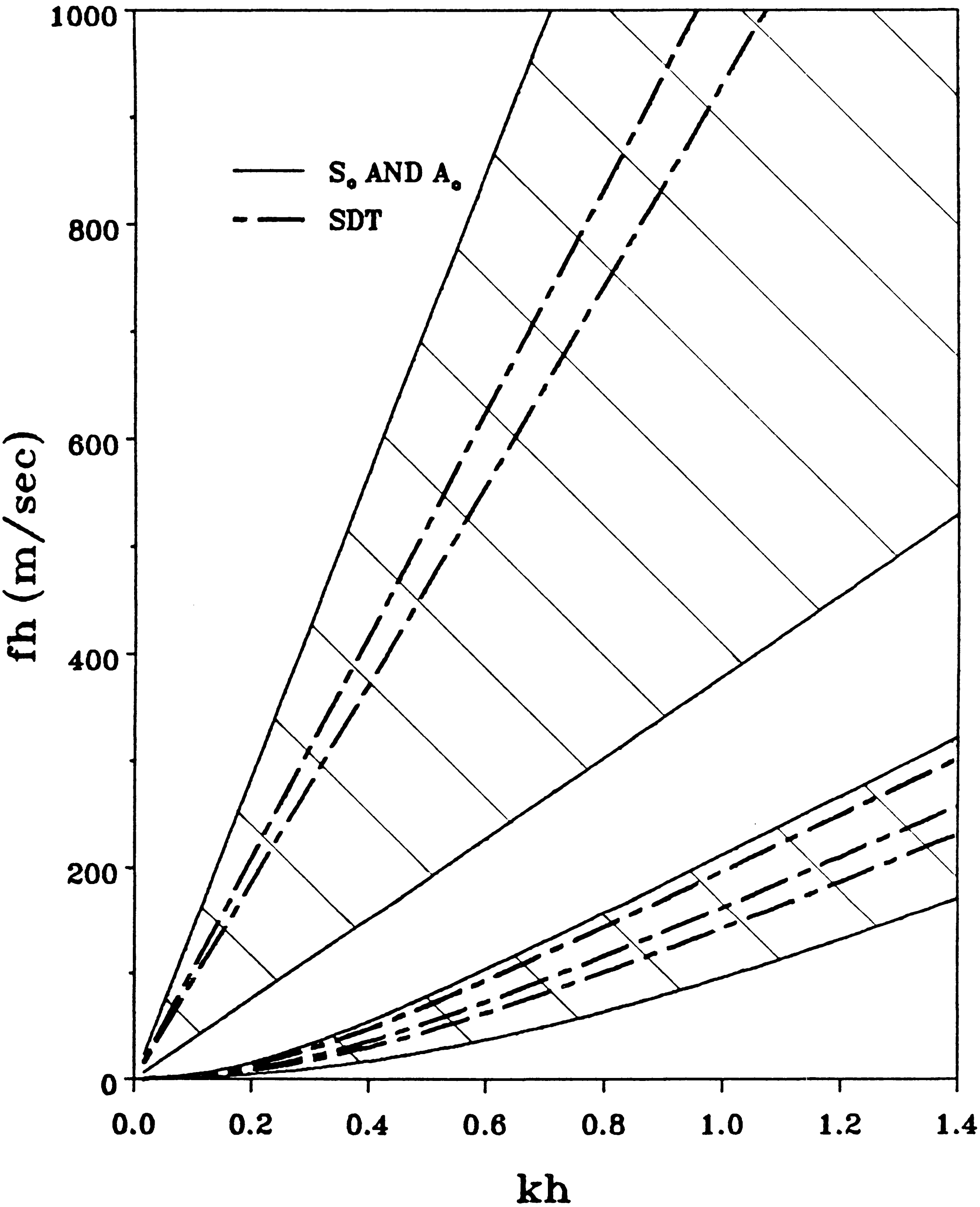

Figure 28. Upper and lower limits of approximate solutions.

VI. APPLICATION TO MONITOR AXIAL STIFFNESS REDUCTION

Lamb waves may be the most adequate nondestructive means to interrogate composite plates. Lamb waves have been used to evaluate delamination and porosity in composite plates in a C-scan type of operation [21]. Measurement of Lamb wave attenuation is another way to evaluate damage. We are interested in relating stiffness reduction of composite laminates caused by damage to the change in Lamb wave velocity.

6.1 *Stiffness Reduction*

In Figure 29, experimental data are compared with theoretical results from the shear deformation theory (SDT) in the low frequency, long wavelength region for a

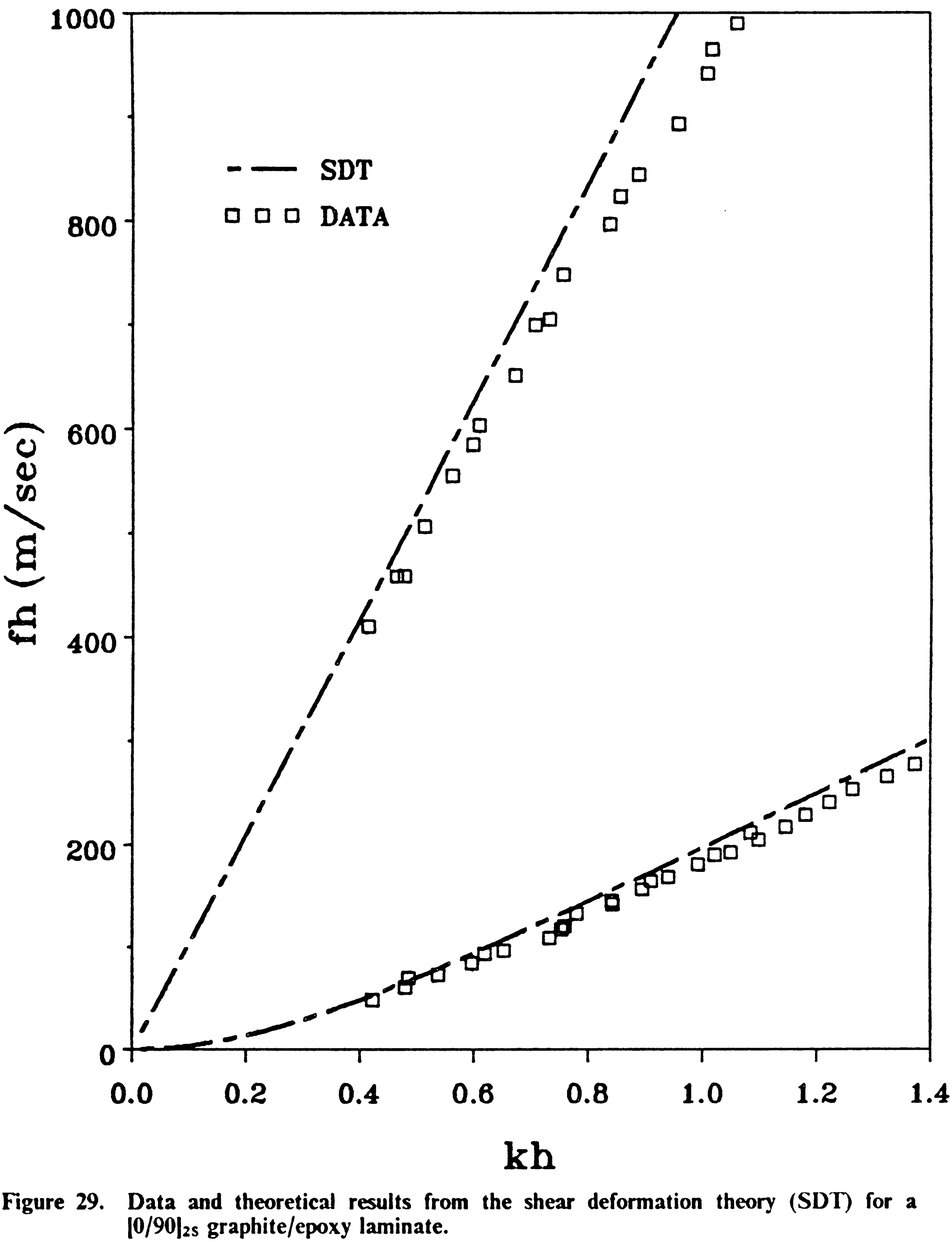

Figure 29. Data and theoretical results from the shear deformation theory (SDT) for a $[0/90]_{2S}$ graphite/epoxy laminate.

$[0/90]_{2s}$ graphite/epoxy laminate. The shear deformation theory is shown to work well in the low frequency, long wavelength region in Chapter 4. By applying load in the 0° direction of the $[0/90]_{2s}$ laminate, transverse cracks are developed in the 90° plies as illustrated graphically in Figure 30. These transverse cracks degrade the laminate and reduce the laminate stiffnesses. To account for the stiffness reduction caused by the damage, the ply discount method is used to analyze the damaged laminate. By setting $E_2 = G_{12} = G_{23} = 0$ for the cracked plies in the ply discount method, the resulting theoretical dispersion curves for Lamb wave propagation in the 0° direction drop relatively as shown in Figure 31. The lower curve which represents the lowest antisymmetric mode is more sensitive to the stiffness reduction of the laminate since it changes more significantly in comparison with the upper curve after the introduction of cracks. In Figure 32, the changes of the theoretical dispersion curves are more dramatic for a $[90/90/90/0]_s$ laminate.

However, in practice, we do not expect the dispersion curves to drop as much as is shown in Figures 31 and 32, even when the 90° plies are fully degraded. Actually, a ply with cracks does not mean that it can no longer carry load and this is not the same as having it completely removed from the laminate. The cracked ply continues to contribute to the stiffnesses of the laminate. To create cracks in the 90° plies and to cause stiffness reduction, a $[90/90/90/0]_s$ graphite/epoxy laminate was bent around a 10 in. diameter cylinder.

Experimental data before damage and after damage are shown in Figure 33. There are some small changes in the experimental dispersion curves for the antisymmetric mode before and after damage. In Figure 34, the previous data for the antisymmetric mode together with new data obtained after further damaging the laminate by bending

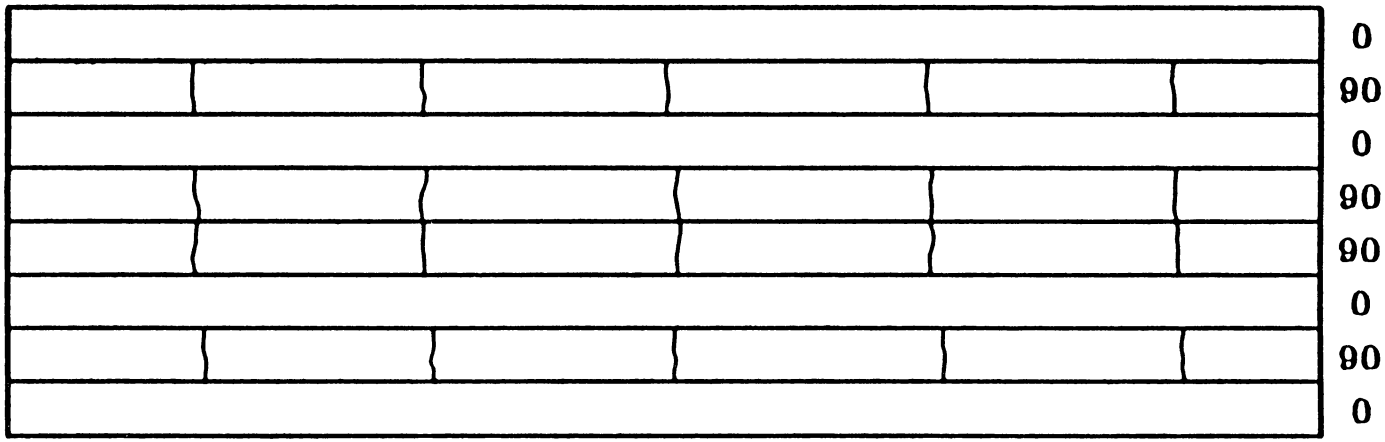

Figure 30. Schematic representation of transverse cracks in a $[0/90]_{2S}$ laminate.

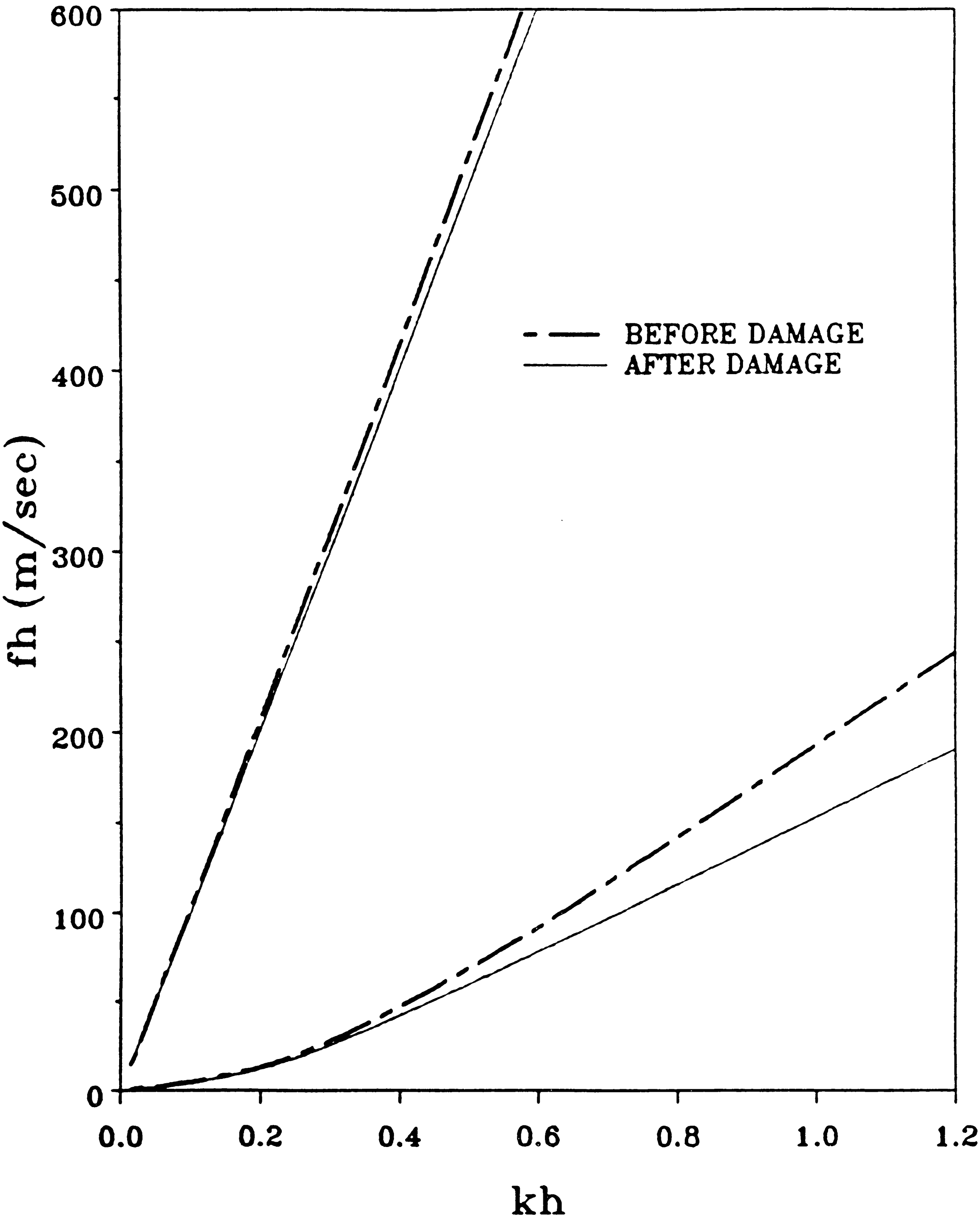

Figure 31. Theoretical dispersion curves for Lamb wave propagation in the 0° direction of a $[0/90]_{2S}$ laminate.

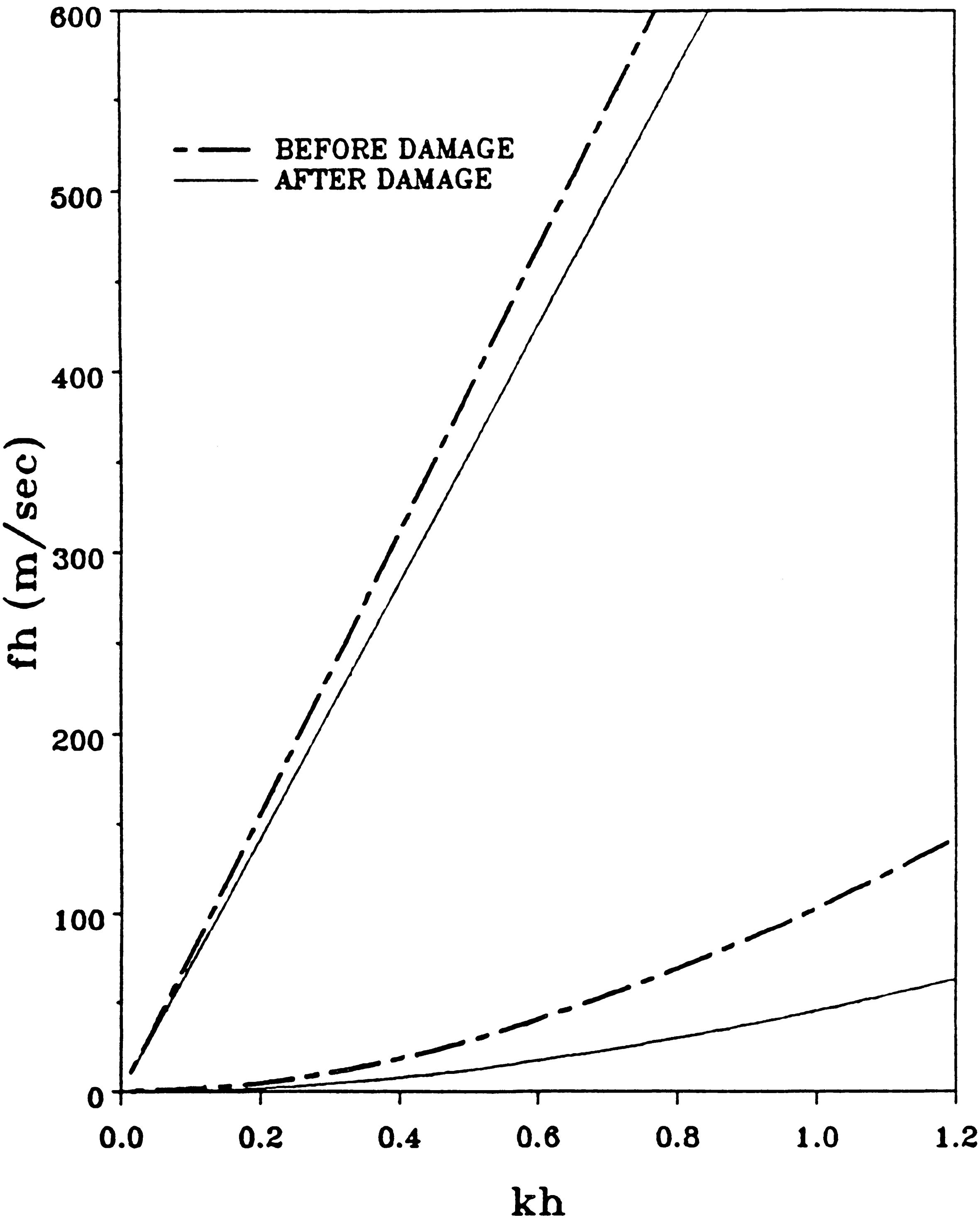

Figure 32. Theoretical dispersion curves for Lamb wave propagation in the 0° direction of a $[90/90/90/0]_s$ laminate.

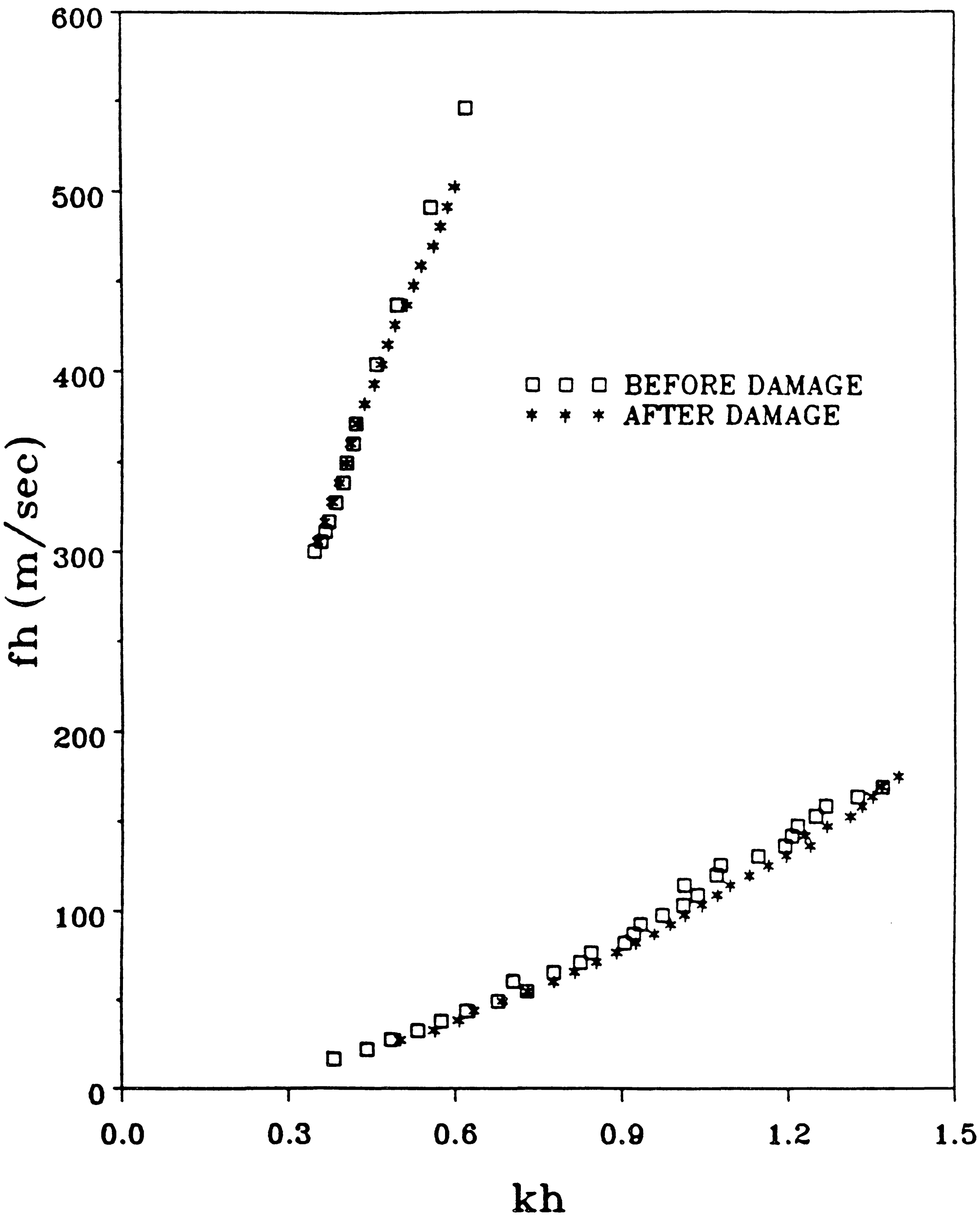

Figure 33. Experimental data for Lamb wave propagation in the 0° direction of a $[90/90/90/0]_s$ graphite/epoxy laminate.

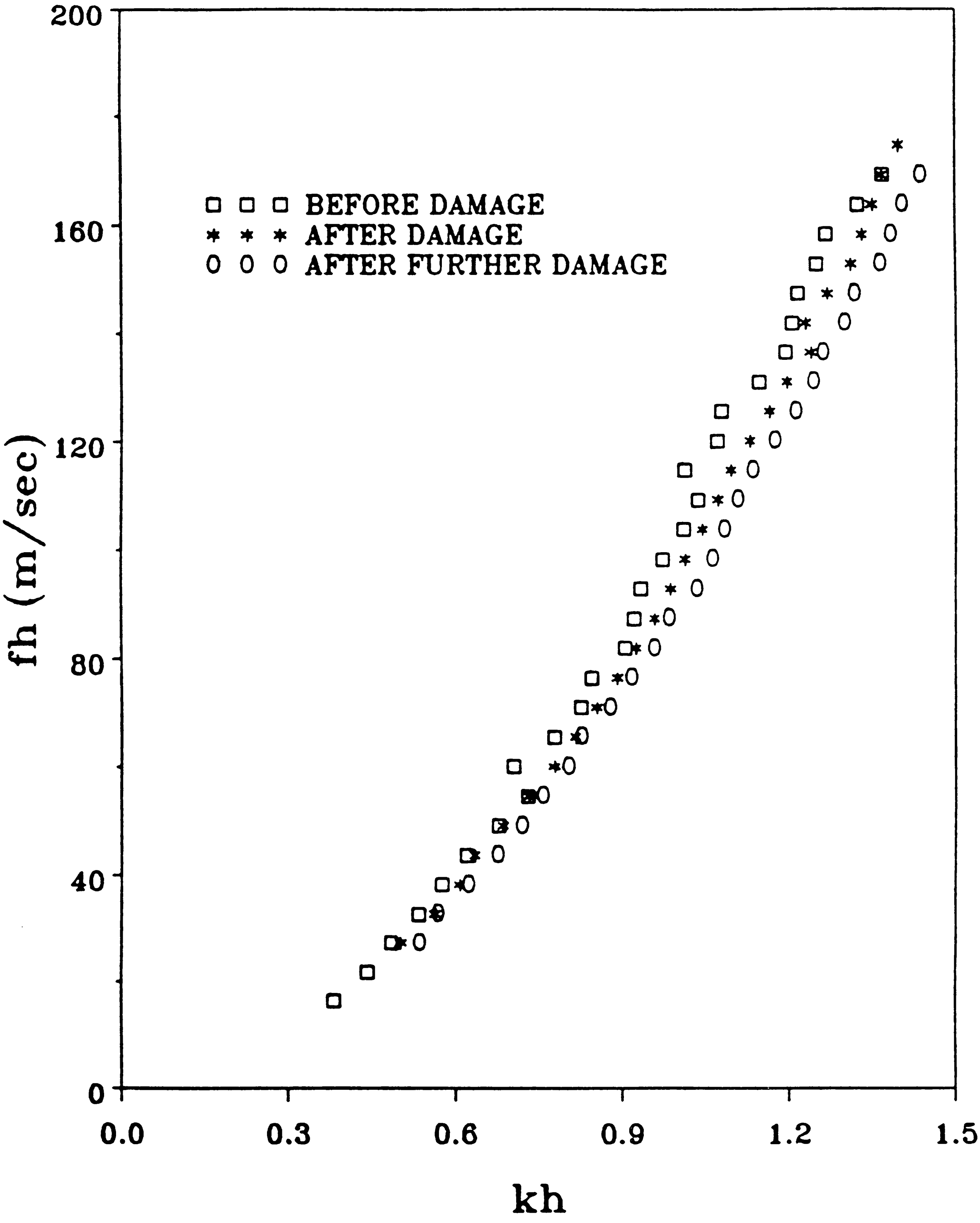

Figure 34. Experimental data for the lowest antisymmetric Lamb mode in the 0° direction of a $[90/90/90/0]_S$ graphite/epoxy laminate.

the plate around a 7 in. diameter cylinder are shown in a different scale. From this figure, it can be concluded that the stiffness reduction caused by damage does indeed reduce the Lamb wave velocity. From observing the crack spacing in the laminate, it was noted that the cracked plies had not reached their characteristic damage state, even after bending around the 7 in. diameter cylinder. More cracks can be introduced into the 90° plies before a saturated spacing is attained. A final comment is that, in order to measure the global effect of the cracks instead of their local effect, it is necessary that the wavelength of the Lamb waves be very long in comparison with the crack spacing. Hence, experimental measurements are restricted to the low frequency, long wavelength region.

6.2 *Modified Method*

Although the previous method successfully gives data that indicate the drop of the dispersion curve with stiffness reduction caused by damage, the method is not generally suitable to use to measure wave propagation in cracked laminates since the cracks in the laminates scatter and reflect waves at their surfaces. These scattered and reflected waves confuse the receiving signal and make it very difficult to follow the signal while moving the receiving transducer. Consequently, a modified method was used to obtain experimental data. In this modified method, instead of moving the receiving transducer a known distance, two transducers with piezoelectric elements of 0.053 in. diameter are used as receivers. These two receivers are separated by a known distance in the direction of the phase velocity. The two receiving signals are overlapped on the oscilloscope by imposing a time delay on the first received signal. From the time delay and the known distance separating the receiving transducers, the same information can be obtained as before.

Figure 35 shows the arrangement of the modified method. The two receiving transducers are held by a fixture which sets them apart by a fixed distance. In the experiment, the two receivers are 1/2 to 1 inch apart with the distance between the transducers determined so as the phase shift between the two receiving signals is small and the corresponding phase points are easy to identify. The experimental results are also checked against the data obtained from the original method to ensure that the correct phase points are identified and overlapped.

In order to maintain the stress free boundary conditions, the fixture holding the transducers is supported so that it does not come into contact with the laminate surface. Also, the receivers are held in position so as to be barely touching the surface of the composite laminate. Water soluble couplant connects the receivers to the laminate. The use of small size receiving transducers and the fixture have the advantages of getting pointwise information and maintaining virtually traction-free boundary conditions at the surfaces. Moreover, using this technique, rather than an immersion technique, strongly reduces the transmission of leaky Lamb waves out of the laminates. The modified method eliminates the difficulty of following the signal while moving the receiving transducer, thus making it easier to obtain experimental data.

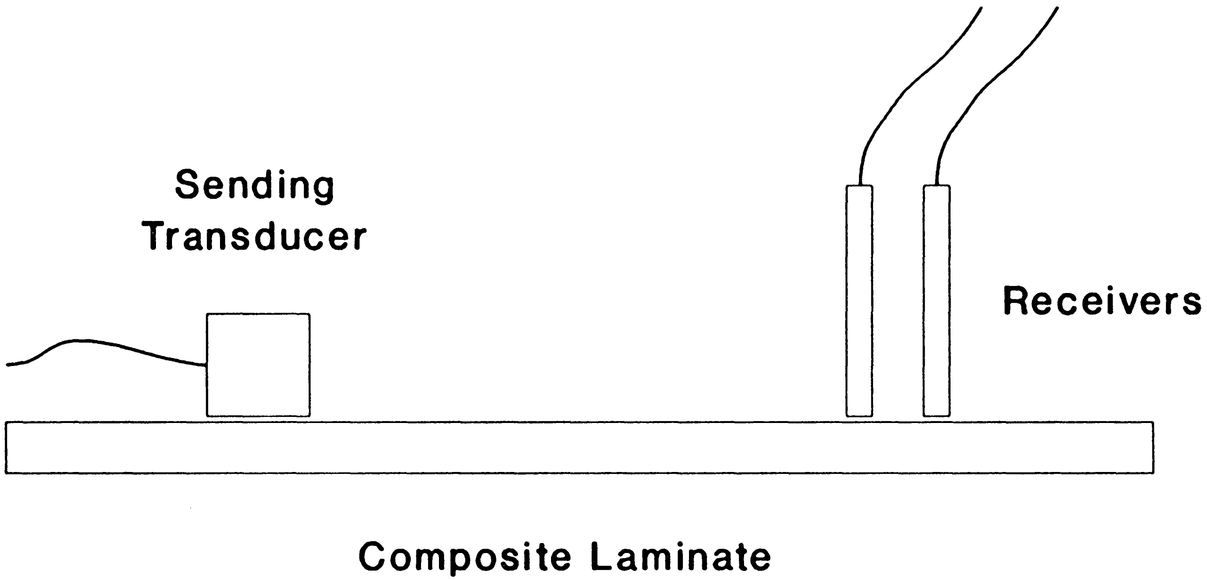

Figure 35. Schematic diagram of the experimental setup for the modified method.

6.3 *Woven Materials*

Two different layups of 8-harness satin woven composite materials were used to further study the relation between Lamb waves and axial stiffness reduction of composite laminates. To bring about damage and stiffness reduction, woven Celion 3000/PMR-15 graphite/polyimide composite laminates of $[0/45/0/45/0/45]_s$ and $[0]_{12}$ were put under tension-tension fatigue loading in the 0° direction at a maximum stress level of 75% of the tensile strength with the ratio of minimum to maximum load of 0.1. Two $[0/45/0/45/0/45]_s$ specimens were subjected to 70,000 and 370,000 fatigue cycles, respectively, and had axial stiffness reductions of 4.9% and 7.7%. In addition, experimental data of the lowest antisymmetric Lamb mode in the 0° direction were obtained before and after axial stiffness changes for the two specimens. Their dispersion curves are shown in Figure 36. From these dispersion curves, it is clear that the lowest antisymmetric Lamb mode can detect axial stiffness changes in composite laminates. Penetrant-enhanced X-ray radiographs of both specimens are shown in Figures 37 and 38. The thick dark lines are Kevlar tracer fibers used by the manufacturer to check ply orientations during layup. Cracks are spaced uniformly and are very densely populated in these specimens. The evidence of the onset of edge delamination can be seen in Figure 38. The $[0]_{12}$ specimen was fatigued to 400,000 cycles and was close to the final stage of its life, but had only a 3% axial stiffness reduction. Very small changes in the dispersion curve is observed in Figure 39.

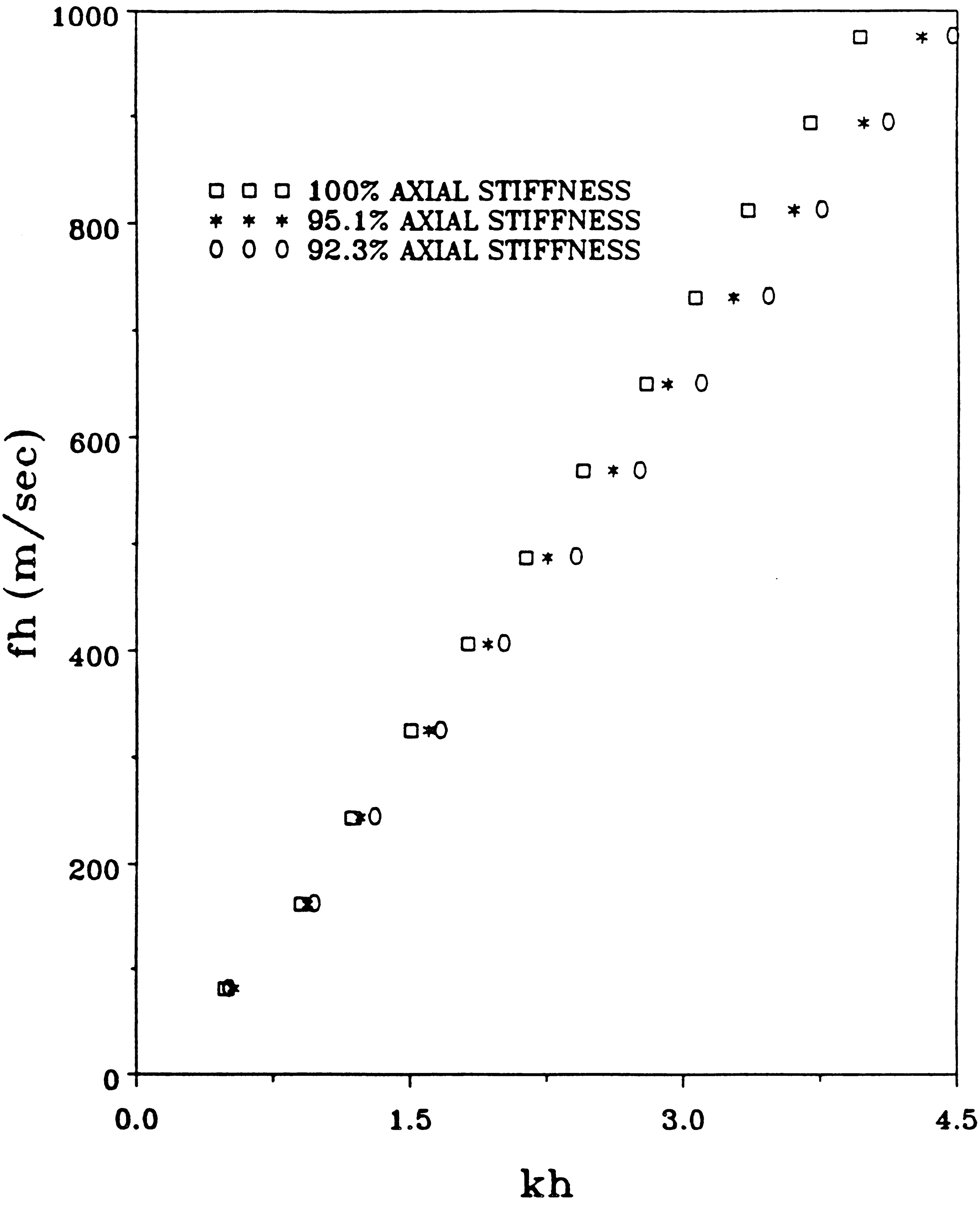

Figure 36. Experimental data for the lowest antisymmetric Lamb mode in the 0° direction of two $[0/45/0/45/0/45]_S$ woven graphite/polyimide specimens.

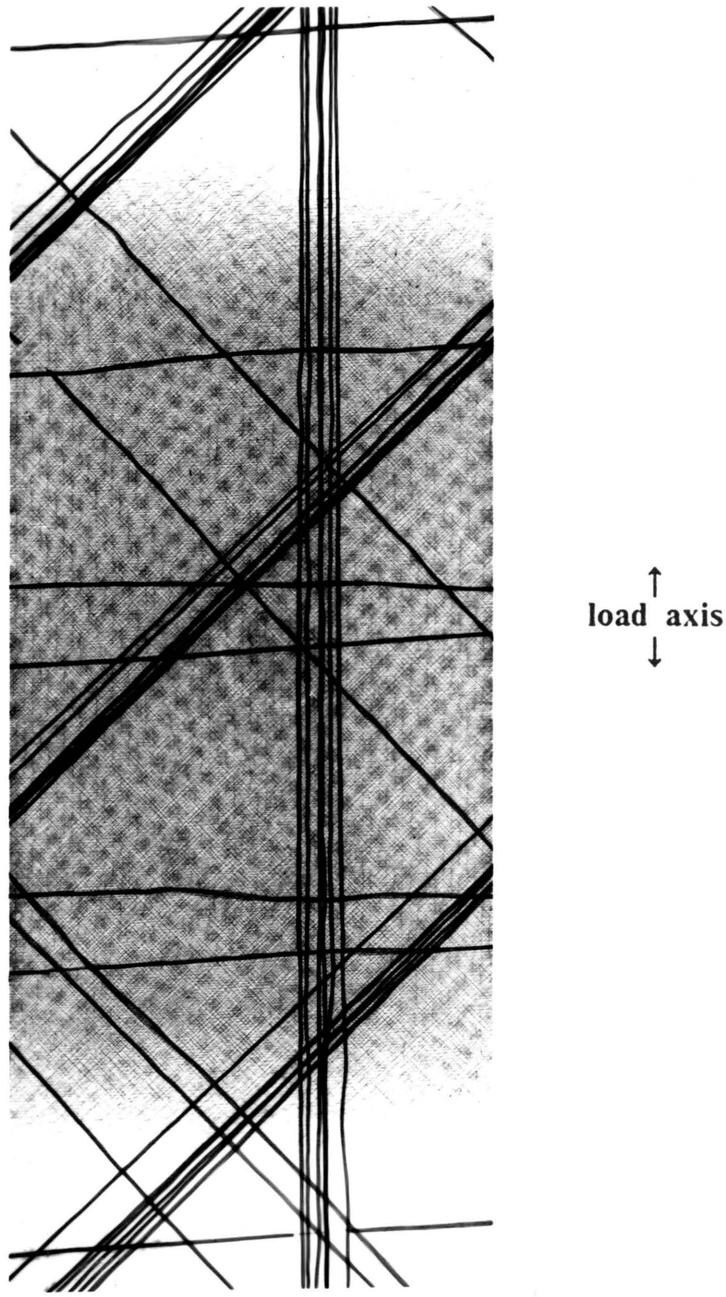

Figure 37. X-ray radiograph of a $[0/45/0/45/0/45]_s$ woven graphite/polyimide specimen after axial stiffness reduction of 4.9%.

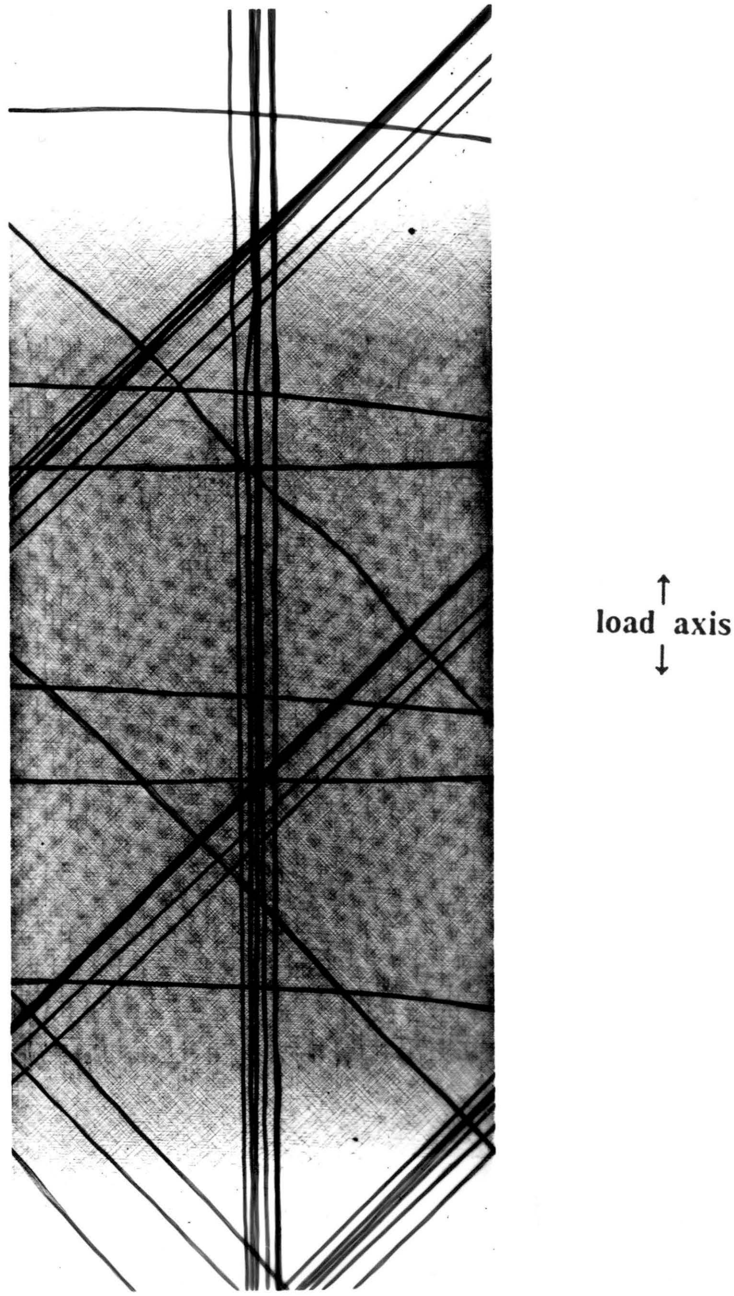

Figure 38. X-ray radiograph of a [0/45/0/45/0/45]$_S$ woven graphite/polyimide specimen after axial stiffness reduction of 7.7%.

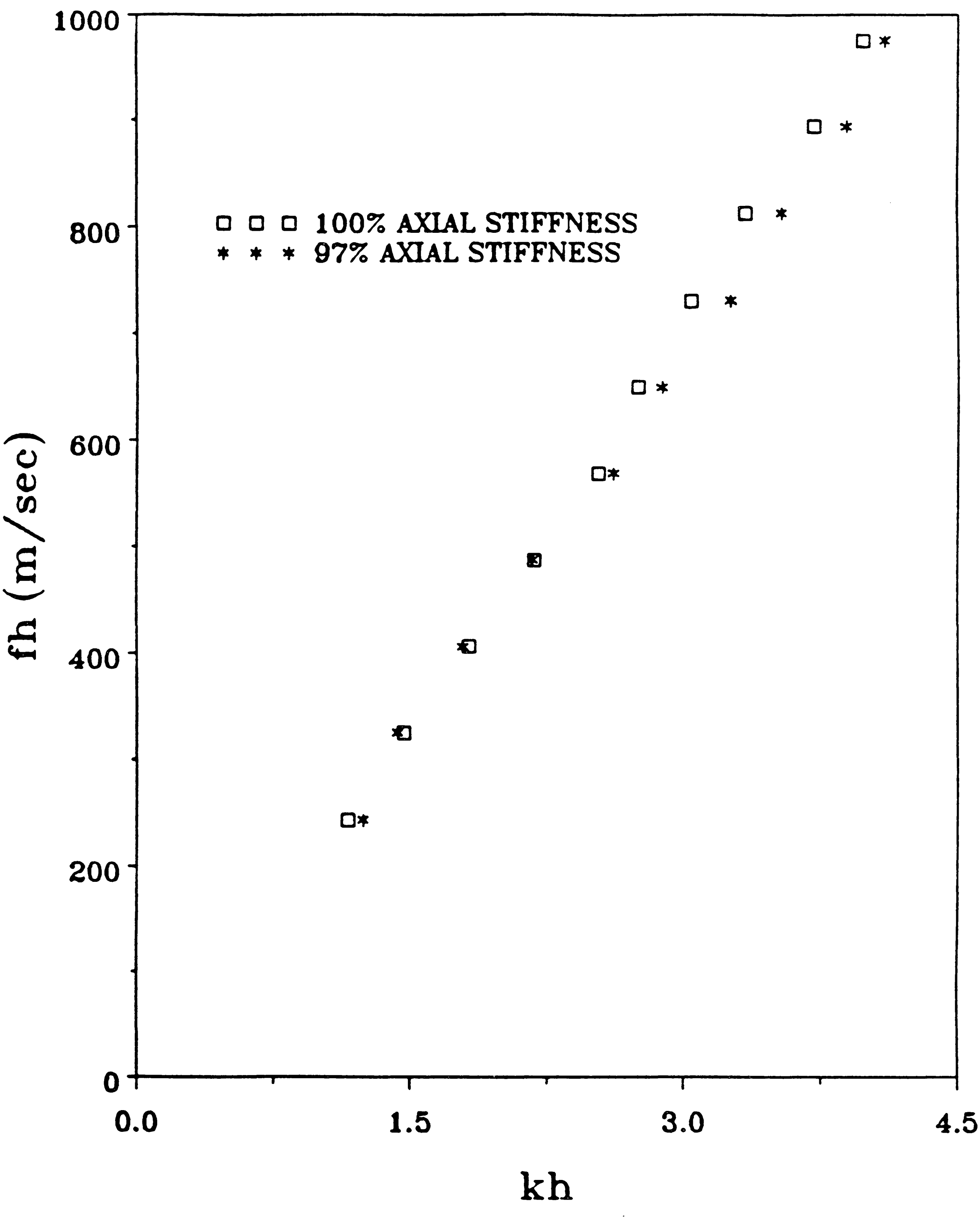

Figure 39. Experimental data for the lowest antisymmetric Lamb mode in the 0° direction of a $[0]_{12}$ woven graphite/polyimide specimen.

VII. CONCLUSIONS

The inclusion of shear deformation and rotary inertia in classical plate theory significantly improves the theoretical dispersion curves for the low frequency antisymmetric Lamb waves propagating in composite laminates, but has relatively little effect on isotropic aluminum plates which are modeled quite well at long wavelengths by the classical plate theory. The shear correction factors for static cylindrical bending are applicable to the problem of low frequency, long wavelength antisymmetric Lamb wave propagation in isotropic plates and unidirectional laminates. Using a higher order approximation of the displacement field may improve our results and the prediction of the higher order modes for transversely isotropic plates and composite laminates. Experimental data for the dispersion curves are obtained by using a simple method similar in configuration to the acousto-ultrasonic technique. For the antisymmetric Lamb modes, the experimental data and the theoretical results in the aluminum plate and the unidirectional laminate agree quite well. The data for the symmetric cross-ply and the symmetric quasi-isotropic laminates definitely have the characteristic of a dispersion curve for antisymmetric Lamb waves.

From the comparison between the experimental data and the exact solutions for the unidirectional laminate and the aluminum plate of both modes, we conclude that this method for measuring Lamb wave phase velocities can be used to obtain data for the Lamb wave dispersion curves, especially for the lowest symmetric and antisymmetric modes. The exact solution for Lamb wave propagation in multilayered composite laminates is not available. However, the Lamb wave dispersion curves for symmetric laminates are probably bounded between the 0° dispersion curves and the 90° dispersion curves, with the 0° dispersion curves as the upper limit and the 90° dispersion curves as the lower limit. There is good correlation between the exact solutions and the solutions from the shear deformation theory in the low frequency, long wavelength region of the lowest symmetric and antisymmetric modes for the unidirectional laminate and the aluminum plate. Agreement is also found in the experimental data and the solutions from the shear deformation theory for the symmetric cross-ply and quasi-isotropic laminates. Thus, these results suggest that the shear deformation theory works in the low frequency, long wavelength region of the lowest symmetric and antisymmetric modes. Finally, the solutions from the shear deformation theory for the symmetric cross-ply and quasi-isotropic laminates are bounded between the upper limit and the lower limit set by the unidirectional laminate results, as we expected.

Lamb waves may be the most adequate nondestructive means to interrogate and to evaluate damage in the in-plane directions of laminated composite plates. Damage in the form of transverse cracks in composite laminates reduces the phase velocities of the Lamb modes. The experimental procedure of generating and detecting the lowest antisymmetric Lamb mode can be used to monitor axial stiffness reduction of composite laminates caused by damage. Furthermore, the modified method improves the efficiency of obtaining experimental data and works extremely well in the case of cracked laminates since there is no need to move the receiver and to follow the receiving signal. However, more sophisticated electronic equipment is required to improve the accuracy of the results and the sensitivity of the experimental technique to detect small axial stiffness changes.

The results of the present work indicate that the shear deformation theory can be used to model the low frequency, long wavelength region of the lowest symmetric and antisymmetric modes for composite laminates. The experimental procedure for measuring phase velocities of the lowest symmetric and antisymmetric modes can be utilized as a nondestructive means to characterize laminated composite plates since each material and stacking sequence gives distinct lowest symmetric and antisymmetric curves. The lowest antisymmetric Lamb mode is sensitive to damage in composite laminates, and is capable of monitoring axial stiffness reduction in these materials.

REFERENCES

1. Ringermacher, H. I., "Ultrasonic Velocity Characterization of Fatigue Damage in Graphite/Epoxy Composites," IEEE 1980 Ultrasonics Symposium Proceedings, B. R. McAvoy, Ed., IEEE, 1980, pp. 957-960.

2. Williams, J. H., Jr. and Lampert, N. R., "Ultrasonic Evaluation of Impact-Damaged Graphite Fiber Composite," Materials Evaluation, Vol. 38, No. 12, 1980, pp. 68-72.

3. Gericke, O. R. and Monagle, B. L., "Detection of Delaminations by Ultrasonic Spectroscopy," IEEE Transactions on Sonics and Ultrasonics, Vol. SU-23, 1976, pp. 339-345.

4. Williams, J. H., Jr., Yuce, H., and Lee, S. S., "Ultrasonic and Mechanical Characterizations of Fatigue States of Graphite Epoxy Composite Laminates," NASA CR-3504, January 1982.

5. Gieske, J. H. and Allred, R. E., "Elastic Constants of B-Al Composites by Ultrasonic Velocity Measurements," Experimental Mechanics, Vol. 14, 1974, pp. 158-165.

6. Zimmer, J. E. and Cost, J. R., "Determination of the Elastic Constants of a Unidirectional Fiber Composite Using Ultrasonic Velocity Measurements," Journal of the Acoustical Society of America, Vol. 47, 1970, pp. 795-803.

7. Reynolds, W. N. and Wilkinson, S. J., "The Analysis of Fibre-Reinforced Porous Composite Materials by the Measurement of Ultrasonic Wave Velocities," Ultrasonics, Vol. 16, 1978, pp. 159-163.

8. Smith, R. E., "Ultrasonic Elastic Constants of Carbon Fibers and Their Composites," Journal of Applied Physics, Vol. 43, 1972, pp. 2555-2561.

9. Blessing, G. V., Elban, W. L., and Foltz, J. V., "Ultrasonic Characterization of Aluminum Matrix Composites for Their Moduli," Ultrasonic Materials Charac-

terization, National Bureau of Standards Special Publication 596, H. Berger and M. Linzer, Eds., National Bureau of Standards, 1980, pp. 137-146.

10. Kriz, R. D., "Mechanical Properties for Thick Fiber Reinforced Composite Materials Having Transversely Isotropic Fibers," M.S. Thesis, College of Engineering, Virginia Polytechnic Institute and State University, Blacksburg, Virginia, May 1976.

11. Brekhovskikh, L. M., Waves in Layered Media, Academic Press, New York, 1960.

12. Ewing, W. M., Jardetzky, W. S., and Press, F., Elastic Waves in Layered Media, McGraw-Hill Book Co., New York, 1957.

13. Lamb, H., "On Waves in an Elastic Plate," Proceedings of the Royal Society of London, Series A, Vol. 93, 1917, pp. 114-128.

14. Solie, L. P. and Auld, B. A., "Elastic Waves in Free Anisotropic Plates," Journal of the Acoustical Society of America, Vol. 54, 1973, pp. 50-65.

15. Habeger, C. C., Mann, R. W., and Baum, G. A., "Ultrasonic Plate Waves in Paper," Ultrasonics, Vol. 17, 1979, pp. 57-62.

16. Moon, F. C., " Wave Surfaces Due to Impact on Anisotropic Plates," Journal of Composite Materials, Vol. 6, 1972, pp. 62-79.

17. Sun, C. T. and Tan, T. M., "Wave Propagation in a Graphite/Epoxy Laminate," Journal of the Astronautical Sciences, Vol. 32, 1984, pp. 269-284.

18. Stiffler, R. C. and Henneke, E. G., II, "The Application of Low Frequency Acoustic Waves for Determining the Extensional and Flexural Stiffnesses in Composite Plates," Interim Report to General Electric Co., Contract No. 14-G-45-480, September 1985.

19. Worlton, D. C., "Experimental Confirmation of Lamb Waves at Megacycle Frequencies," Journal of Applied Physics, Vol. 32, 1961, pp. 967-971.

20. Chimenti, D. E. and Nayfeh, A. H., "Leaky Lamb Waves in Fibrous Composite Laminates," Journal of Applied Physics, Vol. 58, 1985, pp. 4531-4538.

21. Bar-Cohen, Y. and Chimenti, D. E., "Nondestructive Evaluation of Composite Laminates by Leaky Lamb Waves," Review of Progress in Quantitative NDE, D. O. Thompson and D. E. Chimenti, Eds., Vol. 5B, Plenum Press, New York, 1986, pp. 1199-1206.

22. Martin, R. W. and Chimenti, D. E., "Signal Processing of Leaky Lamb Wave Data for Defect Imaging in Composite Laminates," Review of Progress in Quantitative NDE, D. O. Thompson and D. E. Chimenti, Eds., Vol. 6A, Plenum Press, New York, 1987, pp. 815-824.

23. Vary, A. and Bowles, K. J., "Ultrasonic Evaluation of the Strength of Unidirectional Graphite-Polyimide Composites," NASA TM-X-73646, April 1977.

24. Henneke, E. G., II, Duke, J. C., Jr., Stinchcomb, W. W., Govada, A., and Lemascon, A., "A Study of the Stress Wave Factor Technique for the Characterization of Composite Materials," NASA CR-3670, February 1983.

25. Duke, J. C., Jr., Henneke, E. G., II, and Stinchcomb, W. W., "Ultrasonic Stress Wave Characterization of Composite Materials," NASA CR-3976, May 1986.

26. Stiffler, R. C., "Wave Propagation in Composite Plates," Ph.D. Dissertation, College of Engineering, Virginia Polytechnic Institute and State University, Blacksburg, Virginia, November 1986.

27. Chapman, G. B., II, "A Nondestructive Method of Evaluating Adhesive Bond Strength in Fiberglass Reinforced Plastic Assemblies," Joining of Composite Materials, ASTM STP 749, K. T Kedward, Ed., American Society for Testing and Materials, 1981, pp. 32-60.

28. Rose, W. R., Rokhlin, S. I., and Adler, L., "Evaluation of Anisotropic Properties of Graphite/Epoxy Composites Using Lamb Waves," Review of Progress in Quantitative NDE, D. O. Thompson and D. E. Chimenti, Eds., Vol. 6B, Plenum Press, New York, 1987, pp. 1111-1118.

29. Liu, J. M., "The Frequency Dependence of Ultrasonic Wave Propagation in Metal-Matrix Composite Plates," Proceedings of the 15th Symposium on NDE, D. W. Moore and G. A. Matzkanin, Eds., Southwest Research Institute, San Antonio, 1985, pp. 303-310.

30. Wormley, S. J. and Thompson, R. B., "A Semi-Automatic System for the Ultrasonic Measurement of Texture," Review of Progress in Quantitative NDE, D. O. Thompson and D. E. Chimenti, Eds., Vol. 6A, Plenum Press, New York, 1987, pp. 951-956.

31. Yang, P. C., Norris, C. H., and Stavsky, Y., "Elastic Wave Propagation in Heterogeneous Plates," International Journal of Solids and Structures, Vol. 2, 1966, pp. 665-684.

32. Mindlin, R. D., "Influence of Rotatory Inertia and Shear on Flexural Motions of Isotropic, Elastic Plates," Journal of Applied Mechanics, Vol. 18, 1951, pp. 31-38.

33. Green, W. A., "Bending Waves in Strongly Anisotropic Elastic Plates," Quarterly Journal of Mechanics and Applied Mathematics, Vol.35, 1982, pp. 485-507.

34. Mindlin, R. D., "Waves and Vibrations in Isotropic, Elastic Plates," Structural Mechanics, J. N. Goodier and N. J. Hoff, Eds., Pergamon Press, New York, 1960, pp. 199-232.

35. Redwood, M., Mechanical Waveguides, Pergamon Press, New York, 1960.

36. Meeker, T. R. and Meitzler, A. H., "Guided Wave Propagation in Elongated Cylinders and Plates," Physical Acoustics: Principles and Methods, W. P. Mason, Ed., Vol. 1, Pt. A, Academic Press, New York, 1964, pp. 111-167.

37. Viktorov, I. A., Rayleigh and Lamb Waves, Plenum Press, New York, 1967.

38. Henneke, E. G., II and Duke, J. C., Jr., "Analytical Ultrasonics for Evaluation of Composite Material Response," Materials Evaluation, Vol. 43, 1985, pp.740-745.

39. Kriz, R. D. and Stinchcomb, W. W., "Elastic Moduli of Transversely Isotropic Graphite Fibers and Their Composites," Experimental Mechanics, Vol. 19, 1979, pp.41-49.

40. Chow, T. S., "On the Propagation of Flexural Waves in an Orthotropic Laminated Plate and Its Response to an Impulsive Load," Journal of Composite Materials, Vol. 5, 1971, pp. 306-319.

41. Whitney, J. M., "Shear Correction Factors for Orthotropic Laminates Under Static Load," Journal of Applied Mechanics, Vol. 40, 1973, pp.302- 304.

42. Reissner, E., "The Effect of Transverse Shear Deformation on the Bending of Elastic Plates," Journal of Applied Mechanics, Vol. 12, 1945, pp. 69-77.

43. Noor, A. K., "Stability of Multilayered Composite Plates," Fibre Science and Technology, Vol. 8, 1975, pp. 81-89.

APPENDIX A

```
C..............................................................
C
C     THIS COMPUTER PROGRAM IS DESIGNED TO CALCULATE
C     LAMINATE STIFFNESS MATRICES FOR ANY ARBITRARY
C     LAMINATE.
C
C        VARIABLES:
C           E1,E2 = YOUNG'S MODULI
C           V12 = POISSON'S RATIO
C           G12,G13,G23 = SHEAR MODULI
C           N = THE NUMBER OF LAYERS
C           Z(I) = THE DISTANCE FROM THE MIDDLE
C                  SURFACE TO THE INTERFACE
C           ANGLE(I) = ANGLE OF PLY ORIENTATION
C        INPUT:
C           LINE 1: E1,E2,V12,G12,G13,G23
C           LINE 2: N
C           LINE 3: Z(I)
C           LINE 4: ANGLE(I)
C        OUTPUT:
C           A, B, AND D MATRICES
C
C..............................................................
      IMPLICIT REAL*8 (A-H,O-Z)
      DIMENSION A(3,3),B(3,3),D(3,3),Q(3,3),QBAR(3,3),Z(41),ANGLE(40)
      DIMENSION A4455(2,2),QB45(2,2)
C
C
C     BEGIN TO READ INPUT DATA
C
C
      READ(5,*)E1,E2,V12,G12,G13,G23
      READ(5,*)N
      NN=N+1
      READ(5,*)(Z(I),I=1,NN)
      READ(5,*)(ANGLE(I),I=1,N)
C
C
```

```
C     INITIALIZE MATRICES
C
C
      DO 10 I=1,3
      DO 10 J=1,3
      A(I,J)=0.0
      B(I,J)=0.0
      D(I,J)=0.0
      Q(I,J)=0.0
10    QBAR(I,J)=0.0
      DO 17 I=1,2
      DO 17 J=1,2
      A4455(I,J)=0.0
17    QB45(I,J)=0.0
C
C
C     CALCULATE Q MATRIX
C
C
      V21=V12*E2/E1
      Q(1,1)=E1/(1.-V12*V21)
      Q(1,2)=V21*Q(1,1)
      Q(1,3)=0.0
      Q(2,1)=Q(1,2)
      Q(2,2)=Q(1,1)*E2/E1
      Q(2,3)=0.0
      Q(3,1)=0.0
      Q(3,2)=0.0
      Q(3,3)=G12
C
C
C     BEGIN LOOP TO CALCULATE A, B, AND D MATRICES
C
C
      DO 20 K=1,N
C
C
C     CALCULATE QBAR MATRIX OF THE KTH LAYER
C
C
      CALL CQBAR(Q,ANGLE(K),QBAR)
      CALL CQ4455(G13,G23,QB45,ANGLE(K))
C
C
C     PRINT [QB45] MATRIX OF THE KTH LAYER
C
C
      WRITE(6,70)K
70    FORMAT(////,' THE QB45 MATRIX OF THE ',I2,' LAYER IS :',//)
      DO 80 I=1,2
80    WRITE(6,277)(QB45(I,J),J=1,2)
```

```
277  FORMAT(20X,2(1PE11.4,3X),/)
C
C
C     ACCUMULATE VALUES OF A4455 MATRIX FROM EACH LAYERS
C
C
     DO 27 I=1,2
     DO 27 J=1,2
27   A4455(I,J)=A4455(I,J) + QB45(I,J)*(Z(K+1)-Z(K))
C
C
C     ACCUMULATE VALUES OF A, B, AND D MATRICES
C     FROM EACH LAYERS
C
C
     DO 20 I=1,3
     DO 20 J=1,3
     A(I,J)=A(I,J) + QBAR(I,J)*(Z(K+1)-Z(K))
     B(I,J)=B(I,J) + 0.5*QBAR(I,J)*(Z(K+1)**2-Z(K)**2)
20   D(I,J)=D(I,J) + (1./3.)*QBAR(I,J)*(Z(K+1)**3-Z(K)**3)
C
C
C     PRINT A, B, AND D MATRICES
C
C
     WRITE(6,100)
100  FORMAT(////,' THE EXTENSIONAL STIFFNESSES A(I,J) ARE :',//)
     DO 110 I=1,3
110  WRITE(6,200)(A(I,J),J=1,3)
     WRITE(6,120)
120  FORMAT(////,' THE COUPLING STIFFNESSES B(I,J) ARE :',//)
     DO 130 I=1,3
130  WRITE(6,200)(B(I,J),J=1,3)
     WRITE(6,140)
140  FORMAT(////,' THE BENDING STIFFNESSES D(I,J) ARE :',//)
     DO 150 I=1,3
150  WRITE(6,200)(D(I,J),J=1,3)
200  FORMAT(20X,3(1PE11.4,3X),/)
     WRITE(6,177)
177  FORMAT(////,' THE EXTENSIONAL STIFFNESSES A4455 ARE :',//)
     DO 147 I=1,2
147  WRITE(6,277)(A4455(I,J),J=1,2)
     STOP
     END
C
C...............................................................
C
     SUBROUTINE CQ4455(G13,G23,QB45,ANGLE)
     IMPLICIT REAL*8 (A-H,O-Z)
     DIMENSION QB45(2,2)
     ANG=ANGLE*3.14159/180.
```

```
      C=DCOS(ANG)
      S=DSIN(ANG)
      C2=C*C
      S2=S*S
      QB45(1,1)=G23*C2 + G13*S2
      QB45(1,2)=(G23-G13)*C*S
      QB45(2,1)=QB45(1,2)
      QB45(2,2)=G13*C2 + G23*S2
      RETURN
      END
C
C..............................................................
C
      SUBROUTINE CQBAR(Q,ANGLE,QBAR)
      IMPLICIT REAL*8 (A-H,O-Z)
      DIMENSION Q(3,3),QBAR(3,3)
      ANG=ANGLE*3.14159/180.
      C=DCOS(ANG)
      S=DSIN(ANG)
      C2=C*C
      S2=S*S
      C4=C2*C2
      S4=S2*S2
      QBAR(1,1)=Q(1,1)*C4 + 2*(Q(1,2)+2*Q(3,3))*S2*C2 + Q(2,2)*S4
      QBAR(1,2)=(Q(1,1)+Q(2,2)-4*Q(3,3))*S2*C2 + Q(1,2)*(S4+C4)
      QBAR(1,3)=(Q(1,1)-Q(1,2)-2*Q(3,3))*S*C*C2
     +      + (Q(1,2)-Q(2,2)+2*Q(3,3))*S*S2*C
      QBAR(2,1)=QBAR(1,2)
      QBAR(2,2)=Q(1,1)*S4 + 2*(Q(1,2)+2*Q(3,3))*S2*C2 + Q(2,2)*C4
      QBAR(2,3)=(Q(1,1)-Q(1,2)-2*Q(3,3))*S*S2*C
     +      + (Q(1,2)-Q(2,2)+2*Q(3,3))*S*C*C2
      QBAR(3,1)=QBAR(1,3)
      QBAR(3,2)=QBAR(2,3)
      QBAR(3,3)=(Q(1,1)+Q(2,2)-2*Q(1,2)-2*Q(3,3))*S2*C2 + Q(3,3)*(S4+C4)
      RETURN
      END
C
C..............................................................
C
```

APPENDIX B

```
C..............................................................
C
C      THIS COMPUTER PROGRAM IS DESIGNED TO CALCULATE
C      THE SHEAR CORRECTION FACTORS FOR SYMMETRIC
C      CROSS-PLY AND SYMMETRIC QUASI-ISOTROPIC
C      LAMINATES UNDER STATIC CYLINDRICAL BENDING.
C
C         VARIABLES:
C            E1,E2 = YOUNG'S MODULI
C            V12 = POISSON'S RATIO
C            G12,G13,G23 = SHEAR MODULI
C            N = THE NUMBER OF LAYERS
C            Z(I) = THE DISTANCE FROM THE MIDDLE
C                   SURFACE TO THE INTERFACE
C            ANGLE(I) = ANGLE OF PLY ORIENTATION
C         INPUT:
C            LINE 1: E1,E2,V12,G12,G13,G23
C            LINE 2: N
C            LINE 3: Z(I)
C            LINE 4: ANGLE(I)
C         OUTPUT:
C            SHEAR CORRECTION FACTORS
C
C..............................................................
      IMPLICIT REAL*8 (A-H,O-Z)
      DIMENSION A(3,3),B(3,3),D(3,3),Q(3,3),QBAR(16,3,3),Z(17),ANGLE(16)
      DIMENSION A4455(2,2),QB45(16,2,2)
      READ(5,*)E1,E2,V12,G12,G13,G23
      READ(5,*)N
      NN=N+1
      READ(5,*)(Z(I),I=1,NN)
      READ(5,*)(ANGLE(I),I=1,N)
      DO 10 I=1,3
      DO 10 J=1,3
      A(I,J)=0.0
      B(I,J)=0.0
      D(I,J)=0.0
      Q(I,J)=0.0
```

```
      DO 10 K=1,16
10     QBAR(K,I,J)=0.0
      DO 17 I=1,2
      DO 17 J=1,2
      A4455(I,J)=0.0
      DO 17 K=1,16
17     QB45(K,I,J)=0.0
      V21=V12*E2/E1
      Q(1,1)=E1/(1.-V12*V21)
      Q(1,2)=V21*Q(1,1)
      Q(1,3)=0.0
      Q(2,1)=Q(1,2)
      Q(2,2)=Q(1,1)*E2/E1
      Q(2,3)=0.0
      Q(3,1)=0.0
      Q(3,2)=0.0
      Q(3,3)=G12
      DO 20 K=1,N
      CALL CQBAR(Q,ANGLE(K),QBAR,K)
      CALL CQ4455(G13,G23,QB45,ANGLE(K),K)
      DO 27 I=1,2
      DO 27 J=1,2
27     A4455(I,J)=A4455(I,J) + QB45(K,I,J)*(Z(K+1)-Z(K))
      DO 20 I=1,3
      DO 20 J=1,3
      A(I,J)=A(I,J) + QBAR(K,I,J)*(Z(K+1)-Z(K))
      B(I,J)=B(I,J) + 0.5*QBAR(K,I,J)*(Z(K+1)**2-Z(K)**2)
20     D(I,J)=D(I,J) + (1./3.)*QBAR(K,I,J)*(Z(K+1)**3-Z(K)**3)
C
C
C        CALCULATE K52
C
C
      XXA=-0.5D0*QBAR(1,1,1)
      XXB=0.5D0*QBAR(1,1,1)*Z(1)*Z(1)
      ALPHA=(XXA*XXA)/(QB45(1,2,2))
      BETA=(2.D0*XXA*XXB)/(QB45(1,2,2))
      GAMMA=(XXB*XXB)/(QB45(1,2,2))
      SUM=(ALPHA*0.2D0*(Z(2)**5-Z(1)**5))
     +    +(BETA*(Z(2)**3-Z(1)**3)/(3.D0))
     +    +(GAMMA*(Z(2)-Z(1)))
      DO 1000 K=2,N
      KK=K-1
      XXA=-0.5D0*QBAR(K,1,1)
      XXB=(-0.5D0*(QBAR(KK,1,1)-QBAR(K,1,1))*Z(K)*Z(K)) + XXB
      ALPHA=(XXA*XXA)/(QB45(K,2,2))
      BETA=(2.D0*XXA*XXB)/(QB45(K,2,2))
      GAMMA=(XXB*XXB)/(QB45(K,2,2))
1000  SUM=((ALPHA*0.2D0*(Z(K+1)**5-Z(K)**5))
     +    +(BETA*(Z(K+1)**3-Z(K)**3)/(3.D0))
     +    +(GAMMA*(Z(K+1)-Z(K)))) + SUM
```

```
      XXK52=D(1,1)*D(1,1)/(A4455(2,2)*SUM)
C
C
C        PRINT K52
C
C
      WRITE(6,1200)XXK52
 1200 FORMAT(////,' THE SHEAR CORRECTION FACTOR K52 IS ',
     + F7.4,//)
C
C
C        CALCULATE K42
C
C
      XXA=-0.5D0*QBAR(1,2,2)
      XXB=0.5D0*QBAR(1,2,2)*Z(1)*Z(1)
      ALPHA=(XXA*XXA)/(QB45(1,1,1))
      BETA=(2.D0*XXA*XXB)/(QB45(1,1,1))
      GAMMA=(XXB*XXB)/(QB45(1,1,1))
      SUM=(ALPHA*0.2D0*(Z(2)**5-Z(1)**5))
     +   +(BETA*(Z(2)**3-Z(1)**3)/(3.D0))
     +   +(GAMMA*(Z(2)-Z(1)))
      DO 1400 K=2,N
      KK=K-1
      XXA=-0.5D0*QBAR(K,2,2)
      XXB=(-0.5D0*(QBAR(KK,2,2)-QBAR(K,2,2))*Z(K)*Z(K)) + XXB
      ALPHA=(XXA*XXA)/(QB45(K,1,1))
      BETA=(2.D0*XXA*XXB)/(QB45(K,1,1))
      GAMMA=(XXB*XXB)/(QB45(K,1,1))
 1400 SUM=((ALPHA*0.2D0*(Z(K+1)**5-Z(K)**5))
     +   +(BETA*(Z(K+1)**3-Z(K)**3)/(3.D0))
     +   +(GAMMA*(Z(K+1)-Z(K)))) + SUM
      XXK42=D(2,2)*D(2,2)/(A4455(1,1)*SUM)
C
C
C        PRINT K42
C
C
      WRITE(6,1600)XXK42
 1600 FORMAT(////,' THE SHEAR CORRECTION FACTOR K42 IS ',
     + F7.4,//)
      STOP
      END
C
C.................................................................
C
      SUBROUTINE CQ4455(G13,G23,QB45,ANGLE,K)
      IMPLICIT REAL*8 (A-H,O-Z)
      DIMENSION QB45(16,2,2)
      ANG=ANGLE*3.14159/180.
      C=DCOS(ANG)
```

```
      S=DSIN(ANG)
      C2=C*C
      S2=S*S
      QB45(K,1,1)=G23*C2 + G13*S2
      QB45(K,1,2)=(G23-G13)*C*S
      QB45(K,2,1)=QB45(K,1,2)
      QB45(K,2,2)=G13*C2 + G23*S2
      RETURN
      END
C
C..........................................................
C
      SUBROUTINE CQBAR(Q,ANGLE,QBAR,K)
      IMPLICIT REAL*8 (A-H,O-Z)
      DIMENSION Q(3,3),QBAR(16,3,3)
      ANG=ANGLE*3.14159/180.
      C=DCOS(ANG)
      S=DSIN(ANG)
      C2=C*C
      S2=S*S
      C4=C2*C2
      S4=S2*S2
      QBAR(K,1,1)=Q(1,1)*C4 + 2*(Q(1,2)+2*Q(3,3))*S2*C2 + Q(2,2)*S4
      QBAR(K,1,2)=(Q(1,1)+Q(2,2)-4*Q(3,3))*S2*C2 + Q(1,2)*(S4+C4)
      QBAR(K,1,3)=(Q(1,1)-Q(1,2)-2*Q(3,3))*S*C*C2
     +      + (Q(1,2)-Q(2,2)+2*Q(3,3))*S*S2*C
      QBAR(K,2,1)=QBAR(K,1,2)
      QBAR(K,2,2)=Q(1,1)*S4 + 2*(Q(1,2)+2*Q(3,3))*S2*C2 + Q(2,2)*C4
      QBAR(K,2,3)=(Q(1,1)-Q(1,2)-2*Q(3,3))*S*S2*C
     +      + (Q(1,2)-Q(2,2)+2*Q(3,3))*S*C*C2
      QBAR(K,3,1)=QBAR(K,1,3)
      QBAR(K,3,2)=QBAR(K,2,3)
      QBAR(K,3,3)=
     + (Q(1,1)+Q(2,2)-2*Q(1,2)-2*Q(3,3))*S2*C2 + Q(3,3)*(S4+C4)
      RETURN
      END
C
C..........................................................
C
```

The vita has been removed from
the scanned document